YEAR END TECHNICAL REPORT
September 29, 2021 to September 28, 2022

Waste and D&D Engineering and Technology Development

Date submitted:

December 22, 2022

Principal Investigator:

Leonel E. Lagos, Ph.D., PMP®

Florida International University Collaborators:

Leonel E. Lagos, Ph.D., PMP® (Project Manager)
Himanshu Upadhyay, Ph.D., PMP®
Joseph Sinicrope, M.S., MBA
Walter Quintero, M.S.
Santosh Josh, M.S.
Tushar Bhardwaj, Ph.D.
Suresh Peddoju, Ph.D.
Masudur Siddiquee, Ph.D.
Clint Miller, MCSE+Security
Mellissa Komninakis, B.S.
Kexin Jiao, Ph.D.
DOE Fellows

Submitted to:

U.S. Department of Energy
Office of Environmental Management
Under Cooperative Agreement No. DE-EM0005213

Applied Research Center
Florida International University

Addendum:

This document represents one (1) of five (5) reports that comprise the Year End Reports for the period of September 29, 2021 to September 28, 2022 prepared by the Applied Research Center at Florida International University for the U.S. Department of Energy Office of Environmental Management (DOE-EM) under Cooperative Agreement No. DE-EM0005213.

The complete set of FIU's Year End Reports for this reporting period includes the following documents:

Project 1: Chemical Process Alternatives for Radioactive Waste
Document number: FIU-ARC-2021-800012997-04b-006

Project 2: Environmental Remediation Science and Technology
Document number: FIU-ARC-2021-800013918-04b-004

Project 3: Waste and D&D Engineering and Technology Development
Document number: FIU-ARC-2021-800013919-04b-005

Project 4: DOE-FIU Science & Technology Workforce Development Initiative
Document number: FIU-ARC-2021-800013920-04b-017

Project 5: Long-Term Stewardship of Environmental Remedies: Contaminated Soils and Water and STEM Workforce Development
Document number: FIU-ARC-2021-800013922-04b-004

Each document will be submitted to OSTI separately under the respective project title and document number as shown above. In addition, the documents are available at the DOE Research website for the Cooperative Agreement between the U.S. Department of Energy Office of Environmental Management and the Applied Research Center at Florida International University: https://doeresearch.fiu.edu

TABLE OF CONTENTS

LIST OF FIGURES

LIST OF TABLES

PROJECT 3 EXECUTIVE SUMMARY

The Waste and D&D Engineering and Technology Development Project (Project 3) focuses on delivering solutions under the waste, D&D and IT/data science areas for the DOE Office of Environmental Management. This work directly supports D&D activities being conducted across the DOE EM complex to include Oak Ridge, Savannah River, Hanford.

During FIU Year 2, the following DOE Fellows directly supported this project: Aurelien Meray (graduate, Ph.D., Computer Science), Roger Boza (graduate, Ph.D., computer science), Rohan Shanbhag (undergraduate, Computer Science), and Nicholas Espinal (undergraduate, mechanical engineering).

The following ARC researchers are supporting this project and mentoring the DOE-EM Fellows: Himanshu Upadhyay (Ph.D., Engineering/Management, Task 1, 3, 6, 7 & 8, Principal Scientist), Walter Quintero (M.S., Computer Engineering, Task 1, 3 & 6, Research Scientist/IT Team Lead), Santosh Joshi (M.S., Engineering Management, Task 6, 7 & 8, Database Architect), Clint Miller (MCSA, MCSE, CompTIA Security +, C|EH, Cyber Systems Engineer), Masudur Siddiquee ((Ph.D., Computer Science & Engineering, Task 7, Postdoctoral Associate), Joseph Sinicrope (M.S., Technology Leadership/MBA, Task 2, Research Scientist), Mellissa Komninakis (B.S., Biological Eng./Materials Science & Engineering, Task 2, Research Analyst), Kexin Jiao (Ph.D., Material Science & Nanotechnology, Task 2, Postdoctoral Associate), Jose Rivera (B.S., Civil Engineering, Research Analyst), Leonel Lagos (Ph.D., PMP®, Mechanical Eng./Civil/Env. Engineering, PI).

This project included the following tasks during the September 29, 2021 to September 28, 2022 period of performance:

Task 1: Waste Information Management System (WIMS) (HQ)

This task provides direct support to DOE EM for the management, development, and maintenance of a Waste Information Management System (WIMS). WIMS was developed to receive and organize the DOE waste forecast data from across the DOE complex and to automatically generate waste forecast data tables, disposition maps, GIS maps, transportation details, and other custom reports. WIMS is successfully deployed and can be accessed from the web address https://emwims.org/. The waste forecast information is updated annually. WIMS has been designed to be extremely flexible for future additions and is being enhanced on a regular basis.

Task 2: D&D Support to DOE EM for Technology Innovation, Development, Evaluation and Deployment

This task provides direct support to DOE EM for D&D technology innovation, development, evaluation, and deployment. Based on high priority operational requirements expressed by DOE EM HQ, the national labs, and site personnel, FIU will expand its research in technology test and evaluation in the following key areas by: 1) Confirming the experimental designs intended to certify fixative technology performance when exposed to various stressors (e.g., fire, thermal, environmental, water) that are postulated in contingency scenarios in DOE EM-wide Safety Basis Documents; 2) Investigating the application of a down-selected intumescent foam technology and other fire retardant materials to mitigate contaminate release during nuclear pipe dismantling and other D&D activities; 3) Collaborating with ASTM to continue development of standards and testing protocols in support of D&D technologies; and 4) Investigating the potential for multi-functional fixatives intended for mercury abatement during D&D Activities. FIU will further support the EM D&D program by participating in D&D workshops, conferences, and serving as subject matter experts.

Task 3: Knowledge Management Information Tool (KM-IT) (HQ, SRNL, INL, ANL)

The Knowledge Management Information Tool (KM-IT) is a web-based system developed to maintain and preserve the EM knowledge base. The system was developed by Florida International University's Applied Research Center with the support of the D&D community, including DOE-EM, the former DOE ALARA centers, and with the active collaboration and support of the DOE's Energy Facility Contractors Group (EFCOG). The KM-IT is a community driven system tailored to serve the technical issues faced by the workforce across the DOE Complex. The KM-IT can be accessed from web address http://www.dndkm.org.

Task 6: AI for EM Problem Set (D&D): Structural health monitoring of D&D facility to identify cracks and structural defects for Surveillance and Maintenance (SRNL)

This task is focused on investigating specific applications of artificial intelligence and big data technologies to solve DOE-EM problem sets and challenge areas, including potential applications of existing state-of-the-art technologies (e.g., imaging, robotics, big data, and machine learning/deep learning) to assess the structural integrity of aging facilities in support of ongoing surveillance and maintenance (S&M) across the DOE complex. [completed during FIU Year 2].

Task 7: AI for EM Problem Set (Soil and Groundwater) - Exploratory data analysis and machine learning model for Hexavalent Chromium [Cr (VI)] concentration in 100-H Area (PNNL)

To investigate the spatiotemporal correlations between groundwater (GW) and surface water (SW) hexavalent chromium (Cr(VI)) concentrations, the FIU team examined expanded datasets for the 100 Areas of the U.S. Department of Energy Office of Environmental Management's (DOE-EM's) Hanford Site . A suitable strategy for data pre-processing and filtering was created based on the exploratory analysis. An algorithm for spatiotemporal relationship exploration was researched and developed where the machine learning (ML) model's feature scores (GW well time series) for forecasting surface water Cr(VI) content timeseries, were extracted using data filtering techniques and the Random Forest (RF) machine learning (ML) models. To investigate the connection between the distance to each aquifer tube and the feature relevance in the machine learning model, individual aquifer tubes are taken into consideration. Finally, in the assessment of the directions associated with ML model performances, the results show that the minimum mean absolute error (MAE) models associated with arc triangles are located approximately parallel and close to the shoreline for proxy groundwater wells, and an approximately opposite trend was observed for aquifer tubes where the directions are closely perpendicular to the shoreline.

Task 8: AI for EM Problem Set (Soil and Groundwater) – Data analysis and visualization of sensor data from the wells at the SRS F-Area using machine learning (LBNL, SRNL)

The objective of this task is to develop a data interfacing module for the AI system. This type of module will help to ingest the time series and imagery data coming from the sensors deployed by the ALTEMIS project team. Further, research will be performed on algorithms suitable for analysis and pattern identification with a specific focus on spatial and temporal data received from the groundwater wells. It will lead to an AI/ML-based system developed for automatic pattern identification and prediction from the sensor dataset.

MAJOR TECHNICAL ACCOMPLISHMENTS

Task 1: Waste Information Management System (WIMS) (HQ)

- FIU continued to successfully ensure a consistent high level of performance of the WIMS application through day-to-day maintenance and administration tasks. The team continued to use tools like Google Analytics and Google Search Console to monitor the performance of the application.
- The team also updated the script for the Google Map API which supports the GIS module to ensure it was compliant with the new version of the API.
- FIU received a new set of waste stream forecast and transportation forecast data from DOE and completed the data import and all the necessary code updates to the back-end and front-end of the application to accommodate the new waste streams. Two new facilities were added, Unitech and Veolia, which brought the total to 36 sites and 35 disposition facilities. This subtask was completed ahead of schedule on April 25, 2022. This milestone (2021-P3-M3) was completed ahead of schedule.
- FIU successfully ensured the WIMS application remained secure and reliable by consistently engaging with the external FIU security team to do independent testing and with the DOE Fellows to do internal testing. The DOE Fellows are learning to use the latest cyber security tools to get them ready for the workforce as they contribute to this task.
- A poster based on the WIMS application was presented at the Waste Management Symposia 2022 (WM2022).

Task 2: D&D Support to DOE EM for Technology Innovation, Development, Evaluation and Deployment

- The final draft of the "*Radiation Hardened Foam Cold Demo Test Plan - Phase 1: Foam Adhesion, Contamination Fixation, Moisture Stresses, Pipe Cutting, and Thermal Profile Testing*" was approved and signed by all the FIU, SRNL, and F/H Lab Decommissioning team stakeholders in January 2022, and all test objectives outlined in the Phase I Test Plan were fully executed for the first foam technology being evaluated (Hilti 620).
- The final draft of the technical progress report titled, *"Multi-functional 3D Polymer Framework for Mercury Abatement"* was submitted and is being published on OSTI.
- FIU continued to chair the ASTM International E10.03 Subcommittee and led the Fixatives Working Group to update and prepare E3104, *Standard Specification for Strippable & Removable Coatings to Mitigate Spread of Radioactive Contamination* and E3105, *Standard Specification for Permanent Coatings to Mitigate Spread of Radioactive Contamination,* for renewal and balloting.
- Dr. Kexin Jiao et al published a manuscript titled *"Simultaneous Writing and Erasing Using Probe Lithography Synchronized Erasing and Deposition (PLiSED)"* in the peer-reviewed journal - Langmuir. This publication was based on Dr. Jiao's previous research related to polymeric material engineering during the pursuit of his PhD, but certain elements outlined within provided the framework from which to build upon for the functionalization of PDMS-MRs for Hg Remediation.
- Dr. Kexin Jiao was awarded "Best in Track" in the professional poster competition at WM2022 for his research on a multi-functional 3D polymer framework for mercury abatement.

- M. Komninakis et al are in the final stages of completing a manuscript for Nuclear Technology on *Certifying Fixative Technology Performance when Exposed to Impact Stressors as Postulated in Contingency Scenarios Highlighted in Safety Basis Documents*.
- FIU researchers identified another commercial-off-the-shelf foam technology - FOAMBAG - that has been used extensively at Sellafield, UK for decommissioning pipes. F/H labs and SRNL concur it warrants evaluation and will serve as the focal point for the Phase II test plan.

Task 3: Knowledge Management Information Tool (KM-IT) (HQ, SRNL, INL, ANL)

- FIU published 103 technologies, vendors and lessons learned on the KM-IT platform in addition to other relevant resources for the community, such as D&D related training, conferences and workshops. The content management efforts continue to keep the website current and informative for the D&D community.
- FIU attended the 2022 Waste Management Symposia conference where the team hosted a booth to display and demo its research and presented a poster titled *"D&D KM-IT 2022 Updates"*. The poster focused on recent updates to the KM-IT which include the Fixative Module, Research Module, Tech Talks and Responsive Design.
- During this period (Sep 2021 - Oct 2022 vs previous period), the system had a drop in traffic of about 17% shown by User, New Users, Session and Pages per Session. This also affected the Pageview and Avg Session Duration.
- The team developed 9 newsletters for mass communication via email to keep users informed of new system features and other related activities. FIU sent newsletters to the registered users of the KM-IT and to the participants of the Waste Management Symposia with news articles and upcoming events.
- The team hosted 4 Tech Talks during this period of performance (in October 2021, and January, April, and July 2022). This involved collaboration with Idaho National Laboratory (INL), Argonne National Laboratory (ANL) and Florida International University's Applied Research Center (FIU-ARC) research team to present topics relevant to the DOE EM Complex.
- The team has successfully kept the D&D KM-IT application and production environment running with optimal performance. In addition, the team continued to test, maintain, secure and administer the KM-IT system to keep it secured and up to date with industry standards by updating the Secure Socket Layer (SSL) and testing the application on a secure network using cyber security tools like Metasploit.

Task 6: AI for EM Problem Set (D&D): Structural health monitoring of D&D facility to identify cracks and structural defects for Surveillance and Maintenance (SRNL)

- FIU completed this task during FIU Year 2 and final deliverable provided to DOE HQ
- Multiple CNN models were researched and developed with a small memory footprint and high validation accuracy for mobile deployment.
- The model for the YOLOv3 network architecture was improved and is now capable of identifying and locating cracks in real time with better bounding boxes.
- A mobile application was designed and developed to perform image classification and

- object detection predictions using the trained neural network models.
- A Web Service API was developed to expose the trained deep learning models to the mobile app.

Task 7: AI for EM Problem Set (Soil and Groundwater) – Exploratory data analysis and machine learning model for Hexavalent Chromium [Cr (VI)] concentration in 100-H Area (PNNL)

- FIU researched and developed an algorithm for data pre-processing and exploratory analysis which includes time series segregation, missing value handling, sensor locations adjacency identification, time series smoothing, and statistical analysis.
- An algorithm was researched and developed to identify directional and distance-wise spatial segmentation for AI/ML modeling in the case of Cr(VI) spatiotemporal relationship identification for individual groundwater monitoring wells.
- An algorithm was researched and developed to identify the overall trend of the contaminant spatiotemporal relationship between surface water and groundwater in an area of interest.

Task 8: AI for EM Problem Set (Soil and Groundwater) - Data analysis and visualization of sensor data from the wells at the SRS F-Area using machine learning (LBNL, SRNL)

- A prototype interface was developed that can store and preprocess in-situ data which is currently accessed using the HydroVu API.
- The FIU team explored the use of machine and deep learning algorithms to predict contaminant concentrations using proxy variables. It was found that the deep learning methods outperformed the classical machine learning methods.
- The FIU research team completed the milestone 2021-P3-M6 to have an AI system ready for when the ALTEMIS Aqua TROLL sensors come online.

TASK 1: WASTE INFORMATION MANAGEMENT SYSTEM (WIMS) (HQ)

The Waste Information Management System (WIMS) was developed to receive and organize the DOE waste forecast data from across the DOE complex and to automatically generate waste forecast data tables, disposition maps, GIS maps, transportation details, and other custom reports. WIMS is successfully deployed and can be accessed from the web address http://www.emwims.org.

During this period, the team prepared a poster (Figure 1) for the 2022 Waste Management Symposia titled *"Waste Information Management System (WIMS) with 2021-22 Waste Streams."* This poster is focused on informing the community about the new updates to the WIMS application, which includes new waste streams and an updated GIS Google Map.

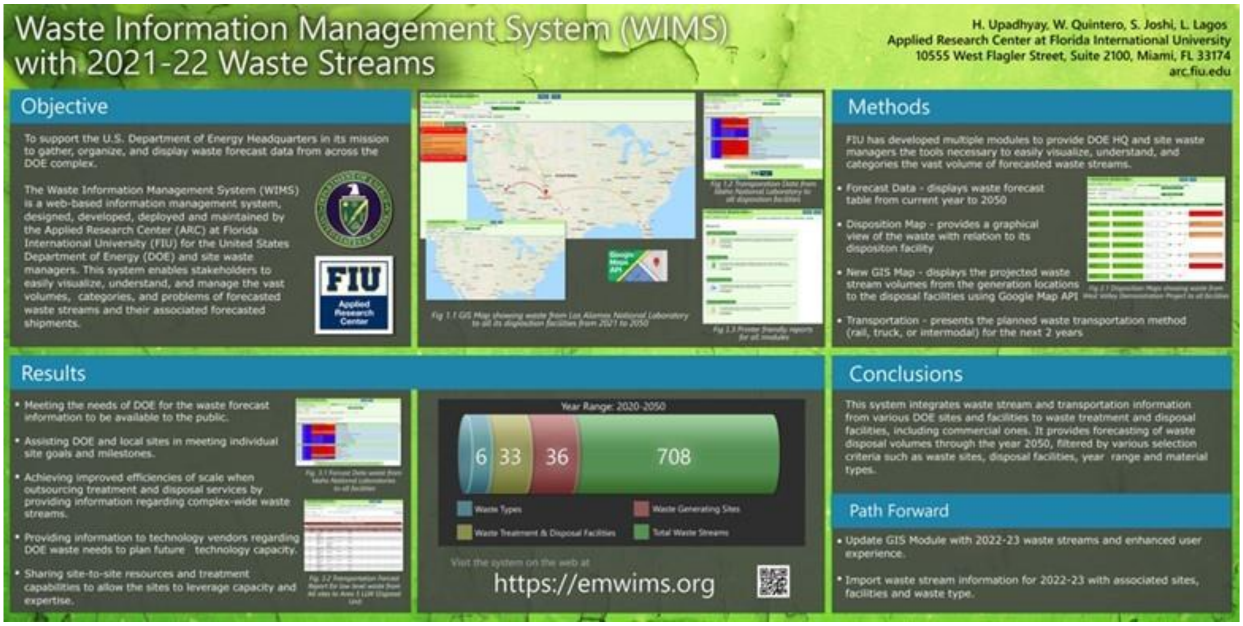

Figure 1. WIMS poster prepared for the 2022 Waste Management Symposia.

The team presented the poster on March 8, 2022, at WM2022. The image below shows the FIU staff (Himanshu Upadhyay and Walter Quintero) and a WM2022 attendee in front of the WIMS poster at the conference.

Figure 2. FIU staff, Himanshu Upadhyay and Walter Quintero, with a WM2022 attendee in front of the WIMS poster.

Subtask 1.1 WIMS System Administration - Database Management, Application Maintenance & Performance Tuning

Subtask 1.1: Introduction

This subtask includes the day-to-day maintenance and administration of the application and the database servers. FIU maintains the WIMS application system to ensure a consistent high level of performance. In addition, the database administrators perform routine maintenance in order to keep the WIMS database and server in a stable condition. The WIMS application is also maintained on the web server by the Web Server Administrator. This administrator monitors the network and server traffic and performs changes necessary to optimize the application performance. In addition, as part of this subtask, FIU will provide application and database security, as well as Help Desk support to DOE site waste managers, HQ managers and other users who need assistance in using WIMS.

Subtask 1.1: Objectives

The objective of this task is to secure the WIMS application (software and hardware) and make it more resilient to cyber-attacks. Cyber threats continue to increase at an exponential rate. The FIU team secures the application by performing routine maintenance and performance tuning. This helps prevent cyber breaches and also improves the user experience by allowing the application to run at optimal performance.

Subtask 1.1: Methodology

FIU is constantly updating the physical environment of the WIMS application. This requires updates of the servers and software, including the IIS (application server), SQL Server (database server), and Microsoft Visual Studio (development tool). This effort supports system availability, security, maintenance, backup and disaster recovery, etc. Keeping the software and hardware up to date facilitates future migration/upgrade processes which also reduces overall maintenance costs.

In addition, FIU performed certain security tasks, including antivirus engine and definition updates on both the web and database servers. Other maintenance tasks included Windows OS updates and patches that were applied to the servers running the emwims.org application.

The team uses multiple tools to monitor the performance of the WIMS application. One of those tools used for web analytics is Google Analytics (GA). The image below (Figure 3) shows the WIMS application web analytics for the period of performance Oct 2021 – Sep 2022 vs the previous period Oct 2020 – Sep 2021.

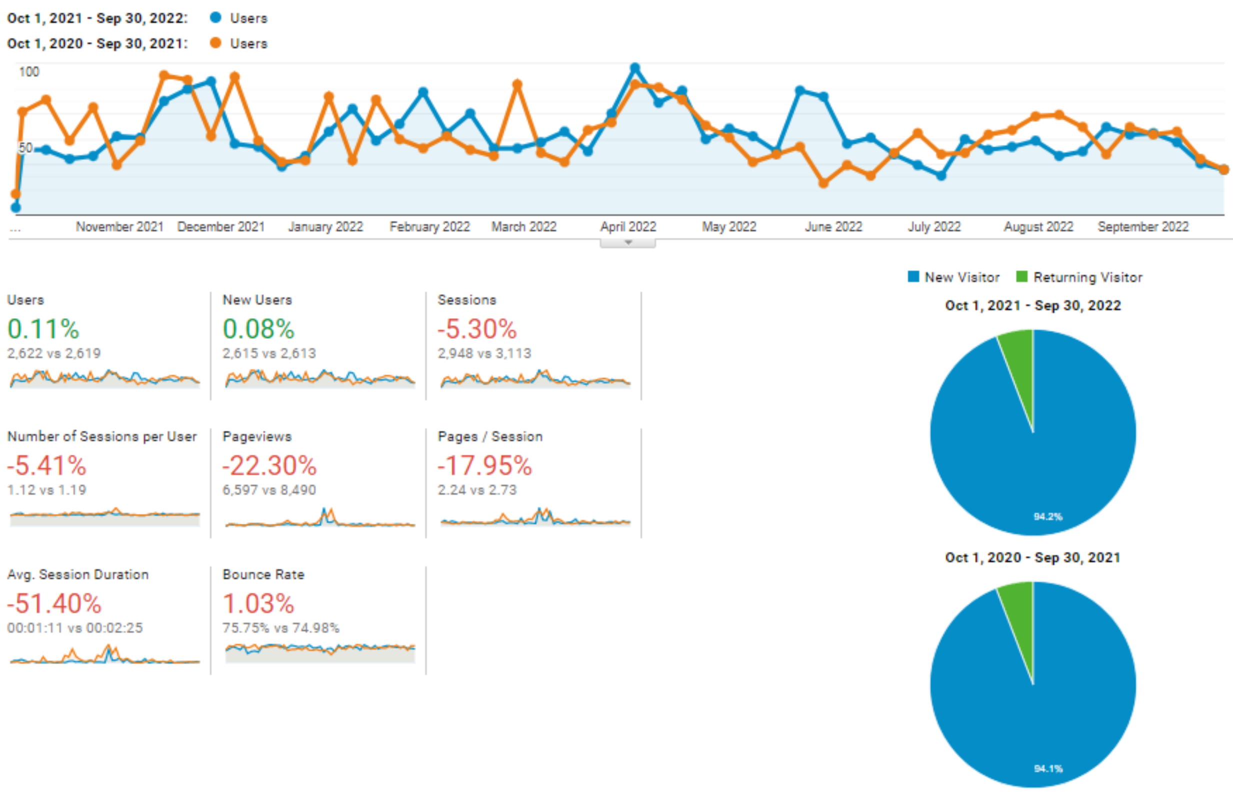

Figure 3. WIMS application web analytics for the period of performance of Oct 2021 – Sep 2022 vs the previous period Oct 2020 – Sep 2021.

The data above showed minimal change on user and new user visits. There was a small percentage drop on Sessions and Number of Session per User and a double-digit percentage drop of Pageviews, Pages per Session and Average Session Duration. Some of these metrics reflect the past year's updates performed on the application. Some of the updates focused on making the WIMS application easier to navigate and on improving performance. This explains the drop of pageviews and the number of pages a user stays on while on the site. So, although there are negative numbers in the report, these numbers validate that the updates performed during the previous period are working.

In addition, the team fixed an issue with the Google Map API account used by the WIMS GIS Map module. The GIS module started to display an error message on the map page with a watermark over the map that said, “for development purposes only” (see Figure 4).

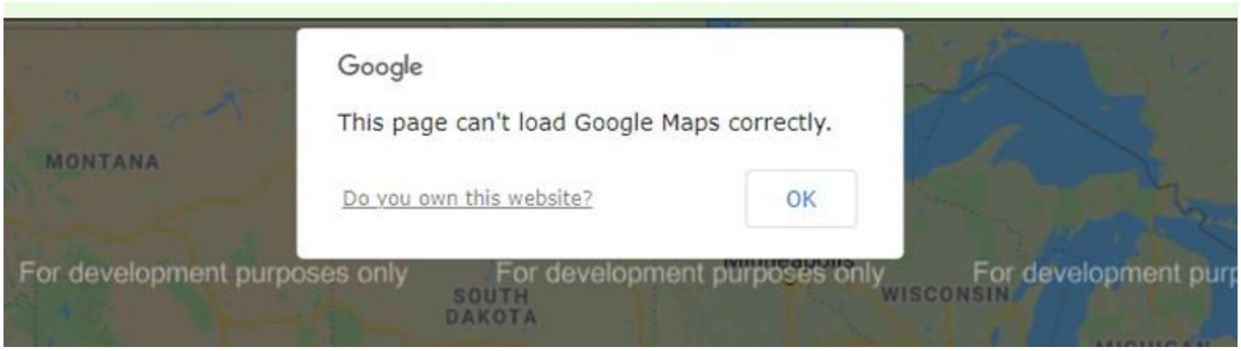

Figure 4. Error message on the WIMS GIS Map module.

The team was able to debug the application and concluded that the setting of the Google Map API account needed an update. After the proper update, the WIMS GIS module was working properly. No code changes were necessary on the application. The following figure shows the WIM GIS map module with no errors (Figure 5).

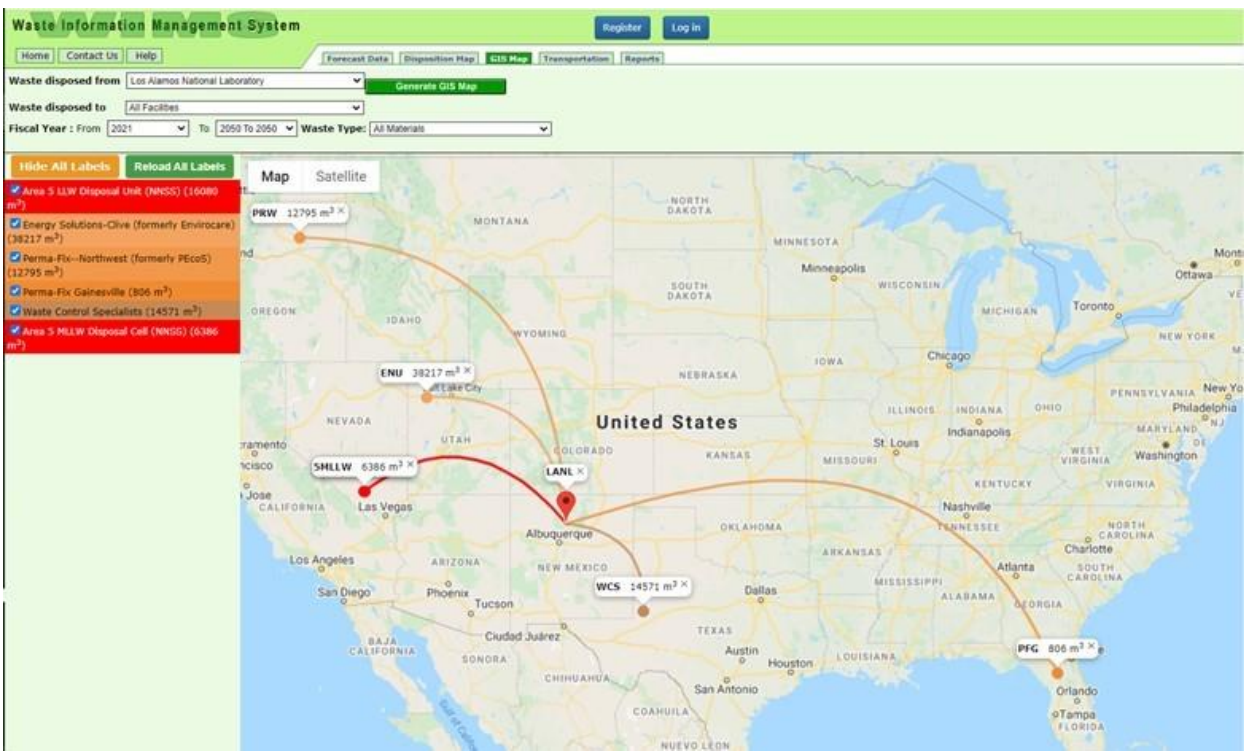

Figure 5. WIMS GIS map module with no errors.

Finally, the team created a Google Search Console profile (formally known as the Google Webmaster Tools) to start tracking WIMS search performance on Google. This is a separate platform from Google Analytics. The team will use this information to identify any issues that Google bots may have when trying to access the WIMS website. The platform will provide information such as broken links, URL errors, sitemap performance, site performance and more. As data becomes available, the team will use this to resolve any issues and report them in the monthly reports. Finally, the team updated the sitemap.xml file and uploaded it to the Google Search Console platform for Google bots to crawl the site.

In addition, the team made some changes to the HTML pages and site settings to help with Search Engine Optimization (SEO). Some of the changes included updating the page title with H1 tags, adding some "alt" description to certain images and updating the XML sitemap file located at https://emwims.org/sitemap.xml. Finally, the robots.txt file was optimized for better search engine coverage. These are common SEO practices that have to be reviewed and updated from time to time to ensure the site is properly crawled by search engines.

Finally, the team replaced the backup storage repository on the backup scripts. The application gets backed up on a regular basis. The hardware that stores this backup was replaced and therefore the backup scripts had to be updated to point to a new destination.

Subtask 1.1: Results and Discussion

FIU continued to perform day-to-day maintenance and administration of the application and the database servers to ensure a consistent high level of performance of the WIMS application system. FIU continued to execute certain security tasks, including antivirus engine and definitions updates on both the web and database servers. Other maintenance tasks included Windows OS updates and patches that were applied to the servers running the emwims.org application. This routine maintenance is necessary in order to keep the WIMS database and server in a stable condition and to monitor the network and server traffic to optimize the application's performance. The updates performed in the previous period were validated by the web analytics report which shows that while users' visits stayed the same, their time on the website was reduced due to a more simplified navigation and faster performance of the application.

Subtask 1.1: Conclusions

This is a continuous task for the purpose of securing the WIMS application (software and hardware). The FIU team has reduced cyber-attacks by securing the application through routine maintenance and performance tuning. This has contributed to the prevention of cyber breaches and improves the user experience by allowing the application to run at optimal performance.

Subtask 1.1: References

Waste Information Management System (WIMS), https://emwims.org/, Applied Research Center, Florida International University.

Subtask 1.2: Waste Stream Annual Data Integration

Subtask 1.2: Introduction

Under this subtask, FIU receives revised waste forecast data as well as transportation data as formatted data files on an annual basis. To incorporate these new files, FIU built a data interface to allow the files to be received by the WIMS application and imported into SQL Server. SQL server is the database server where the actual WIMS data is maintained. This data is typically received from DOE in the April/May timeframe.

Subtask 1.2: Objectives

The objective of this subtask is to consolidate waste forecast information from separate DOE sites and build forecast data tables, disposition maps, and GIS maps on the web. An integrated system was needed to receive and consolidate waste forecast information from all DOE sites and facilities and to make this information available to all stakeholders and the public. As there was no off-the-shelf computer application or solution available for creating disposition maps and forecast data, FIU built a DOE complex-wide, high performance, n-tier web-based system for generating waste forecast information, disposition maps, GIS Maps, successor stream relationships, summary information and custom reports based on DOE requirements.

Subtask 1.2: Methodology

FIU receives revised waste forecast data and transportation data as formatted data files from DOE EM on an annual basis. To incorporate these new files, FIU built a data interface to allow the files to be received by the WIMS application and imported into SQL Server. SQL server is the database server where the actual WIMS data is maintained. Once integrated, reviewed and verified, the new waste data replaces the existing/previous waste data and becomes fully viewable and operational in WIMS.

Subtask 1.2: Results and Discussion

Under this subtask, FIU receives and incorporates the revised waste forecast data files into the system on a yearly basis. The new waste data replaces the existing waste data and becomes fully viewable and operational in WIMS. During March timeframe, FIU receives revised waste forecast data from DOE-HQ as formatted data files. To incorporate these new files, FIU builds a data interface to allow these specific files to be formatted for the WIMS application and imported into SQL Server. This data is imported and mapped to the 2022 waste stream structure which will update the Forecast Data, Disposition map, Successor stream map, Transportation and Reports.

FIU was notified in early March by DOE HQ that the annual data had been collected. After DOE HQ verified the data, FIU received the data in late-March. The team got to work right away on getting it incorporated into the WIMS application by importing the data into the development database environment and updating the application to consume the new waste stream data. The team created the development environment to facilitate working on the application without interruption of the production site. The team verified the data, normalized it in order to prepare it for input into the SQL server, and performed the input using SQL import service packages developed for WIMS. The team had to make some modifications to the code to accommodate the new waste stream data. The team also updated the report module as well as other modules to make sure all the data is properly displayed.

The team has updated the application and database. The application was moved to a staging server for DOE Fellows and DOE officials to test the application and verify the data. Once DOE confirmed that all the data had been imported properly and reflected on the application, the team moved the application to the production environment.

FIU addressed all the feedback and comments from DOE HQ and moved the WIMS application from the staging server to the production server at https://emwims.org. The screenshot below shows the WIMS application with the new 2022 data streams.

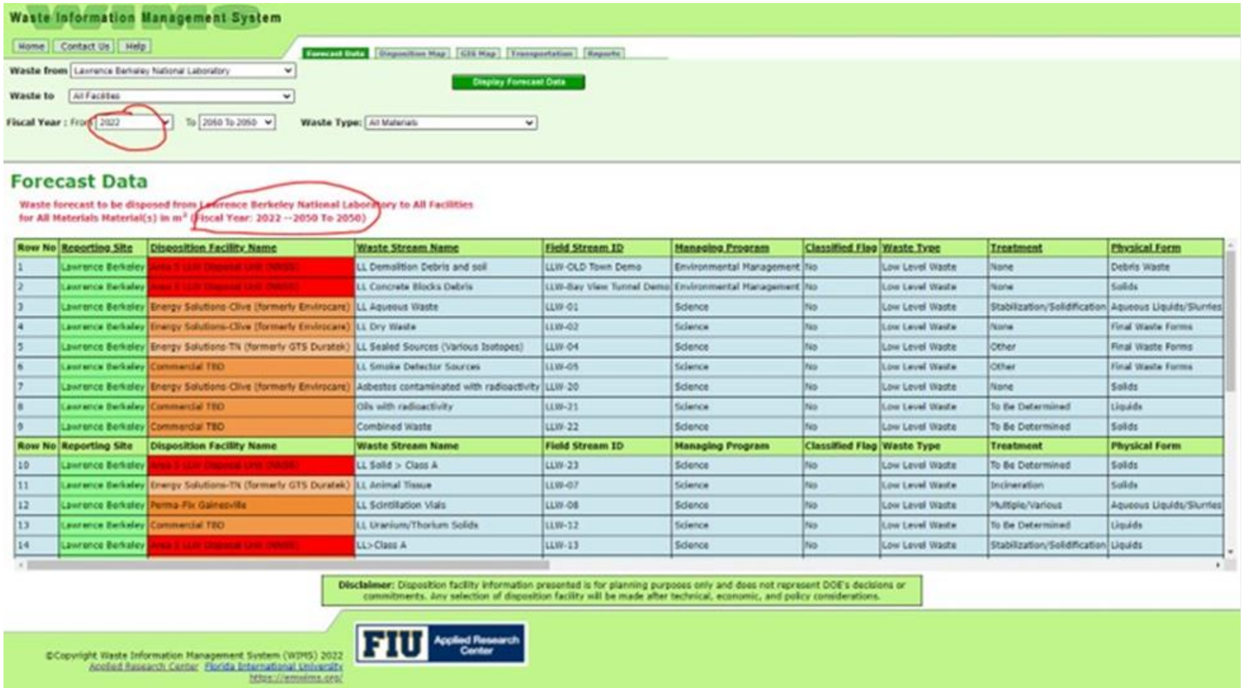

Figure 6. Forecast Data module showing 2022 waste stream data from Lawrence Berkeley National Laboratory to All Facilities.

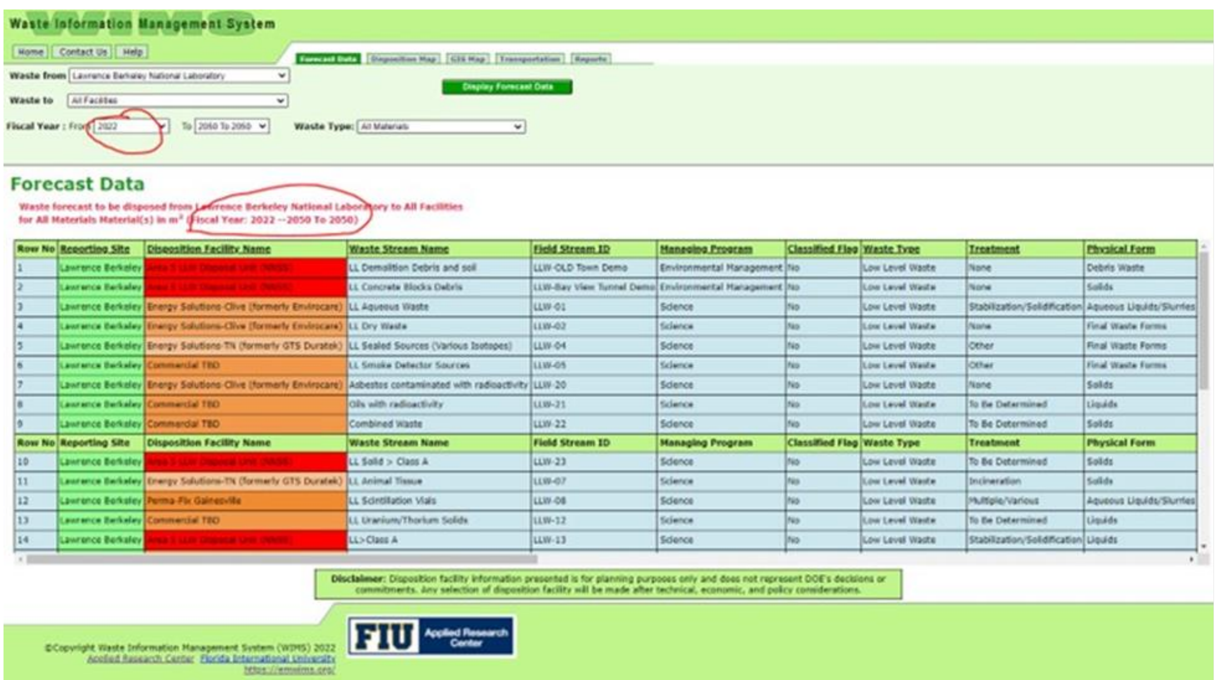

Figure 7. Disposition map showing 2022 waste stream from Bettis Atomic Power Laboratory to All Facilities.

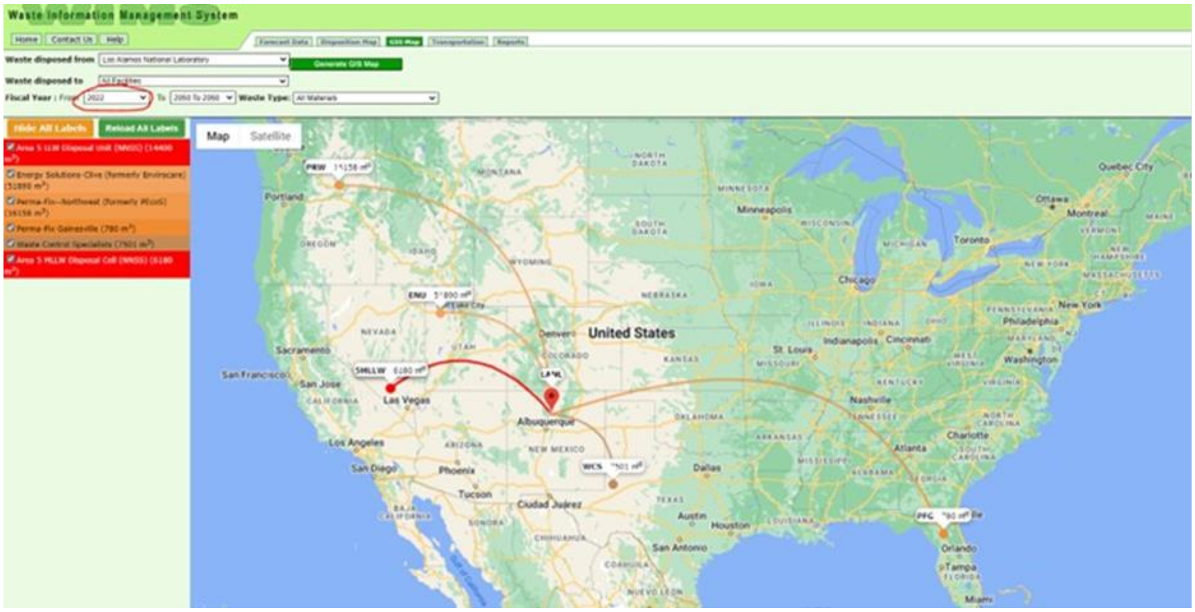

Figure 8. GIS Module showing 2022 waste steam data from Los Alamos National Laboratory to All Facilities.

The team sent a notification of completion email to DOE HQ on April 25, 2022. This milestone (2021-P3-M3) was completed ahead of schedule.

As of the end of this period, the WIMS application has supported the following waste types:

- All Materials
- Unknown
- Low-Level Waste
- Mixed Low-Level Waste
- 11e.(2) Byproduct Material
- Other Material

In addition, the waste can be forecasted among 36 sites and 34 disposition facilities. The names of each of the locations are listed below. These include new disposition facilities named Unitech and Veolia.

Table 1. List of Sites and Facilities Supported by WIMS

	SITES		FACILITIES
1	Ames Laboratory	1	200 Area Burial Ground (HANF)
2	Argonne National Laboratory	2	746-U Landfill (Paducah)
3	Bettis Atomic Power Laboratory	3	Area 5 LLW Disposal Unit (NTS)
4	Brookhaven National Laboratory	4	Area 5 MLLW Disposal Cell (NTS)
5	Energy Technology Engineering Center	5	Clean Harbors
6	Fermi National Accelerator Laboratory	6	Commercial TBD
7	Hanford Site-RL	7	E-Area Disposal (SRS)
8	Hanford Site-RP	8	EMWMF Disposal Cell (ORR)
9	Idaho National Laboratory	9	Energy Solutions-Clive (formerly Envirocare)

10	Kansas City Plant	10	Energy Solutions-TN (formerly GTS Duratek)
11	Knolls Atomic Power Laboratory - Kesselring	11	ERDF (HANF)
12	Knolls Atomic Power Laboratory - Schenectady	12	Impact Services-TN
13	Lawrence Berkeley National Laboratory	13	INL CERCLA Cell (INL)
14	Lawrence Livermore National Laboratory	14	Integrated Disposal Facility (HANF)
15	Los Alamos National Laboratory	15	New RH LLW Vaults (INL)
16	Naval Reactor Facility	16	Omega Waste Logistics
17	Nevada Test Site	17	OSWDF(Portsmouth)
18	NG Newport News	18	Paducah CERCLA
19	Norfolk Naval Shipyard	19	Perma-Fix Gainesville
20	Nuclear Fuel Services, Inc. (cleanup site)	20	Perma-Fix--Diversified Scientific Services, Inc.
21	Oak Ridge Reservation	21	Perma-Fix--Northwest (formerly PEcoS)
22	Paducah Gaseous Diffusion Plant	22	Perma-Fix/Materials & Energy Corp
23	Pantex Plant	23	Remote Waste Disposition Project (INL)
24	Pearl Harbor Naval Shipyard	24	River Metals
25	Pacific Northwest National Laboratory	25	RMW Trenches (MLLW/LLW) (HANF)
26	Portsmouth Gaseous Diffusion Plant	26	RMW Trenches/IDF (HANF)
27	Portsmouth Naval Shipyard	27	RWMC (LLW disposal) (INL)
28	Princeton Plasma Physics Laboratory	28	Siemens
29	Puget Sound Naval Shipyard	29	Smokey Mountain Solutions
30	Sandia National Laboratories - NM	30	TA 54/Area G (LLW disposal) (LANL)
31	Savannah River Site	31	To Be Determined
32	Stanford Linear Accelerator Center	32	Unitech
33	Separations Process Research Unit	33	US Ecology-Idaho
34	Thomas Jefferson National Accelerator Facility	34	Veolia
35	Waste Isolation Pilot Plant	35	Waste Control Specialist
36	West Valley Demonstration Project		

Subtask 1.2: Conclusions

WIMS continues to successfully accomplish the goals and objectives set forth by DOE. WIMS has replaced the historic process of each DOE site gathering, organizing, and reporting their waste forecast information utilizing different database and display technologies. In addition, WIMS meets DOE's objective to have the complex-wide waste forecast information available to all stakeholders and the public in one easy-to-navigate system. The data includes low-level and mixed low-level radioactive waste forecast data supplied by all DOE programs in addition to transportation information. After a final review, the FIU team published the application to the production server running live at https://emwims.org/. This subtask (2021-P3-M3) was completed ahead of schedule on April 25, 2022.

Subtask 1.2: References

Office of Environmental Management (DOE-EM), https://www.energy.gov/em/office-environmental-management*, U.S. Department of Energy.*

Waste Information Management System (WIMS), https://emwims.org/, Applied Research Center, Florida International University.

Subtask 1.5: Cyber Security of WIMS Infrastructure

Subtask 1.5: Introduction

The cyber security of WIMS Infrastructure involves securing the network not only by system administration tasks mentioned above (), but also by conducting routine cyber security tasks to test the network's vulnerability. This involves coordination between the FIU security team and DOE Fellows who also learn cybersecurity skills while assisting staff do penetration testing and other tasks to test the overall security of the system at the application, database, and infrastructure levels.

Subtask 1.5: Objectives

The objective of this task is to focus on specific cyber security threats that could affect the WIMS application and framework. The team achieves this by implementing the latest industry security standards on the application and network to protect the WIMS application from malicious attacks.

Subtask 1.5: Methodology

Cyber security of WIMS involves securing the network infrastructure by performing routine cyber security tasks to test the network's vulnerability. The team involves coordination between the FIU security team and DOE Fellows to achieve this goal. The FIU security team performs independent security scans to test the vulnerability of the system. The reports of these scans are shared with the developer team which uses the information to focus on critical areas. The DOE Fellows perform internal tests on the environment. They use commonly used industry cyber security tools to test system vulnerability. By using these tools, the DOE Fellows are trained on the latest penetration test standards performed in the industry.

During the last period, the team, with the assistance of DOE Fellows, created a local private network where the WIMS application infrastructure could be duplicated. The purpose is to use cybersecurity tools to perform penetration testing to find vulnerabilities on the application. The team used the Nessus vulnerability scanner to find a host on the network. It then scanned the host for possible vulnerabilities. If one was found, the team used Metasploit to gain access to the system. After access is gained, the machine is prone to all kinds of attacks and the entire network could also be compromised. The team uses these kinds of exercises to train DOE Fellows on industry cybersecurity tasks and to apply these techniques to existing production environments such as the WIMS and D&D KM-IT. The team also used this information to properly secure the WIMS application running on the production environment.

Finally, during this period, the team focused on maintaining the development and staging environment used in Subtask 1.2. These environments had to be maintained and secured during the development and testing on the staging server. Also, since this milestone was completed, the team began dismantling the development environment and making backups for redundancies.

Subtask 1.5: Results and Discussion

The teams continued to secure the application on a constant basis. This effort needs to be performed regularly as new security threads are developed daily. The team has engaged with the external FIU security team to do independent testing and engaged the DOE Fellows to do internal testing. As a result, the WIMS application has remained secure and reliable. The DOE Fellows are learning to use the latest cyber security tools to get them ready for the workforce as they contribute to this task.

Subtask 1.5: Conclusions

As mentioned above, this is a continuous task in which multiple teams work together to achieve the goal of securing the WIMS application. The team has been successful in keeping the application secure and is always looking for new tools to test the application security. As new threats are identified on the internet, the team tests the application against those threats and quickly applies the appropriate patches and software updates to minimize the system vulnerability.

Subtask 1.5: References

Waste Information Management System (WIMS), https://emwims.org/, Applied Research Center, Florida International University.

TASK 2: D&D SUPPORT TO DOE EM FOR TECHNOLOGY INNOVATION, DEVELOPMENT, EVALUATION AND DEPLOYMENT

Subtask 2.1: Development of Uniform Testing Protocols and Standard Specifications for Dust Suppressant Technologies in support of Open-Air Demolition during D&D

Subtask 2.1: Introduction

The U.S. Department of Energy's Office of Environmental Management (DOE-EM) has taken a leading role in investing the research and development (R&D) of critical technologies to support the safe and efficient decommissioning of legacy nuclear facilities. In order to facilitate the complex-wide deployment and adoption of those technologies from the laboratory to end users, and to maximize return on investment of government-sponsored R&D projects, DOE-EM proactively solicits and evaluates initiatives intended to enhance achievement of these goals. One such case study emerged and involved the successful deployment of an intumescent fixative technology in support of the SRS 235-F PuFF Facility Risk Reduction Program. A detailed analysis confirmed that a critical enabler and key contributor to this effort was a deliberate, methodical approach to leverage an international, consensus-based standards organization from the onset. This approach ensured uniform standard specifications and testing protocols were used to confirm technology performance, which correspondingly mitigated the risk to the end user for acceptance and adoption of the new technological solution. There is a substantial body of literature that supports the crucial role of standards in technology programs across all phases of development - from concept, to deployment, to large-scale diffusion - in other industries. There are several federal directives that recognize the essential role of standards. For example, Section 12(d) of the National Technology Transfer and Advancement Act (Public Law 104-113), directs federal departments to achieve a greater reliance on voluntary consensus standards, and this mantra is also required by the Office of Management and Budget's Circular A-119, "Federal Participation in the Development and Use of Voluntary Consensus Standards and in Conformity Assessment Activities."

Given that standards-based testing and evaluation is a critical enabler to the successful transition and deployment of D&D technologies from the lab to the end user, FIU will continue to actively participate in ASTM International's E10 and E10.03 Committees to develop and promulgate uniform performance metrics and testing protocols for D&D technologies, with a particular emphasis on dust suppressant technologies in support of open-air demolition. To date, this effort has produced five (5) new international standard specifications and testing practices for fixative technologies which have been fully integrated into D&D technology test plans across the DOE-EM complex.

These efforts help to ensure that the FIU three-phased Technology Test and Evaluation Model is uniform in its application and defensible in its findings and results. As part of these efforts, FIU will attend and participate in the two planned ASTM International Conferences per year throughout this period of performance. The ultimate outcome of these efforts is to reduce the risks associated with implementing new technologies and further support the update of existing directives and guidance handbooks to account for the recent advancements in technology development in D&D.

Subtask 2.1: Objectives

Under this task, FIU ARC continues to actively participate in ASTM International's E10 and E10.03 Committees to develop and promulgate uniform performance metrics and testing protocols for D&D technologies, with a particular emphasis on fixatives and foams. This activity directly supports the planned operational deployment of those technologies on site, as well as establishes the groundwork for updating the DOE-HDBK-3010. Providing a uniform certification methodology for fixative technologies has been deemed an essential goal under this activity.

Subtask 2.1: Methodology

Leveraging the incombustible fixatives research and development activity being led by Savannah River National Laboratory (SRNL) and Florida International University's Applied Research Center (FIU ARC) on behalf of DOE EM's Office of Infrastructure and D&D, a holistic technology deployment approach was devised for the adoption of intumescent technologies as fire resistant fixatives. SRNL's close relationship with the SRS 235-F PuFF Facility Risk Reduction Team and FIU's involvement with the American Society for Testing and Materials (ASTM) International's E10.03 Subcommittee on Radiological Protection for D&D of Nuclear Facilities and Components provided an ideal vehicle to test the initiative. New international standard specifications for fixative technologies have been formally published and promulgated by ASTM. More importantly, this effort has been an important pillar for the test and evaluation of a fixative technology that has been successfully deployed in the entry hood and process cell #7 at the SRS 235-F PuFF Facility and serves as the basis for promoting the planned deployment of a foam technology on site in FY'24/25.

Subtask 2.1: Results and Discussion

In discussions with DOE EM, as well as commercial entities conducting the environmental restoration of various nuclear sites, it was determined that many of these human factor concerns could be alleviated by:

1. Leveraging an international, consensus-based organization that develops and promulgates international standards and testing protocols for fixative technologies used in D&D, and
2. Referencing these new standards to update dated regulations and directives guiding the environmental restoration of nuclear sites.

Immediately addressing these concerns would provide tremendous credibility to the R&D effort and yield a significant return on investment as the fixative technology would be tested, evaluated, and compared to a set of uniformly accepted standards and metrics that ensure it satisfactorily addresses the three pillars of test and evaluation – quality, productivity, and safety. This requirement becomes even more pressing and prominent when technologies are on the higher end of the technology readiness level (e.g., 7-9) and are ready for acquisition and deployment.

The ASTM International E10.03 Subcommittee on Radiological Protection during Decontamination and Decommissioning of Nuclear Facilities and Components is answering this challenge. It boasts a robust international membership that spans the entire spectrum of stakeholders and is perfectly postured to lead a collaborative process that bridges the organizational boundaries and cultures to achieve consensus on industry standards to facilitate uniform testing and evaluation of technologies and processes. Specifically, FIU continued to chair the ASTM International E10.03 Subcommittee and led the Fixatives Working Group to update and prepare E3104, *Standard Specification for Strippable & Removable Coatings to Mitigate Spread* *of Radioactive Contamination* and E3105, S*tandard Specification for Permanent Coatings to Mitigate Spread of Radioactive Contamination* for renewal and balloting.

Subtask 2.1: Conclusions

The ASTM International E10.03 Subcommittee will continue pursuing further testing protocol and standards development for fixatives and other technology categories associated with D&D, creating consensus-based standards for D&D technologies that are not only aligned with technical specifications, but also account for the safety, regulatory, and operational requirements encountered during D&D activities. Addressing existing shortfalls through standards will provide credibility, yield a significant return on investment, and allow all types of D&D technologies (robotics, fixatives, characterization, decontamination, demolition, etc.) to be developed, tested, evaluated, and compared to a set of uniformly accepted metrics.

International standards and testing protocol development plays a critical role in successful technology development and deployment programs. These standards lay the groundwork for setting the necessary conditions to successfully test, evaluate, compare, transition, and employ technologies in support of D&D activities in the highly regulated, safety conscience, risk adverse industry in which work is done. Universally accepted standards are essential in building the bridge to full field deployment of new technologies. This is particularly relevant when working at the higher ends of the TRL readiness scale and addresses many concerns on the part of all stakeholders – from researchers and developers to end users, regulatory agencies, and the public.

Subtask 2.1: References

ASTM International. (2017). *E3104-17 Standard Specification for Strippable & Removable Coatings to Mitigate Spread of Radioactive Contamination.* Retrieved from https://doi.org/10.1520/E3104-17

ASTM International. (2017). *E3105-17 Standard Specification for Permanent Coatings Used to Mitigate Spread of Radioactive Contamination.* Retrieved from https://doi.org/10.1520/E3105-17

ASTM International. (2018). *E3191-18 Standard Specification for Permanent Foaming Fixatives Used to Mitigate Spread of Radioactive Contamination.* Retrieved from https://doi.org/10.1520/E3191-18

ASTM International. (2019). *E3190-19 Standard Practice for Preparation of Fixed Radiological/Surrogate Contamination on Porous Test Coupon Surfaces for Evaluation of Decontamination Techniques.* Retrieved from https://doi.org/10.1520/E3190-19

ASTM International. (2021). *E3283-21 Standard Practice for Preparation of Loose Radiological/Surrogate Contamination on Nonporous Test Coupon Surfaces for Evaluation of Decontamination Techniques.* Retrieved from https://doi.org/10.1520/E3283-21

Subtask 2.2: Applications of Intumescent Foams and Other Fire-Retardant Materials to Mitigate Contaminate Release during Nuclear Pipe Dismantling and other D&D Activities

Subtask 2.2: Introduction

In support of the DOE-FIU Cooperative Agreement under Project 3 (Waste and D&D Engineering and Technology Development), Task 2 (D&D Support for Technology Innovation, Development, Evaluation and Deployment), the FIU Applied Research Center (ARC) focused its research activities on identifying, testing and evaluating commercial-off-the-shelf (COTS) intumescent material technologies as fire resistant fixative solutions that have a high potential to: 1) successfully address postulated contingency scenarios outlined in Basis for Interim Operations (BIO)/Safety Basis documents across the complex; and, 2) demonstrate a high probability of transitioning to an operational test and evaluation in a radioactive environment on site. This approach resulted in one intumescent coating technology being deployed in the Entry Hood to Process Cell 1 and Process Cell 7 at the SRS 235-F PUFF Facility in September/October of 2018. It has also led to the identification of another COTS intumescent foam technology that has demonstrated initial promise during proof-of-concept experiments this year in addressing an operational requirement for a rigid, fire-resistant fixative technology to immobilize and/or isolate residual contamination within a 3-dimensional void space of various volumes at sites across the complex.

An operational concept has been developed and proposed using the intumescent foam technology as an internal barrier, or "plug", prior to cutting contaminated pipework during dismantling and demolition operations on nuclear sites. Phase I of this research activity involved down-selecting a potential intumescent foam against some initial operational parameters outlined in ASTM E3191-18, Standard Specification for Permanent Foam Fixatives, specifically developed by the ASTM International E10.03 Subcommittee to support this broader activity. These included: 1) the ability to immobilize contamination and fill 3D spaces; 2) resistance to extreme temperatures and thermal stressors; 3) the ability to withstand certain environmental factors such as water; 4) mechanical properties such as rigidity and adhesion to ensure the material can act as a "plug" in piping and not be adversely affected when exposed to expected impact stressors; and, 5) confirmation of temperature profiles related to curing and uniform application of the material. Based on the initial findings and through extensive discussions with SRNL and other stakeholders across DOE EM, a COTS intumescent polyurethane foam has been identified and downselected as a technology that warrants further investigation. The research plan for the next phase is to develop, in close collaboration with SRNL and site personnel, an operationally focused test plan designed to directly evaluate the technology in terms of immediate, high priority requirements from safety basis personnel to conduct an operational test and evaluation on a DOE EM site by 2024.

During this performance year, the Radiation Hardened Foam Cold Demo Test Plan was developed. This document outlined the Phase-I test objectives and implementation plan for a downselected foam fixative technology intended to facilitate activities in support of the Savannah River Site (SRS) F/H labs' D&D efforts. It is a collaborative effort between SRNL, FIU, and the SRS F/H labs' team intended to test and evaluate the potential of an intumescent, fire-retardant foam in mitigating the release of contamination during dismantling operations on radioactively contaminated piping in legacy facilities. The cold demo test plan addresses specific requirements highlighted by site and safety personnel and will be executed in FIU's Outdoor Test and Evaluation Facility using a mock-up that replicates the operational conditions at the proposed hot test location at the F/H labs. Results from the cold test plan will inform the hot test at the F/H labs, which will use the foam fixative to confine and/or isolate residual contamination within a 3-dimensional void space of Hastelloy C-22 piping designated for removal from the site and transported to a proper disposal facility.

Subtask 2.2: Objectives

Phase I of the cold demo test plan outlined the following objectives:

- Evaluate the adhesion and bonding properties of the foam plug to Hastelloy C-22 piping
- Evaluate the adhesion and bonding properties of the foam plug to Hastelloy C-22 piping under various moisture conditions
- Determine the heat profile of the foam during curing in Hastelloy C-22 piping
- Establish the relationship between piping diameter and necessary quantity of Hilti CP-620 foam
- Determine the internal pipe pressure after foam deployment and curing time
- Develop a leak test standard operating procedure to test for the effectiveness of the foam plug
- Conduct a literature review to determine if using a hot tap is a viable method to deliver foam into piping
- Gather information and reference material to initiate the construction of the mock-up test of the F/H labs' courtyard

Subtask 2.2: Methodology

The COTS intumescent foam selected for evaluation is a two-component polyurethane foam that expands up to six times in volume upon application and cures in approximately one minute. The volume of foam produced per cartridge is up to 110 in^3. Per the application instructions, the first five pumps of the dispenser (or until the foam in the mixer nozzle has a consistent red color) will be discarded because this initial portion is unevenly mixed.

Evaluation of the adhesion and bonding properties of the foam plug to Hastelloy C-22 piping

Adhesion capabilities of the intumescent foam to Hastelloy C-22 piping will ultimately decide whether an intumescent foam fixative plug can confine and immobilize residual contamination in piping prior to transportation and disposition. The adhesion test will assess if any potential incidental impact could cause the Hilti CP-620 foam to delaminate from Hastelloy C-22 piping, causing the release of contamination. The tensile adhesion, compressive and shear properties of the foam itself have been baselined by FIU and SRNL in accordance with ASTM D1623: *Test method for tensile adhesion properties of rigid cellular plastics4,* ASTM D1621: *Standard Test Method for Compressive Properties of Rigid Cellular Plastics*, and ASTM D3574E: *Foam Tension Testing*. Furthermore, FIU and SRNL previously developed a series of testing practices specifically designed to evaluate the foam's ability to perform and function as a permanent plug in a pipe under normal operating conditions and when exposed to a variety of environmental and impact stressors. Using the MTS Criterion series 43 Tensile Tester with compression plates, shown in Figure 9, the amount of force required to push a foam plug out of a 3" D x 14" L pipe segment was determined. This test will be used on foam plugs in Hastelloy C-22 pipes, and the data will be compared with that obtained from the 304 stainless steel pipes to ascertain any differences in adhesion and bonding properties between the two pipe materials.

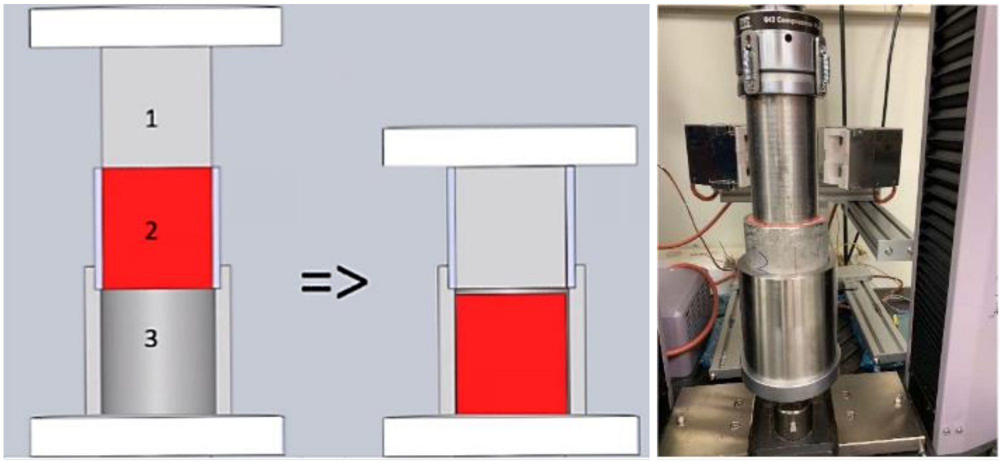

Figure 9. Plug strength test schematic (left) and plug strength testing for pipe samples using the "plunger – bucket" method on an MTS testing device (right).

Determination of the heat profile of the foam during curing in Hastelloy C-22 piping

Section 7.10 of *ASTM E3191-18: Standard specification for permanent foaming fixatives used to mitigate spread of radioactive contamination* states that "the foaming fixative shall not generate heat sufficient to compromise any of the components within the enclosure to which it is applied". Based on initial data from a series of experiments done at FIU, the curing temperature profile of Hilti CP-620 foam when applied in 1.5-inch diameter 304 stainless steel piping reached a maximum temperature range of 255.6°F to 276.0°F. Confirmation of the temperature profile of the curing process of the Hilti foam in Hastelloy C-22 piping on a larger sample size will be performed using the Extech SDL200 datalogger and Extech TP870 Type K thermocouples. The heat profile of the foam curing over time will be recorded until the cured foam has cooled to a temperature at which the pipe can be safely handled by workers. The monitoring time of the foam and the temperature needed to be reached for safe handling by workers will be determined by SRNL, FIU, and the F/H labs during testing.

Determine internal pipe pressure after foam deployment and curing time

The experimental setup is shown in Figure 10, where the pressure will be monitored for 24-hours using a digital pressure gauge. The SRS Manual 1S LLW WAC Section 5.3 identifies the maximum amount of allowable pressure within a pressurized container to be 1.5 atm (22 psi).

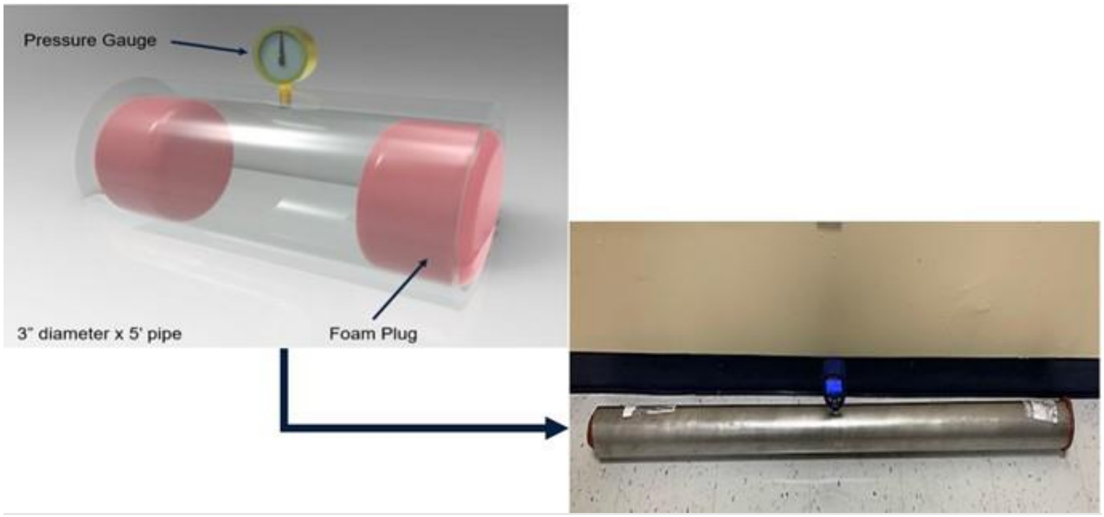

Figure 10. Experimental design for determining the internal pipe pressure after foam deployment.

Develop a leak test standard operating procedure to test for the effectiveness of the Hilti CP-620 foam plug

During Phase-I, the Cold Test Team will develop a consensus-based standard operating procedure (SOP) in consultation with the respective stakeholders (site personnel, SRNL, DOE-EM, F/H labs, FIU, EH&S, etc.). The developed water leak SOP will be used in Phase-II to evaluate the effectiveness of the Hilti CP-620 foam plug after injection and curing. Leak testing on the Hilti CP-620 foam plug in Hastelloy C-22 piping will be performed in accordance with Engineering Standard 15889: Confinement Ventilation Systems Design Criteria, Section 5.2.1.1, which states that the pass/fail criterion for leak tests should be comparable to solids/liquids applied to a cell or glovebox. The expected maximum permissible leak rate is expected to be 0.1% of pipe volume per hour at a differential pressure of 2 inches water column (2" WC). Upon completion, the water leak test SOP developed by the Cold Test Team will be submitted for review as a formal testing practice to ASTM International's E10 Committee on Nuclear Technology and Applications and its associated E10.03 Subcommittee on Radiological Protection for Decontamination and Decommissioning of Nuclear Facilities and Components. This will allow for the Cold Test Team to codify the leak test experimental design as an international standard for this technology.

Conduct a literature review to determine if using a hot tap is a viable method to deliver foam into piping

The Savannah River Site (SRS) has routinely used hot taps to make connections to existing piping. The hot tap method has been demonstrated for both stainless steel piping and carbon alloy piping; however, it is unknown (a) if the standard hot tap method will be effective at tapping into Hastelloy C-22 piping and (b) if the Hilti CP-620 foam can be injected into Hastelloy C-22 piping using a hot tap. This literature review will assess previous uses of hot taps on Hastelloy C-22 piping. The information will be compiled together and SRNL, FIU, and the F/H labs will develop a Phase-II test plan to test for the implementation of Hilti CP-620 foam using hot taps in a mock-up facility at FIU.

Subtask 2.2: Results and Discussion

Evaluation of the adhesion and bonding properties of the Hilti foam plug to Hastelloy C-22 piping

The intumescent foam was applied into C-22 and 304-stainless steel pipes for comparison and then tested using the MTS Criterion. The results for the Hastelloy pipes are shown in Table 2. The average failure load was 7,733 lbf with a standard deviation of 1,213 and none of the data points were statistical outliers. The results for the 304-stainless steel pipes are shown in Table 3. There was a slight issue with a setting on the MTS machine so two of the stainless-steel samples were disregarded. Overall, the stainless-steel average load before failure is still within the deviation of the previous data, 7,447 ± 1,110 lbf. The difference in pipe material seems to have little to no effect on the plug strength of the foam.

Table 2. Maximum Failure Load for Hastelloy C-22 Baseline Hilti Foam Samples

Baseline Testing Values				
	Load (lbf)	std	Stress (psi)	std
C-22-1	7250.07			
C-22-2	6940.50			
C-22-3	9983.59			
C-22-8	6963.39			
C-22-9	6988.26			
C-22-10	8273.61			
AVERAGE	**7733.24**	1213.72	**58.61**	0.44

Table 3. Maximum Failure Load for 304-Stainless Steel Baseline Hilti Foam Samples

Baseline Testing Values				
	Load (lbf)	std	Stress (psi)	std
304-1	8792.23			
304-2	7996.41			
304-3	8798.43			
304-4	-			
304-5	-			
304-6	8952.68			
AVERAGE	**8634.94**	432.11	**65.44**	0.50

FIU tested the plug strength of the intumescent foam in Hastelloy C22 pipes 24 hours after application. Previous results revealed that the average baseline plug strength of the foam in

Hastelloy piping is 7,733 lbf ± 1,214 lbf. However, these previous samples were tested a few days after foam application. As seen in Table 4, there was no significant change in the plug strength just 24 hours after foam application when compared to previous results.

Table 4. Maximum Failure Load for Hastelloy C-22 Hilti Foam Samples – 24 Hours After Application

24 Hours After Application				
	Load (lbf)	Standard Deviation - Load	Stress (psi)	Standard Deviation - Stress
C22-3	7094.31			
C22-7	8283.25			
C22-8	9130.68			
AVERAGE	**8169.41**	1022.95	**61.91**	0.47

Evaluation of the adhesion and bonding properties of the Hilti foam plug to Hastelloy C-22 piping under moisture conditions

An initial proof-of-concept for Objective 2 involved spraying/misting a known amount of water around the inside of the Hastelloy pipes, so that all sides of the pipes were wet. Then the intumescent foam was applied immediately following the misting. The foam was allowed to fully cure before testing the effects of moisture/water on the plug strength using the MTS Criterion tester. The plug strength results in Table 5 show an average failure load of 888 lbf. The average baseline plug strength determined previously was 7,733 lbf under ideal conditions. This initial moisture test suggests that the foam does not adhere well to wet surfaces, and it negatively affects the strength of the foam.

Table 5. Initial Moisture – Maximum Failure Load for Hastelloy C-22 Baseline Hilti Foam Samples

Initial Moisture Test				
	Load (lbf)	Standard Deviation - Load	Stress (psi)	Standard Deviation - Stress
C-22-1	1120.20			
C-22-2	846.80			
C-22-3	245.84			
C-22-10	1339.23			
AVERAGE	**888.01**	473.14	**6.73**	0.05

In addition, an initial water leak test was conducted with the intumescent foam in clear PVC piping. The foam was applied inside the pipe and allowed to cure before adding water with a blue UV-reactive dye. Enough water was added to the pipe to create one inch of standing water when the pipe was laying horizontally. The pipe was then stood up vertically and monitored for over a week to see if the foam would be impermeable. As seen in Figure 11, no water leaked out of the pipe after more than one week.

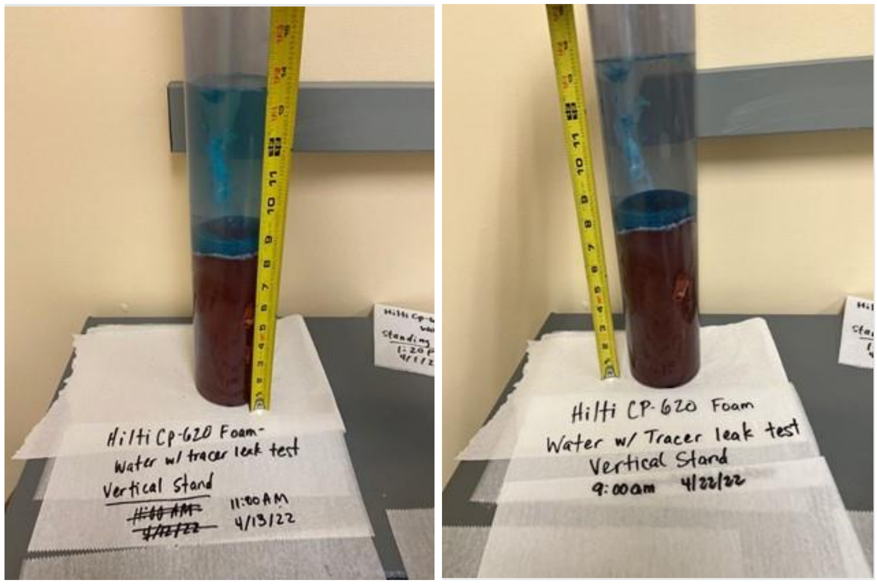

Figure 11. Initial water leak test in clear PVC pipe with Hilti foam.

Determination of the heat profile of the Hilti foam during curing in Hastelloy C-22 piping

Determining the heat profile involved inserting four thermocouples at varying depths into the pipes to determine the internal temperature of the foam while curing. The internal temperature was monitored for 24 hours after the application of the foam. A thermal camera was also used to monitor the external temperature of the Hastelloy pipes for 20 minutes after the application of the foam. The results of the internal temperature profile, in Figure 12, showed that the average maximum internal temperature of the foam during curing was 261.5°F, with a standard deviation of 1.9, and it took about 2.5 hours for that temperature to return to 70°F. The results of the external temperature test, in the images below, show that the maximum external temperature was around 75°F.

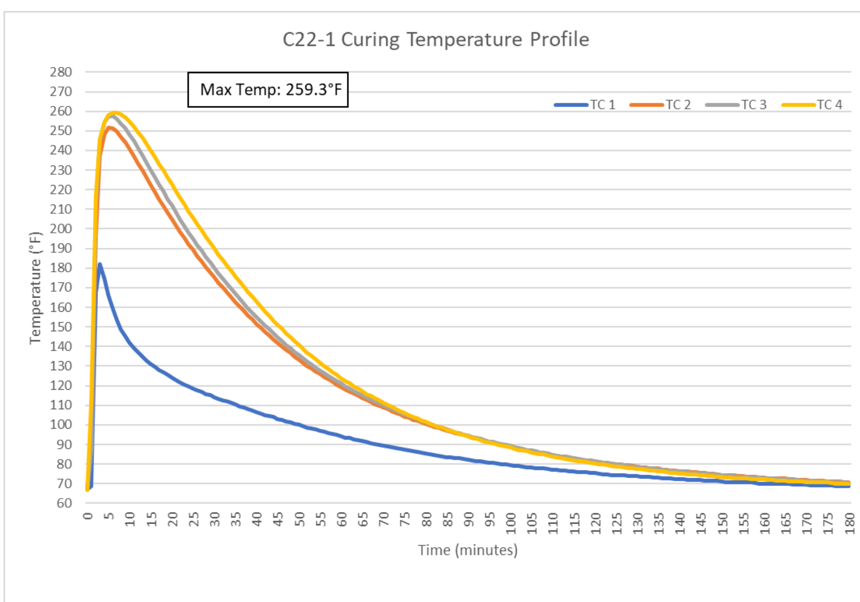

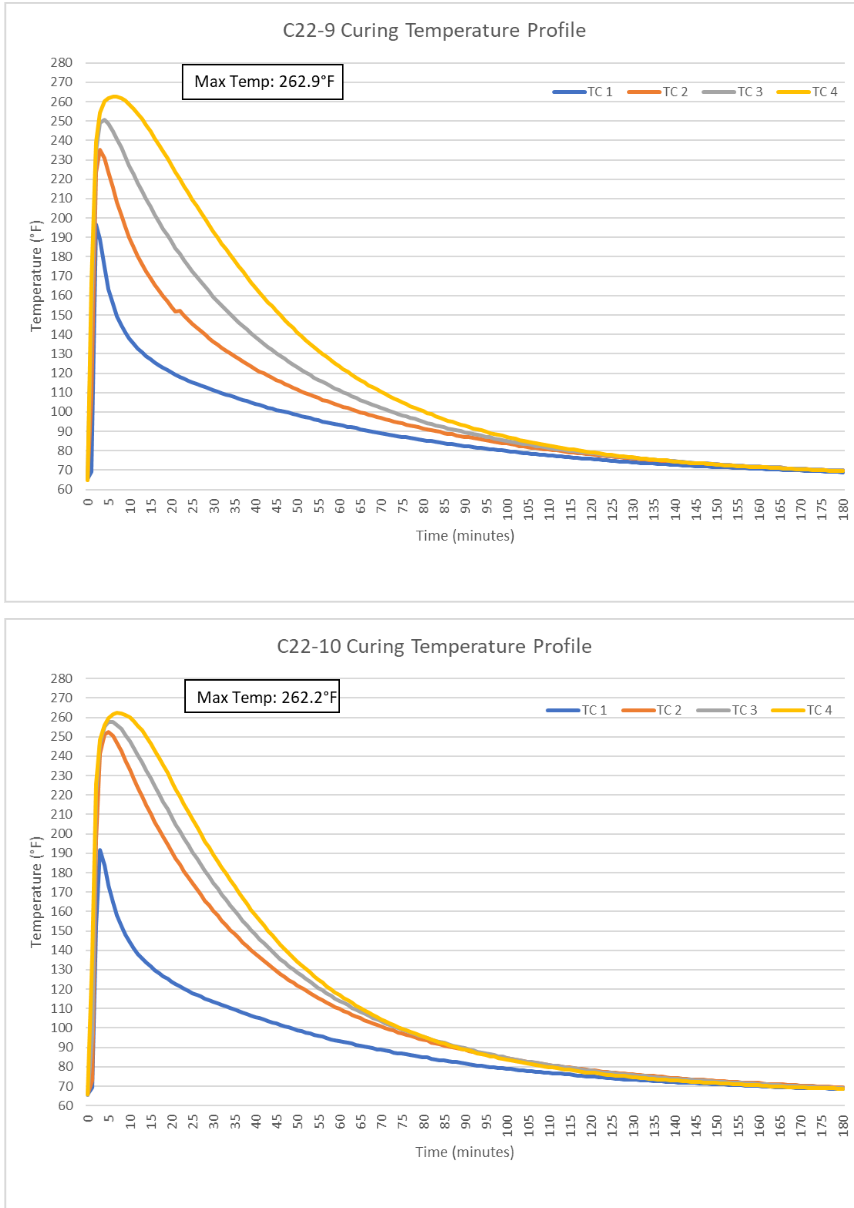

Figure 12. Hilti foam curing temperature profile graphs in Hastelloy C-22 pipes.

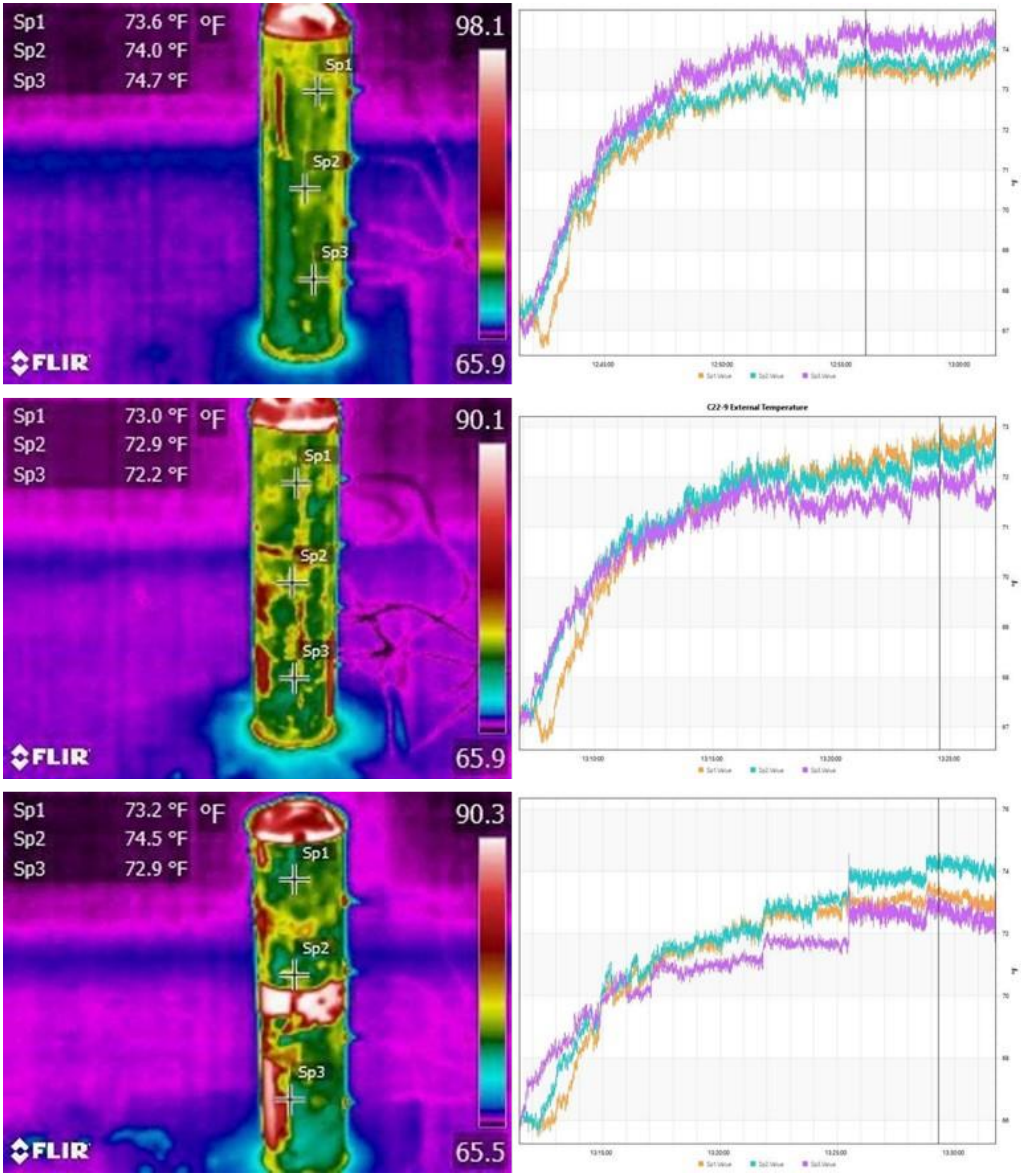

Figure 13. External temperature profiles for C22-1 (top), C22-9 (middle), and C22-10 (bottom) Hilti samples.

Determine the internal pipe pressure after foam deployment and curing time

FIU machined a five-foot long Hastelloy pipe to be able to attach a pressure gauge for completion of this objective. As seen in Figure 14, the machining was successful, and the pressure gauge was able to be attached. An initial test was conducted, and the maximum pressure observed during this experiment was 1 psi (0.07 atm). However, additional tests and/or reconfiguration of the experimental design is needed to further confirm these results.

Figure 14. Hastelloy pipe after drilling and tapping hole for pressure gauge (left) and with pressure gauge successfully attached (right).

Conduct a literature review to determine if using a hot tap is a viable method to deliver foam into piping

FIU initiated a literature review of foam technologies that would be viable for delivery through a hot tap. The technology for mitigating release during pipe dismantling has shifted to the FOAMBAG™ technology and initial purchase orders have been submitted. FOAMBAG™ is an expanding polyurethane resin foam that is injected into the semiporous bag via an injection tube which passes up through the standpipe assembly. The bag holds the foam in place as it expands and at full expansion, some of the foam seeps through the semi-porous material to adhere to the pipe wall, as shown in Figure 15. This technology is more compatible with hot tapping procedures, has been used in the UK at Sellafield, and it meets the UK gas industry technical standard T/SP/E/59.

Figure 15. Depiction of FOAMBAG™ technology, which holds the resin foam in place as it expands. At full expansion, some of the foam seeps through the semi-porous panels of the bag to form an adhesive seal with the pipe.

Subtask 2.2: Conclusions

FIU in collaboration with SRNL and the F/H Lab Deactivation Site Team have begun discussions on a Phase II Cold Demo Test Plan for this activity. Phase II testing will be performed to characterize the mechanical properties of FOAMBAG™ foam fixative when exposed to various stressors that may impact its effectiveness as a 3D fixative in Hastelloy C-22 pipes. Specifically, testing will address the following:

- Evaluation of the adhesion and bonding properties of the FOAMBAG™ foam plug to Hastelloy C-22 piping.
- Evaluation of the adhesion and bonding properties of the FOAMBAG™ foam plug to Hastelloy C-22 piping under various moisture conditions.
- Determination of the heat profile of FOAMBAG™ foam during curing in Hastelloy C-22 piping.
- Determination of the internal pipe pressure after FOAMBAG™ foam deployment and curing.
- Determination the effectiveness of FOAMBAG™ using a standard leak test
- Evaluation of off-gas formed during FOAMBAG™ curing
- Evaluation of the impacts of temperature and humidity on FOAMBAG™ stability during environmental chamber testing

Subtask 2.2: References

A. Materials, "C1892: Nominal Joint Strength of End-Plug Joints in Advanced Ceramic Tubes at Ambient and Elevated Temperatures".

ASTM International. (2016). *D1621-16 Standard Test Method for Compressive Properties of Rigid Cellular Plastics.* Retrieved from https://doi.org/10.1520/D1621-16

ASTM International. (2017). *D1623-17 Standard Test Method for Tensile and Tensile Adhesion Properties of Rigid Cellular Plastics.* Retrieved from https://doi.org/10.1520/D1623-17

ASTM International. (2018). *E3191-18 Standard Specification for Permanent Foaming Fixatives Used to Mitigate Spread of Radioactive Contamination.* Retrieved from https://doi.org/10.1520/E3191-18

Extech Instruments. (2016). *Product Datasheet SDL200.* Retrieved from Extech: http://www.extech.com/resources/SDL200_DS-en.pdf

Fabricatore, E.D., Moore, P.M., Sinicrope, J., McDonald, F.S., Walker, R., Wohlwend, J.L. Permanent Foam Fixatives for Radioactive Contamination Control: Environmental Chamber Testing (SRNL-STI-2022-00004), February 2022. https://doi.org/10.2172/1846768.

FLIR. (2019). *Electrical/Mechanical Applications FLIR EXX-Series.* Retrieved from https://www.flir.com/globalassets/imported-assets/document/17-3307-ins-e53-_-exx-series-datasheet-mfg-web.pdf

Hilti. (2015). *Hilti CP 620 Instruction for use.* Retrieved from Hilti: https://www.hilti.com/medias/sys_master/documents/h4a/9158089048094/Instruction-for-use-INT-CP-620-Instruction-for-use-PUB-5188045-000.pdf

Hilti. (2016). *Hilti Firestop Foam solid CFS-F SOL; CP 620 Safety information for 2-Component-Products.* Retrieved from Hilti: https://www.hilti.com/medias/sys_master/documents/hfc/9178915405854/Documentation-ASSET-DOC-APPROVAL-0564.pdf

Lagos, L., Sinicrope, J., Shoffner, P., Komninakis, M., Simoes-Ponce, T., Nuñez, J., & Rendon, J. (2019). *Testing and Evaluating Intumescent Foams in Operational Scenarios - Test Plan.* Miami: Applied Research Center - Florida International University.

Lagos, L., Sinicrope, J., Shoffner, P., Viera, J., Simoes-Ponce, T., & Nuñez, J. (2018). *Testing and Evaluating Radiological Shielding Foams Resistance to Thermal Stressors - Test Plan.* Miami: Applied Research Center - Florida International University.

Klempner, D., & Sendijarevic, V. "Polymeric foams and foam technology," Hanser, 2004.

MTS Criterion® Series 40. (2014). Retrieved from Product Information: https://engineering.jhu.edu/labs/wp-content/uploads/sites/76/2016/04/MTS-Criterion-40-Product-User-Manual.pdf

Mahmood, N. "Investigations on the adhesion and interfacial properties of polyurethane foam/thermoplastic materials," 2007. [Online]. Available: https://www.academia.edu/6047100/Investigations_on_the_adhesion_and_interfacial_properties_of_polyurethane_foam_thermoplastic_materials.

Marinzuli, G., Surace, R., & Ludovico, A. "A preliminary study on adhesion on steel cylinder filled with aluminum foam," 213.

Nicholson, D., Peters, B., Washington, D., & Wilson, J. (2016). *Fabrication and Evaluation of Radiation Hardened Polyurethane Foams for D&D Activities (SRNL-L3100-2016-00231).* Savannah River National Laboratory.

Subtask 2.3: Certifying Fixative Technology Performance when Exposed to Impact Stressors as Postulated in Contingency Scenarios Highlighted in Safety Basis Documents

Subtask 2.3: Introduction

In considering the vast number of facilities still awaiting final disposition within DOE, fixative platforms are being evaluated for use as a safety measure for mitigating the release of residual hold up material that could subsequently be released to the public or environment during interim operations. These fixative technologies could provide the means necessary to extend the lifetime of an interim operations facility and significantly reduce the risk of radiological release during the path to final disposition. Safety basis calculations support the safety considerations necessary for legacy nuclear facilities as they transition from active use, through limited operations and standby modes, until final disposition is achieved. Many of the calculations involve estimating doses to a co-located worker at 100 meters from the source term and at the site boundary. These dose values are governed in part by the values presented in DOE-HDBK-3010 in the form of airborne release of radioactive material resulting from penetration of the facility per seismic activity, full facility fires, and/or explosions.

The current version of the DOE-HDBK-3010 does not consider the positive impacts these fixative technologies may have on immobilizing residual contamination once encapsulated in a solid polymer material. This solid-state polymer form significantly mitigates the potential of release under normal operating conditions, during demolition activities, and contingency-based scenarios postulated in BIOs across the DOE complex. This change of state significantly reduces the Airborne Release Fraction/Respirable Fraction (ARF/RF) values, leading to a more accurate reduced material at risk (MAR) through this mitigating method. Reduced analysis conservatism based on quantified attributes will result in better safety calculations given to the MAR across all applicable facilities, resulting in cost reductions based on less material deemed as "loose powder" per the DOE-HDBK-3010, transitioning to lower ARF/RF values. Reduction in MAR will lead to less safety controls necessary for the building during its time on the final disposition path, reducing the cost to maintain the facility. It will also facilitate quantification of fixative technologies designed to mitigate contingency scenarios outlined in complex-wide BIOs and lay the groundwork for uniform international standards and testing protocols through ASTM.

Under this subtask, FIU evaluated fixative performance when exposed to impact stressors associated with safety basis analysis in response to high priority requirements identified across the DOE complex. This research effort has the added benefit of potentially providing essential data points on the positive effects of fixative technologies on mitigating airborne release fractions, respirable fractions, and resuspension rates used in safety basis calculations and the Source Term Formula outlined in DOE-HDBK-3010.

Subtask 2.3: Objectives

1. **Develop and validate experimental design for the quantification of contamination release during impact stress.**
   This objective focuses on the experimental methodology for impact stress and includes four main aspects: surrogate contaminant, impact test chamber, collection of released particulates, and analysis.
2. **Reevaluate ARF coefficients for powder contaminants under impact stress.**
   This approach will either confirm or dispute the original ARFs for powder contamination as determined in the DOE-HDBK-3010. Since there have been new technological advances in analytical techniques, it is possible that the coefficients in the present version of the handbook are outdated and do not accurately reflect the airborne release.
3. **Determine ARF coefficients for fixative materials under impact stress.**
   This objective focuses on investigating the ARFs for fixatives applied over powder contamination under impact. Initially, two polymer fixatives will be used as a starting point to provide data to substantiate the Fixative State for this stressor. Based on previous research conducted, the use of fixatives will produce much lower ARFs.

Subtask 2.3: Methodology

Throughout numerous DOE nuclear facilities, there are many different types of substrates to which the fixatives may be applied. However, these initial experiments only consider non-porous substrates (stainless steel coupons). All testing is performed on: (1) coupons without a fixative as a baseline and to confirm the original data for ARFs for powder contaminants under impact, and (2) two fixatives (FD and PBS) as a starting point to provide data to substantiate the fixative/polymer state under impact. There are four main aspects to this experimental methodology: surrogate contaminant, impact test chamber, collection of released particulates, and analysis.

Surrogate Contaminant and Controlled Contamination of Test Coupons

Cesium chloride (CsCl) is the surrogate contaminant used as it is a non-radioactive soluble powder and contains a unique chemical element that will be detectable in the analysis component. It is essential that the coupons are weighed before and after contaminant application in order to quantify the initial amount of contamination prior to any stressor for proper release measurements. Another main aspect is to be able to uniformly contaminate the test coupons for all experiments. Previous work and existing standards, such as ASTM E3283-21 “Standard Practice for Preparation of Loose Radiological/Surrogate Contamination on Nonporous Test Coupon Surfaces for Evaluation of Decontamination Techniques”, are being leveraged for this design.

A small known quantity of CsCl was used to create a solution in deionized (DI) water. The contaminant solution was mixed homogenously and then applied to 304-stainless steel coupons at different points. 10 µL drops of contaminant solution were stippled in a pattern towards the center of the coupon, per ASTM E3283, which created a uniform distribution and reduced the risk of run-off at the edge of the coupon. The coupons were undisturbed while the solvent was allowed to evaporate. After evaporation, the coupons were weighed to initially quantify the amount of contaminant present. The fixative could then be applied and cured to the manufacturer’s requirements. The coating thickness was confirmed using the Defelsko PosiTector 6000. The Defelsko PosiTest LPD pin-hole detector is used, where appropriate, to confirm that there are no small cracks/holes in the coating application before all testing.

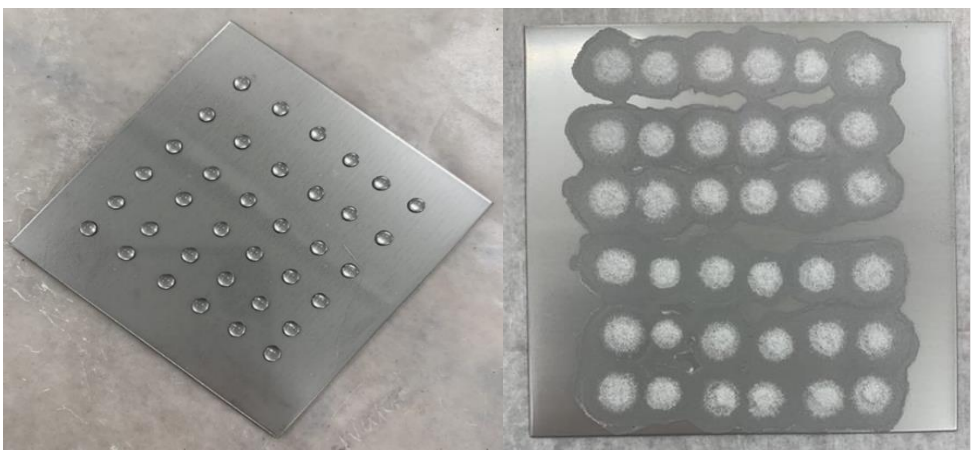

Figure 16. Stippled contaminant solution on 304-SS coupon (left) and after solvent evaporation (right).

Impact Stressor

BYK-Gardner PF-5546 Extra Heavy-Duty Impact Tester has a maximum force of 320 in-lb and is used to evaluate impact resistance and determine the exact point of failure and/or establish pass/fail specifications. It specifically complies with ASTM D2794, “Standard Test Method for Resistance of Organic Coatings to the Effects of Impact”. While this method was not originally designed to test for contamination release, it establishes a standard method to test a coating’s response to rapid deformation. The coupons are required to have the following dimensions: 3.0” length, 3.0” height; and 0.024” width. Additionally, an acrylic housing assembly was placed around the device which will allow for artificially contaminated coupons to be tested for release fractions.

Figure 17. BYK-Gardner PF-5546 Extra Heavy-Duty Impact Tester.

Contamination Release Collection

In order to quantify a total release, effective collection methods must be used to ensure accuracy of the data. Collection of released contamination includes airborne and any particulates that may have resettled on the stressor apparatus or test chamber surfaces. Mixed cellulose ester (MCE) filter cassettes and an air-sampling pump were used to collect any suspended airborne particulates. Any contamination that has settled on the walls of the test chamber or stress apparatus can be collected using sampling wipes. Then the filters and wipes are dissolved in an acidic medium for the analysis process.

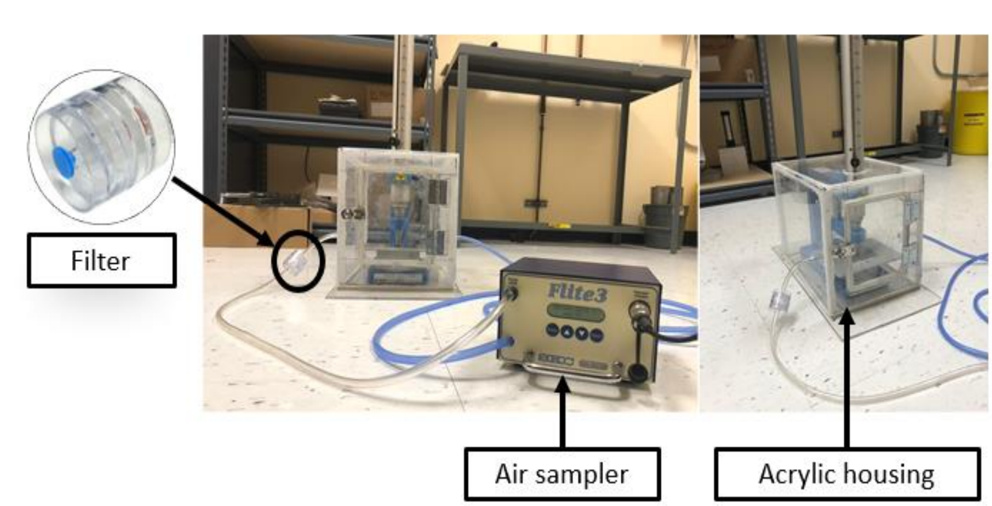

Figure 18. Impact tester with acrylic impact housing and Flite 3 901-3011 air sampler setup.

Analysis

After collection of the released contaminant, it can be analyzed using mass spectrometry. The surrogate contamination has a unique signature that can be detected using ICP-MS. Mass spectroscopy detects charged particle impacts following a deflection by a magnetic field that separates ions by mass/charge ratios. Carefully tracked dilutions or dissolutions are required to correctly determine the amount of collected contaminant. These analysis methods will detect only the specified element in the surrogate (Cesium), which is imperative in certifying and quantifying fixative performance.

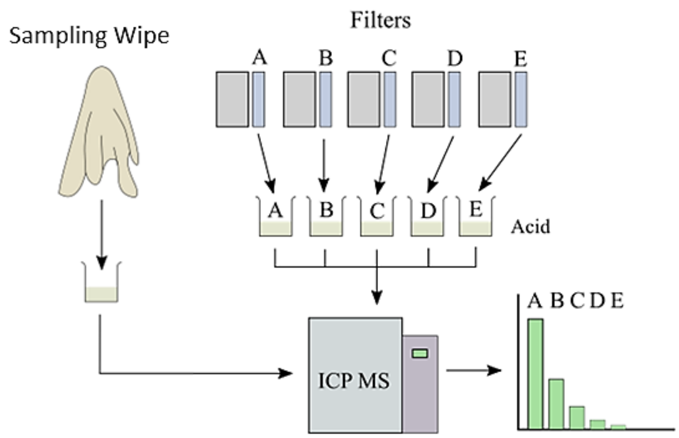

Figure 19. Collection and analysis process.

Subtask 2.3: Results and Discussion

FIU performed ICP-MS analysis on additional baseline powder samples on lower impact forces. The complete results are shown in Table 6and this average airborne release fraction of 3.47e-4, is very similar to the ARF value presented in the DOE-HDBK-3010, 3e-4.

Table 6. ICP-MS Analysis and the Associated Airborne Release Fractions for Baseline Powder Contamination under Impact Stress

	Impact (in-lb) / (kg-cm)	Average Airborne Release Fraction
Powder	320 / 368	2.27E-04
	240 / 276	1.08E-04
	200 / 230	1.05E-05
	160 / 184	6.32E-07
Total Average		3.47E-04

In addition, testing proceeded on contaminated coupons with fixatives to determine its impact on ARFs, as shown in Figure 20. The impact forces used are at varying intervals from 160 in-lb to 320 in-lb (maximum).

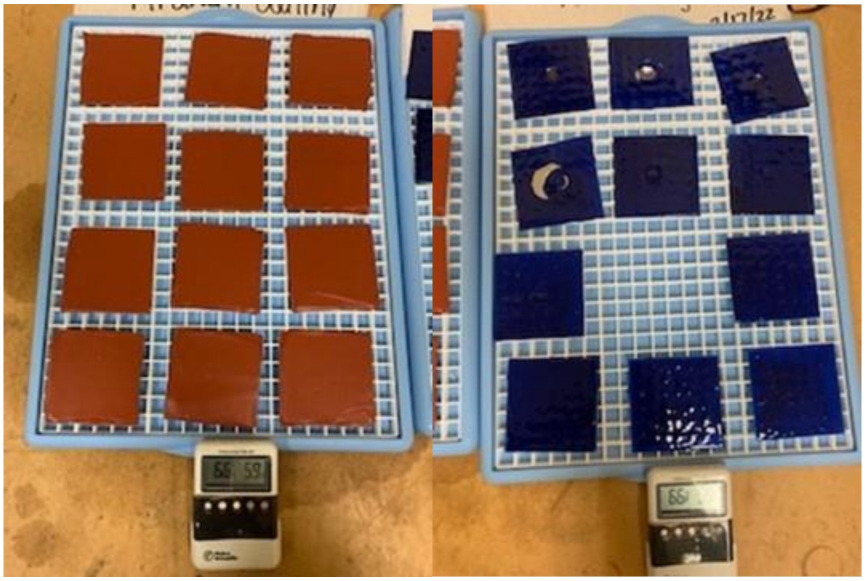

Figure 20. Contaminated coupon samples with FD coating (left) and PBS coating (right) prepared for impact testing.

ICP-MS testing was completed on impact samples for FD coating. The results, displayed in Table 7, show a significant reduction in the ARFs for powder contaminants. This data provides evidence that supports that there is a different ARF coefficient that should be implemented for fixatives in the DOE-HDBK-3010.

Table 7. Average Airborne Release Fractions for FD Coating under Impact Stress

	Impact Force (in-lb) / (kg-cm)	**Average Airborne Release Fraction**
FD	320 / 368	5.55E-07
	240 / 276	6.78E-07
	200 / 230	8.34E-07
	160 / 184	3.33E-08
Total Average		**5.25E-07**

Similarly, FIU performed ICP-MS testing on the additional BPBS-coated samples. The results are shown in Table 8. The average airborne release fraction (ARF) for BBPS was similar to the results from the FD-coated samples, 4.96e-7 and 5.25e-7 respectively. Overall, this lower ARF for fixative coatings further confirms the idea of a “fixative/polymer state”, which should be included in the DOE-HDBK-3010 so that this reduction can be credited in safety basis calculations.

Table 8. Average Airborne Release Fractions for BPBS Coating under Impact Stress

	Impact Force (in-lb) / (kg-cm)	Average Airborne Release Fraction
BPBS	320 / 368	5.55E-07
	240 / 276	6.78E-07
	200 / 230	8.34E-07
	160 / 184	3.33E-08
Total Average		**5.25E-07**

Subtask 2.3: Conclusions

The data collected during this performance year supports the original ARF for powder contaminants in the DOE-HDBK-3010 and the idea of a fixative/polymer state. These initial results for fixatives support an ARF that is less than that of a liquid contaminant, as shown in Figure 21.

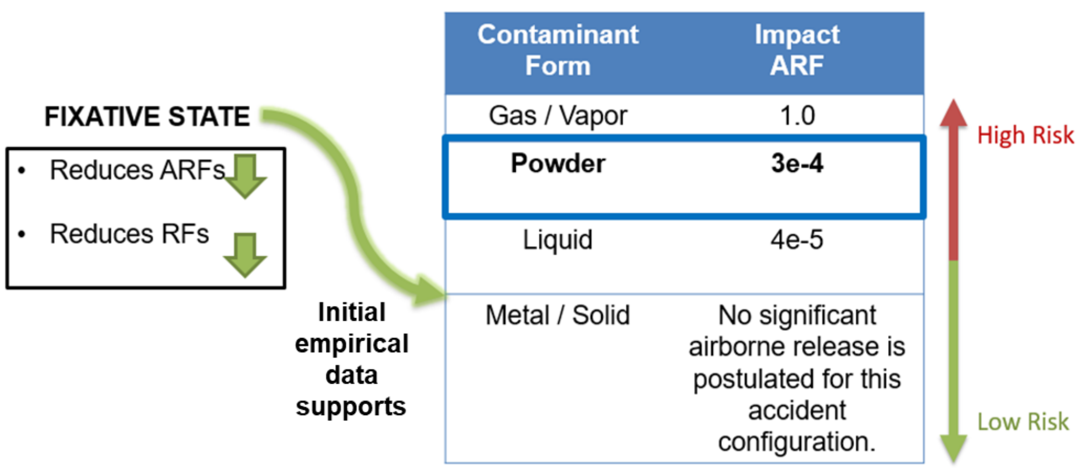

Figure 21. DOE-HDBK-3010 ARF coefficients for various contaminant forms under impact stress. Initial data indicates a fixative state with an ARF less than a liquid contaminant.

FIU will continue collaboration with SRNL and other sites to leverage ASTM practices and principles to further define operational parameters. FIU will proceed with any additional testing required to quantify release and the performance of fixative technologies to support and update the DOE-HDBK-3010. Various substrate types and/or thicknesses will be considered for future testing.

Subtask 2.3: References

U.S. Department of Energy, "Airborne Release Fractions/Rates and Respirable Fractions for Nonreactor Nuclear Facilities (DOE-HDBK-3010-94)," December 1994. [Online]. Available: https://www.nrc.gov/docs/ML1307/ML13078A031.pdf.

ASTM International, "E3283-21 Standard Practice for Preparation of Loose Radiological/Surrogate Contamination on Nonporous Test Coupon Surfaces for Evaluation of Decontamination Techniques," 2021. Available: https://doi.org/10.1520/E3283-21.

SKC Inc., "Flite 3 High Flow Air Sampler Product Data Sheet," [Online]. Available: https://www.skcinc.com/catalog/pdf/instructions/1806.pdf.

ASTM International, "D522/D522M-17 Standard Test Methods for Mandrel Bend Test of Attached Organic Coatings," 2017. Available: https://doi.org/10.1520/D0522_D0522M-17.

ASTM International, "D2794-93(2019) Standard Test Method for Resistance of Organic Coatings to the Effects of Rapid Deformation (Impact)," 2019. Available: https://doi.org/10.1520/D2794-93R19.

3M, "3M Fire Protection Products 3M™ FireDam™ Spray 200". Available: https://multimedia.3m.com/mws/media/373702O/3m-firedam-spray-200-flyer.pdf.

3M, "3M™ FireDam™ Spray 200 Product Data Sheet". Available: https://multimedia.3m.com/mws/media/373703O/3m-firedam-spray-200-flyer-technical-data-sheet.pdf.

BHI Energy, "Specialty Coatings". Available: https://www.bhienergy.com/services/power-services/technologies/specialty-coatings/.

Bartlett Nuclear, Inc. , "Product Data Sheet Polymeric Barrier System (PBS)". Available: https://www.dndkm.org/DOEKMDocuments/GetMedia/Technology/1620-PBS%20Data%20Sheet.pdf.

BHI Energy, "Material Safety Data Sheet Polymeric Barrier System (PBS)". Available: http://www.bhienergy.com/assets/PBS-MSDS-2015Revised-3-15.pdf.

3M, "Safety Data Sheet 3M FireDam Spray 200 - Red," 13 April 2020. Available: https://multimedia.3m.com/mws/mediawebserver?mwsId=SSSSSuUn_zu8l00xM82vn8tUOv70k17zHvu9lxtD7SSSSSS--.

R. Demmer, D. Fox, S. Reese, A. Banford and J. Dodds, "Fixatives Used for Decommissioning and Maintenance of Radiological Facilities – 17537," in *Waste Management Symposia*, Phoenix, AZ, 2017.

J. Hubbard, T. Boyle, E. Zepper, A. Brown and T. Settecerri, "Airborne Release Fractions from Surrogate Nuclear Waste Fires Containing Lanthanide Nitrates and Depleted Uranium Nitrate in 30% Tributyl Phosphate in Kerosene," *Nuclear Technology,* vol. 207, no. 1, pp. 103-118, 2020.

ASTM International, "D7091-13 Standard Practice for Nondestructive Measurement of Dry Film Thickness of Nonmagnetic Coatings Applied to Ferrous Metals and

Nonmagnetic, Nonconductive Coatings Applied to Non-Ferrous Metals," 2013. Available: https://doi.org/10.1520/D7091-13.

ASTM International, "E3190-19 Standard Practice for Preparation of Fixed Radiological/Surrogate Contamination on Porous Test Coupon Surfaces for Evaluation of Decontamination Techniques," 2019. Available: https://doi.org/10.1520/E3190-19.

Sinicrope, J., Komninakis, M., Gabaldon, D., Moore, P., Lagos, L., Nicholson, J.C., Wohlwend, J.L. Certifying Fixatives - Impact Technical Progress Report (FIU-ARC-2020-800013919-04c-006), September 2021.

Subtask 2.4: Multi-functional 3D Polymer Framework for Mercury Abatement

Subtask 2.4: Introduction

The development of innovative, new generation mercury abatement technologies containing high fixative efficiency, low environmental toxicity, high selectivity, low cost, and high recyclability is of great interest to DOE-EM. During Year 1, FIU investigated the feasibility of using a 3D polymeric filtration/absorption matrix containing self-assembled and functionalized polymer micro-ribbons (MRs) for Hg(II) abatement in aqueous systems. FIU developed methods for functionalization of PDMS-MR surfaces for mercury abatement. FIU selected (3-Mercaptopropyl)-trimethoxysilane (MPTMS) as the sulfur source and performed a self-assembled monolayer (SAM) silanization to functionalize PDMS-MR surfaces. FIU also investigated the effects of solvent, MPTMS concentration, reaction temperature, reaction time, and cleaning procedure on PDMS-MR surface silanization quality. The PDMS-MR surfaces were successfully functionalized using this optimized method.

Under this subtask, FIU will explore the feasibility of using a 3D polymeric filtration/absorption matrix containing self-assembled and functionalized polymer MRs for Hg(II) abatement in aqueous systems. The benefits of this strategy include:

- The self-supported 3D polymeric matrix does not require additional supporting foundation during Hg filtration.
- The backbones of the polymer MRs are composed of siloxanes, which are environmentally friendly and non-hazardous to human beings.
- The surfaces of the polymer MRs are rich in silanol groups which enable versatile functionalization at their surfaces for selective heavy metal removal.
- The 3D polymeric matrix forms a self-assembled network which can be easily recycled and regenerated.

For FIU Performance Year 2, FIU focused on the investigation of mercury abatement performance of functionalized PDMS-MRs under different environmental conditions. Specifically, FIU studied the effects of temperature, pH, ionic strength, organic compound composition in water, and repeated use of PDMS-MRs on mercury abatement performance including the abatement efficiency, binding strength, and abatement selectivity of functionalized PMDS-MRs. Moreover, a method was developed to enable magnetic field responsibility of PDMS-MRs by embedding magnetic nanoparticles in the PDMS-MRs or at the PDMS-MRs surfaces. The effect of environmental conditions on the magnetic field responsibility of PDMS-MRs was also investigated. Finally, FIU explored the possibility of using surface functionalized magnetic PDMS-MRs for mercury abatement and collection.

Subtask 2.4: Objectives

1. Investigate the effects of environmental conditions on mercury abatement ability (mercury abatement efficiency, binding strength, and selectivity) of PDMS-MRs.
    a. Effect of temperature change
    b. Effect of pH change
    c. Effect of ionic strength change
    d. Effect of the change of organic compound composition and content
    e. Effect of other heavy metal contaminants
    f. Regeneration of PDMS-MRs after oil/water separation
2. Magnetic PDMS-MR synthesis and characterization of the effect of environmental conditions on the magnetic field responsibility of PDMS-MRs.
    a. Synthesis of magnetic field responsive PDMS-MRs
    b. Effect of temperature change
    c. Effect of pH change
    d. Effect of ionic strength change
    e. Regeneration of PDMS-MRs after oil/water separation
3. Lab-scale demonstration of using surface functionalized magnetic PDMS-MRs for mercury abatement, collection, and regeneration.
4. Test the ability of PDMS-MRs in removing organic mercury.

Subtask 2.4: Methodology

PDMS-MR Fabrication

In a typical fabrication route, the PDMS-MRs were synthesized by spin-coating a mixture composed of PDMS Part A and B with a ratio of 10:1 on a clean glass slide followed by curing at 100 °C for 15 min. The glass slide with cured PDMS film was heated above 400ºC in the furnace for a few minutes followed by natural cooling in the air. The synthesis procedure was varied to find the optimal conditions for PDMS-MR formation.

PDMS-MR Surface Functionalization

The PDMS-MRs were post-heated at 330 ºC for ~ 3 h followed by filtration using ethanol through a stainless-steel mesh with 50 µm pores twice. The filtered and cleaned PDMS-MRs were added into 0.05 M MPTMS ethanol solution. For 0.5g PDMS-MRs, about 20 mL solution was needed. The solution containing PDMS-MRs was placed for 30 min on a stirrer. For the 20 mL solution, ~ 1-2 drops of acetic acid was added while stirring. The solution was stirred for another 30 min followed by rinsing of the PDMS-MRs using copious amounts of ethanol to remove the excess

MPTMS at the PDMS-MR surfaces. The rinsed PDMS-MRs were placed in a glass container and heated to 80ºC to complete the polymerization of MPTMS.

Mercury-contaminated Water Sample Preparation

The inorganic mercury-contaminated water samples were prepared by diluting the original 1,000 ppm to 1 ppm stock solution using distilled water. During the test, 0.5 mL stock solution was added to 9.5 mL distilled water to make a 0.05 ppm Hg^{2+} solution.

The organic mercury-contaminated water samples were prepared by diluting the original 1M methylmercury hydroxide solution to 1 ppm stock solution. During the test, 0.5 mL stock solution was added to 9.5 mL distilled water to make a 0.05 ppm Hg^{2+} solution.

Mercury Abatement Test

For inorganic mercury abatement and organic mercury abatement tests, 10 µm of PDMS-MRs was added to each 10 mL inorganic or organic mercury-contaminated water sample respectively. The mixture was sealed and then shaken on an orbital shaker for different durations. About 1 mL of cleaning solution was transferred to a new vial for further tests from the original mixture using a syringe. Transfer of the PDMS-MRs was carefully avoided.

Subtask 2.4: Results and Discussion

PDMS-MRs Fabrication and Optimization

FIU explored the lab-scale fabrication conditions for PDMS-MR formation on glass slides. Specifically, FIU explored the effects of starting PDMS film thickness and heating temperature on PDMS-MR formation. The results are shown in Table 9.

Table 9. The heated glass slides with PDMS films after cooling. The starting film thicknesses and heating temperatures are different from sample to sample.

	4,000 RPM, 30s	4,500 RPM, 30s	5,000RPM, 30s
450°C, 4 min	 Unpatterned cracks were formed during cooling. Thick and less curled MRs were formed during cooling.	 Unpatterned cracks were formed during cooling. Thick and less curled MRs were formed during cooling.	 Patterned cracks were formed. Long and curled MRs were formed.
460°C, 4 min	 Unpatterned cracks were formed during cooling. Thick and less curled MRs were formed during cooling.	 Patterned cracks were formed. The MRs were curled but short in length.	 Patterned cracks were formed. Long and curled MRs were formed.

470°C, 4 min	 Unpatterned cracks were formed during cooling. Thick and less curled MRs were formed during cooling.	 Massive fine cracks were formed during heating. No MRs formed.	 Massive fine cracks were formed during heating. No MRs formed.

To summarize, the starting PDMS film thickness, the heating temperature, the heating duration, and the cleanliness of the glass surface all affect the formation and quality of the PDMS-MRs. A series of experiments and characterizations were performed to investigate the principle and the effects of different factors on PDMS-MR formation. A manuscript will be developed based on the findings with the aim of publishing it in a high-impact factor peer-reviewed journal next year. At this point, it has been concluded that the PDMS-MRs with the proper shape, number, and length will be formed under these conditions: spin-coating speed of 5,000 RPM for 30s, followed by 4 min heating at 450°C. Close-up views of the formed PDMS-MRs are shown in Figure 22.

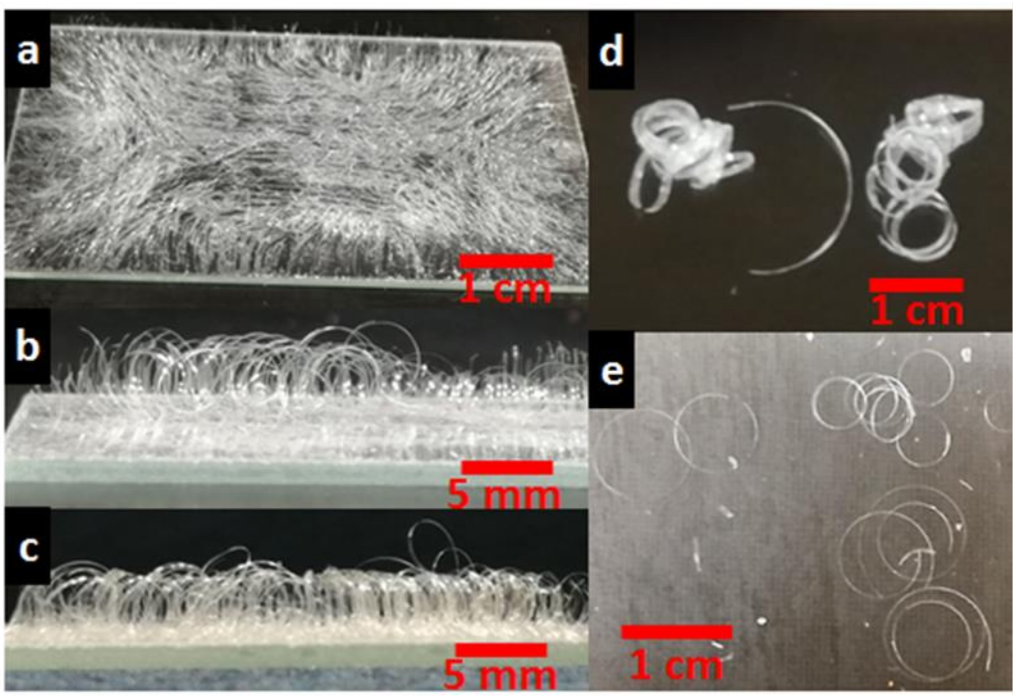

Figure 22. Close-up views of oPDMS-MRs. (a) Top view of the oPDMS-MRs formed on a glass slide. (b) and (c) Side view of the oPDMS-MRs formed on a glass slide. (d) The entangled oPDMS-MRs. (e) Spiral-shaped PDMS MRs.

Once the optimized synthesis conditions were determined, FIU massively fabricated the PDMS-MRs following the optimized fabricating conditions. During the fabrication, PDMS-MRs with larger length (> 5 mm), smaller width (< 200 µm), and highly curled shapes were guaranteed and massively produced (Figure 23a). The fabricated PDMS-MRs (Figure 23b and c) were collected for further cleaning, surface functionalization, and characterization. The PDMS-MR has a low bulk density due to its high porosity. Figure 23b shows the volume for ~0.5g PDMS-MRs in a glass vial.

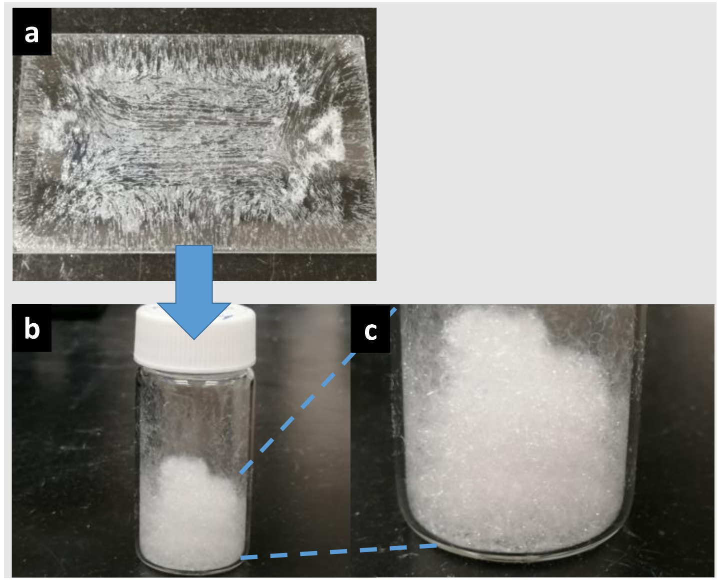

Figure 23. The PDMS-MRs were fabricated on a glass slide under optimized conditions (a) and collected in a glass vial (b). A magnified view of the collected PDMS-MRs is shown in (c).

Self-Entanglement Test of PDMS-MRs

The investigation indicated that the hydrophobic PDMS-MRs tend to self-entangle via physical entanglement to minimize the contact between their hydrophobic surfaces and the water molecules. Figure 24A shows the behavior of 0.5g PDMS-MRs in clean water. The low density of PDMS-MRs and the air portal formed in the pores of the PDMS-MRs matrix float the PDMS-MRs at the water surface. The PDMS-MRs were entangled and repelled water when being pushed into the water using a spatula. This entanglement is stable and recovers after being untangled by the external shear force, for example, water turbulence. This is an important character of PDMS-MRs which makes PDMS-MRs a superior sorbent candidate. To test the self-entanglement ability of PDMS-MRs in water, 10 mL of silicon bath oil was added to 200 mL water to make an oil-water mixture while stirring. A large number of emulsions were observed in the mixture without PDMS-MRs after 5 min (Figure 24B). However, an oil phase with a clear oil/water interface formed within a few seconds after stirring in the mixture containing 0.5g PDMS-MRs (Figure 24C). This was attributed to the selective affinity of PDMS-MRs to oil molecules due to their hydrophobic surface and the self-entangling behavior in water under shearing force.

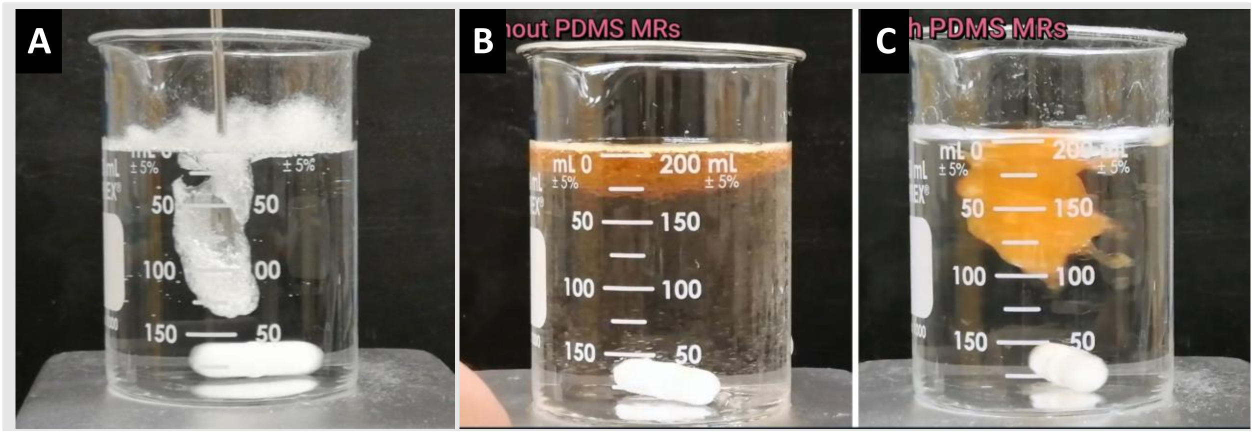

Figure 24. (A) PDMS-MRs in water. (B) Oil-water mixture after stirring without PDMS-MRs. (C) Oil-water mixture after stirring, containing 0.5g PDMS-MRs.

Surface Activation of PDMS-MRs

Thiol-functionalized micro/nano/mesostructures have been reported to have a strong affinity to mercury and are applied as mercury binding sites. FIU functionalized the PDMS-MR surface using MPTMS via self-assembled monolayer (SAM) technology to enhance its mercury adsorbing ability. However, SAMs can only be applied on hydroxyl group-enriched surfaces. To ensure a successful surface functionalization, the hydroxyl group-enriched PDMS-MRs precursor was fabricated by reheating the PDMS-MRs in the air to partially thermally oxidize their surfaces. As mentioned before, a proper hydrophobicity degree is important to the self-entanglement of PDMS-MRs in water. Therefore, the heating conditions were optimized to have a balance between the PDMS-MRs surface activity for MPTMS and the overall hydrophobicity of PDMS-MRs to maintain their self-entanglement ability. The heating conditions for different trials are shown in Table 10. It was observed that the increased heating temperature and heating time led to a higher thermal oxidation degree of PDMS-MRs, which can be reflected in the easier wetting and tendency to precipitation of PDMS-MRs in water (Figure 25). The results suggest an optimized heating condition of 350 ºC with 3h heating time to have a proper balanced thermal oxidation of PDMS-MRs which were used for MPTMS functionalization in the next step.

Table 10. Heating Conditions of PDMS-MRs Thermal Oxidation

Heating temperature (ºC)	300	300	330	330	350	350	350	350	350
Heating time (h)	24	60	2	3	3	6	24	48	60

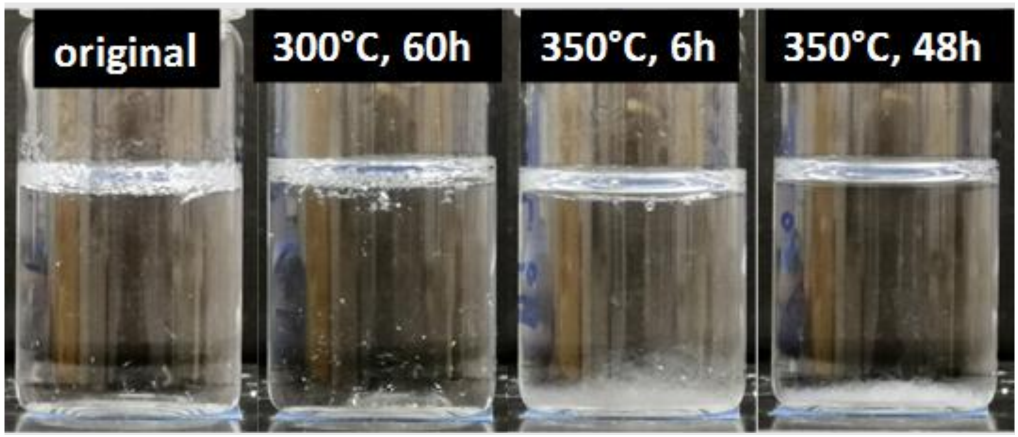

Figure 25. Partially thermal oxidized PDMS-MRs in water. The oxidation degree increases from left to right.

Mercury Abatement Test of PDMS-MRs

To have a better practical meaning, FIU evaluated the mercury removal ability of PDMS-MRs for inorganic mercury (Hg^{2+}) and organic mercury (CH_3Hg^+) respectively. The mercury-contaminated water samples were prepared by diluting the original mercury stock solutions to desired concentrations. For each 10 mL mercury-containing sample, 5 mg of PDMS-MRs was added. The mixtures were shaken for different durations before being transferred to new vials using syringes for DMA analysis. The detailed compositions are shown in Table 11.

Table 11. Mercury Abatement Samples Containing Functionalized PDMS-MRs for DMA Test

	Inorganic mercury		Organic mercury	
	0.5 ppm $Hg(NO_3)_2$	PDMS-MRs	0.5 ppm CH_3HgOH	PDMS-MRs
Background	5 mL		5 mL	
5 min	5 mL	5 mg	5 mL	5 mg
10 min	5 mL	5 mg	5 mL	5 mg
30 min	5 mL	5 mg	5 mL	5 mg
60 min	5 mL	5 mg	5 mL	5 mg

The result was shown in Figure 26. In Figure 26A, the reason that thermal oxidized PDMS-MRs have better performance and higher mercury adsorbing efficiency than unoxidized PDMS-MRs can be explained by: (1) The increased hydrophobicity of PDMS-MRs increased the contact area between PDMS-MRs and water-soluble mercury species. (2) The increased surface hydroxyl group density increased the surface activity for MPTMS functionalization. During the tests, it was found that the small pieces or residue of PDMS-MRs produced during the fabrication route may significantly decrease the mercury adsorbing efficiency. The small or residue species have similar inner structures and porosity in their matrixes but larger specific surface areas than that of bulk PDMS-MRs. Those small or residue PDMS-MRs adsorb mercury in the water and may be transferred to the vials for the DMA test through the syringe needle. This caused the irrational increased mercury concentration in the DMA test sample to be higher than that of the original sample without cleaning, which is shown in the first column group in Figure 26B. Therefore, the

PDMS-MRs were filtered twice using a stainless-steel mesh with a pore size of 50 µm to remove the small residue pieces of PDMS-MRs before adding them to the sample. The mercury removal efficiencies of PDMS-MRs with one filtration and two filtrations are shown in the second and third column groups in Figure 26B respectively. A clear increase in mercury removal efficiency was observed for the PDMS-MRs filtrated twice. The further improved removal efficiencies of inorganic mercury (~ 33.6%) and organic mercury (~53.9%) after 30 min cleaning using PDMS-MRs were achieved under optimized post-heating conditions of PDMS-MRs (the fourth column group in Figure 26B). This result suggested that excessive post-heating of PDMS-MRs results in a decreased mercury removal efficiency for inorganic and organic mercury. This was attributed to the increased pore size and consequently the decreased total surface area of nanoporous PDMS-MRs after excessive thermal oxidation. The decreased total surface area leads to the decreased capacity of PDMS-MRs for mercury adsorption and the decreased number of thiol-ended functional groups at PDMS-MR surfaces for mercury species to interact with.

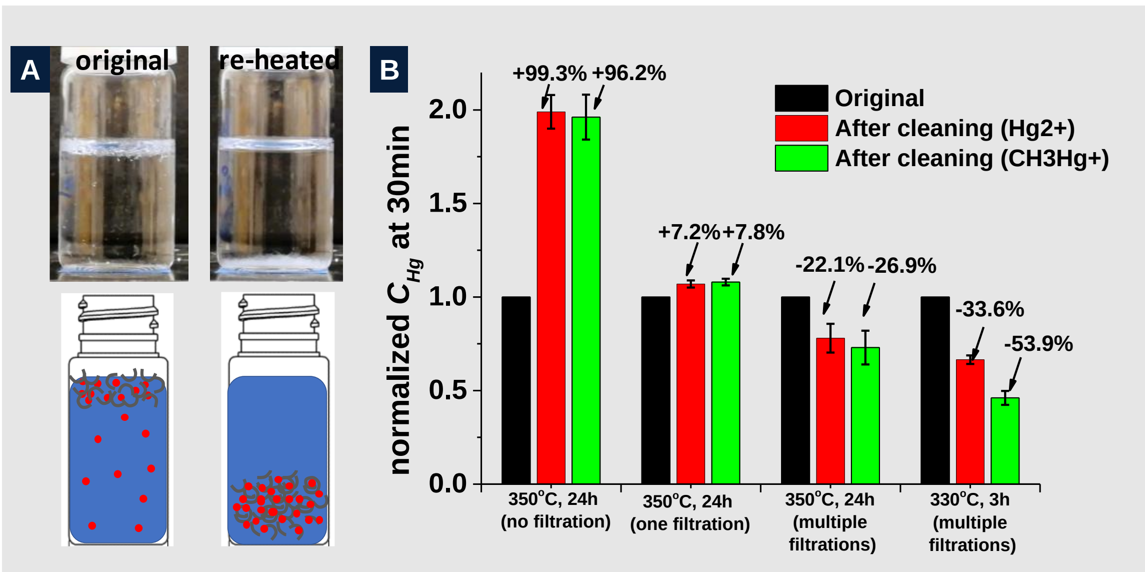

Figure 26. (A) Illustration of thermally oxidized PDMS-MRs and the interaction between the PDMS-MRs and mercury species. (B) Hg abatement performance of unfiltered, one-time filtered, and multiple-times filtered PDMS-MRs for inorganic Hg (Hg^{2+}) and MeHg (CH_3Hg^+) respectively. The result at immersing time of 30 min was selected and was normalized to the Hg concentration in the solution before abatement (0.5 ppm).

Subtask 2.4: Conclusions

FIU confirmed that PDMS-MR is a great candidate for mercury remediation in water due to its unique physical and chemical properties. The superiority of PDMS-MR in mercury cleaning finds expression in its high adsorbing efficiency, low cost, easy recycling, and environmental friendliness. The PDMS-MR surface can be turned into a silica-like surface via thermal oxidization which embodies enormous potential in different types of contaminant remediation. FIU will continue the investigations into optimizing the PDMS-MR properties, figuring out the proper working conditions of PDMS-MRs in mercury abatement, improving the performance of PDMS-MRs in mercury remediation, and organizing large-scale tests or on-spot demos of mercury remediation using PDMS-MRs to meet the requirements from different stakeholders. The primary objectives of this research include:

1. Investigation of the adsorption kinetics and capacity of PDMS-MRs for inorganic mercury, organic mercury, and mercury-natural organic matter (Hg-NOM) complexes.
2. Investigation of the effects of environmental conditions on the mercury adsorption performance of PDMS-MRs.
3. Development of magnetic responsive PDMS-MRs for easy recycling. Testing of the mercury adsorption capacity, recycling feasibility, and stability under different environmental conditions of magnetic responsive PDMS-MRs.

Development of a method for fabricating PDMS-MRs on a large scale and if possible, an industrial scale.

Subtask 2.4: References

Miranda, I. *et al*. Properties and Applications of PDMS for Biomedical Engineering: A Review. *J Funct Biomater* **13**, doi:10.3390/jfb13010002 (2021).

Yu, J.-G. *et al.* Removal of mercury by adsorption: a review. *Environmental Science and Pollution Research* **23**, 5056-5076, doi:10.1007/s11356-015-5880-x (2016).

Sams, C. Methylmercury Contamination: Impacts on Aquatic Systems and Terrestrial Species, and Insights for Abatement. (2007).

Bernhoft, R. A. Mercury Toxicity and Treatment: A Review of the Literature. *Journal of Environmental and Public Health* **2012**, 460508, doi:10.1155/2012/460508 (2012).

Zhang, D., Yin, Y. & Liu, J. Removal of Hg2+ and methylmercury in waters by functionalized multi-walled carbon nanotubes: adsorption behavior and the impacts of some environmentally relevant factors. *Chemical Speciation & Bioavailability* **29**, 161-169, doi:10.1080/09542299.2017.1378596 (2017).

Huang, Y., Gong, Y., Tang, J. & Xia, S. Effective removal of inorganic mercury and methylmercury from aqueous solution using novel thiol-functionalized graphene oxide/Fe-Mn composite. *Journal of Hazardous Materials* **366**, 130-139, doi:https://doi.org/10.1016/j.jhazmat.2018.11.074 (2019).

Hua, K. *et al.* Effective Removal of Mercury Ions in Aqueous Solutions: A Review. *Current Nanoscience* **16**, 363-375, doi:http://dx.doi.org/10.2174/1573413715666190112110659 (2020).

Liu, Z. *et al.* Mercury Removal Based on Adsorption and Oxidation by Fly Ash: A Review. *Energy & Fuels* **34**, 11840-11866, doi:10.1021/acs.energyfuels.0c02209 (2020).

Gworek, B., Bemowska-Kałabun, O., Kijeńska, M. & Wrzosek-Jakubowska, J. Mercury in Marine and Oceanic Waters—a Review. *Water, Air, & Soil Pollution* **227**, 371, doi:10.1007/s11270-016-3060-3 (2016).

Moreau, J. W. *et al.* The Effect of Natural Organic Matter on Mercury Methylation by Desulfobulbus propionicus 1pr3. *Frontiers in Microbiology* **6**, doi:10.3389/fmicb.2015.01389 (2015).

Henneberry, Y. K. *et al.* Removal of inorganic mercury and methylmercury from surface waters following coagulation of dissolved organic matter with metal-based salts. *Sci Total Environ* **409**, 631-637, doi:10.1016/j.scitotenv.2010.10.030 (2011).

Peterson, M. J. *et al.* Mercury Remediation Technology Development for Lower East Fort Poplar Creek - FY2018 Update. doi:10.2172/1490603 (2018).

Liu, H. *et al.* A nanozyme-based enhanced system for total removal of organic mercury and SERS sensing. *Journal of Hazardous Materials* **405**, 124642, doi:https://doi.org/10.1016/j.jhazmat.2020.124642 (2021).

Dong, W., Liang, L., Brooks, S., Southworth, G. & Gu, B. Roles of dissolved organic matter in the speciation of mercury and methylmercury in a contaminated ecosystem in Oak Ridge, Tennessee. *Environmental Chemistry* **7**, 94-102, doi:https://doi.org/10.1071/EN09091 (2010).

Gu, B. *et al.* Mercury reduction and complexation by natural organic matter in anoxic environments. *Proceedings of the National Academy of Sciences* **108**, 1479-1483, doi:doi:10.1073/pnas.1008747108 (2011).

Pacyna, J. M. *et al.* An Assessment of Costs and Benefits Associated with Mercury Emission Reductions from Major Anthropogenic Sources. *Journal of the Air & Waste Management Association* **60**, 302-315, doi:10.3155/1047-3289.60.3.302 (2010).

Otto, M. & Bajpai, S. Treatment technologies for mercury in soil, waste, and water. *Remediation Journal* **18**, 21-28, doi:https://doi.org/10.1002/rem.20150 (2007).

Gökaltun, A., Kang, Y. B., Yarmush, M. L., Usta, O. B. & Asatekin, A. Simple Surface Modification of Poly(dimethylsiloxane) via Surface Segregating Smart Polymers for Biomicrofluidics. *Scientific Reports* **9**, 7377, doi:10.1038/s41598-019-43625-5 (2019).

Billinge, S. J. L. *et al.* Mercury Binding Sites in Thiol-Functionalized Mesostructured Silica. *Journal of the American Chemical Society* **127**, 8492-8498, doi:10.1021/ja0506859 (2005).

Ulman, A. Formation and Structure of Self-Assembled Monolayers. *Chemical Reviews* **96**, 1533-1554, doi:10.1021/cr9502357 (1996).

Lessel, M. *et al.* Self-assembled silane monolayers: an efficient step-by-step recipe for high-quality, low energy surfaces. *Surface and Interface Analysis* **47**, 557-564, doi:https://doi.org/10.1002/sia.5729 (2015).

TASK 3: KNOWLEDGE MANAGEMENT INFORMATION TOOL (KM-IT) (HQ, SRNL, INL, ANL)

Subtask 3.4: Content Management

Subtask 3.4: Introduction

Content Management includes publishing D&D technologies and QA/QC of existing content in the system. This is accomplished with the assistance of DOE Fellows who do most of the data mining across the system. Addition of vendors, lessons learned, best practices, D&D news, and conferences are also a part of content management.

Subtask 3.4: Objectives

The objective of this effort is for FIU to continue to publish additional technologies, vendors, and lessons learned on the KM-IT platform in addition to other relevant resources for the community, such as D&D-related training, conferences and workshops to maintain fresh and informative content on the website.

Subtask 3.4: Methodology

FIU used factsheets, conference material (agenda, proceedings, brochures, etc.), vendor website, publications, DOE newsletters, and other sources to continue to publish additional technologies, vendors and lessons learned on the KM-IT platform. In addition, the team used other relevant resources for the community, such as D&D-related training, seminars and workshops to share information with the D&D community.

The team monitored the website data analytics on the D&D KM-IT website and looked for anomalies, spikes in traffic, and other information that should be addressed. By using data analytics, the developers and team members can focus on critical issues affecting the website. It can also provide great insight into features that should be enhanced and/or added to the website based on user behavior.

Subtask 3.4: Results and Discussion

FIU continues to publish additional technologies, vendors, and lessons learned on the KM-IT platform in addition to other relevant resources for the community, such as D&D-related training, conferences and workshops. There were 103 technologies published on the D&D KM-IT website. Below is the breakdown by quarter.

- First Quarter (Sep – Dec, 2021) – 23 technologies published
- Second Quarter (Jan – Mar, 2022) – 31 technologies published
- Third Quarter (Apr – Jun, 2022) – 39 technologies published
- Fourth Quarter (Jul – Sep, 2022) – 10 technologies published

In addition to technologies and vendors, training and conference opportunities related to D&D were also added to the system.

Content management has allowed the D&D KM-IT to increase its content. The graph below (Figure 27) summarizes the growth over the years. As of August 2022, the system had 1,544 D&D technologies, 1,117 registered users, 996 D&D vendors, and 108 subject matter specialists.

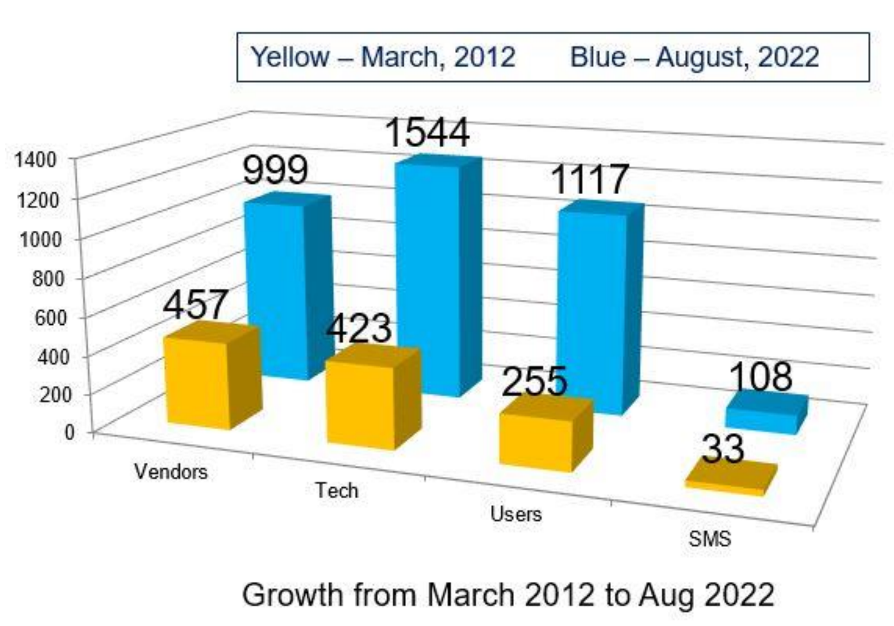

Figure 27. Number of vendors, technologies, users, and SMS as of August 2022.

As part of this task, the team also tracks web activity on the D&D KM-IT website. The following figure (Figure 28) shows the most relevant key metrics from Google Analytics (GA). During this period (Sep 2021 - Oct 2022 vs previous period), the system had a drop in traffic of about 17% shown by User, New Users, Session and Pages per Session. This also affected the Pageview and Avg Session Duration.

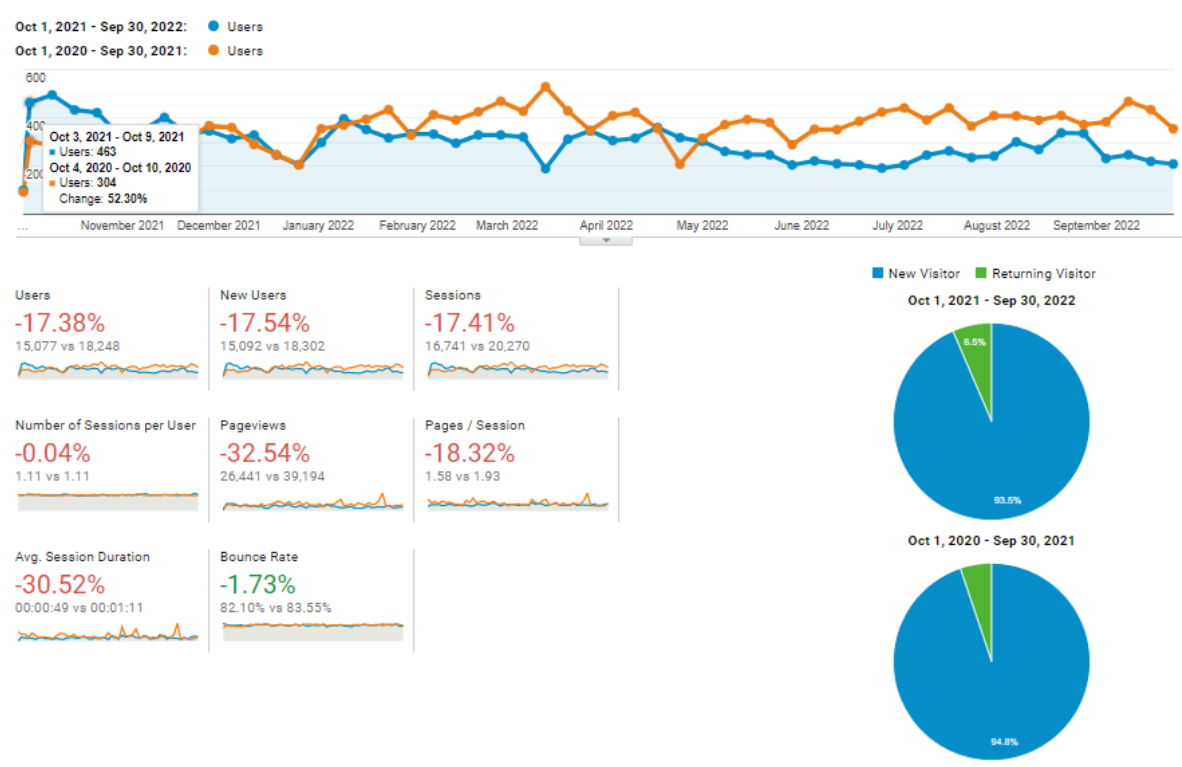

Figure 28. Google Analytics activity 2021 vs. 2022.

The GA data analytics captures some interesting information, such as the location of a user visiting the website. The map below (Figure 29) shows the changes in the amount of activity by state. Notice the shading of each of the states. The darker color shows more activity, so from this image one can conclude that the top five states that visited the website were Illinois, Virginia, California, Texas and New York.

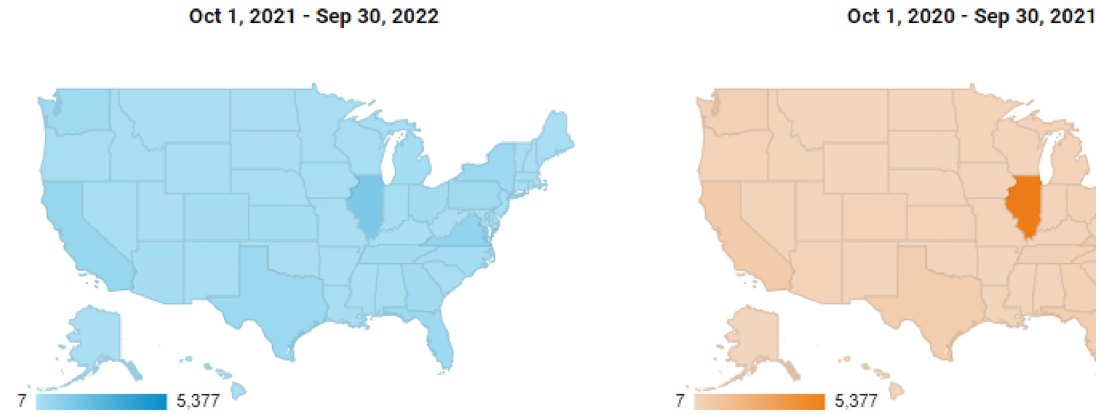

Figure 29. D&D KM-IT activity by state (2020 vs. 2021).

Other information captured by GA is the type of devices used by the visitors, operating system, mobile devices, and even browsers. Below are some comparisons of each of these metrics to the previous period (Figure 30). Notice on the top left image (Pageviews by Device Category) that there was a significant increase of about 11% on mobile device usage compared to the previous period. This fact is more evident when we see the Pageviews by Operating System (top right image), where the iOS and Android operating system (mobile operating system) increased by 4% and 6% respectively. More information about the mobile devices used to visit the system can be found on the lower left image (Pageviews by Mobile Device Info) where we see that the iPhone is the most used mobile device. Finally, we can also see which desktop browsers were used to access the D&D KM-IT on the lower right image (Pageviews by Browser) where Chrome is the top browser used.

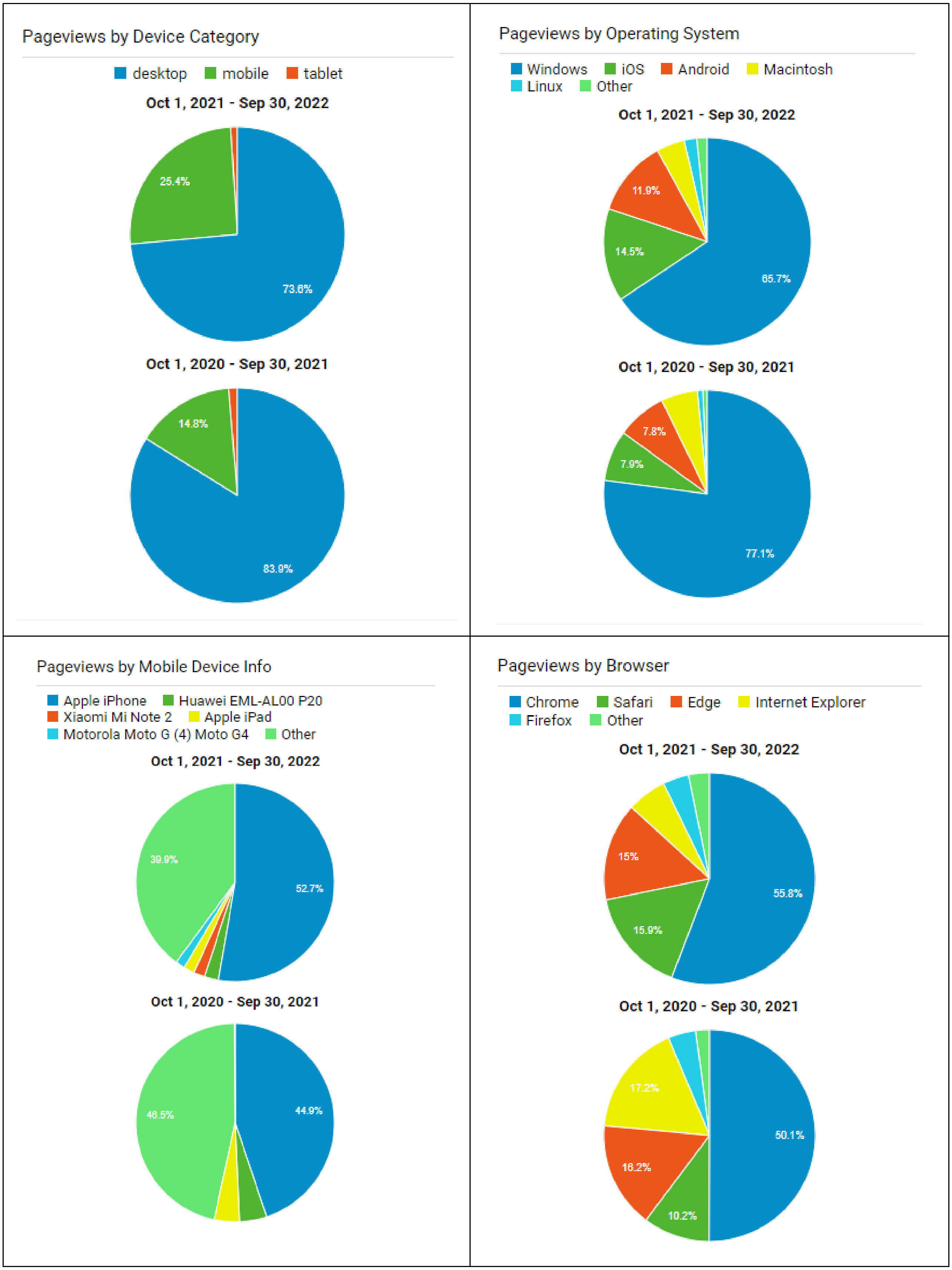

Figure 30. Google Analytics metrics for D&D KM-IT.

Subtask 3.4: Conclusions

FIU achieved the abovementioned objectives by publishing 103 technologies on the D&D KM-IT website over the past year. In addition, website data analytics captured key metrics that helped the FIU developer focus on specific issues on the website. The content management efforts continue to keep the website current and informative for the D&D community.

Subtask 3.4: References

Waste Information Management System (WIMS), https://emwims.org/, Applied Research Center, Florida International University.

Google Analytics, https://analytics.google.com, Google Analytics, Google Inc.

Google Search Console, https://search.google.com/search-console/, Google Search Console, Google Inc.

Subtask 3.5: Marketing and Outreach

Subtask 3.5: Introduction

This task involves reaching out to sites/national labs to increase KM-IT user involvement as well as presentations at conferences and collaboration with other organization involved in D&D. In addition, the team focused on increasing engagement from DOE sites and national labs on D&D KM-IT by a series of methods such as TechTalks, public and internal newsletters.

Some specific activities for outreach and marketing of KM-IT included the following:

Newsletters and Mass Communications**:** Newsletters and online promotions are a great way to bring waves of traffic to the website. By using the registered users as recipients, users were kept up to date on new features and content on the D&D KM-IT.

Conferences and Workshops**:** Participation and presentations of KM-IT at industry conferences boosts awareness of the website and its capabilities to the target users. FIU presented KM-IT at conferences, such as the Waste Management Symposia, through a combination of oral and poster presentations as well as individual and small-group demonstrations and workshops hosted in the exhibition hall. At these events, the site features can be explained in detail and participants can share their feedback and ideas.

User Support and Ad Hoc Specialized Reports: This task includes supporting KM-IT users with a help desk role to resolve issues on a day-to-day basis, as well as developing specialized reports using the KM-IT system for unforeseen data requests from DOE or the EM community of practice.

Subtask 3.5: Objectives

The objective of this task is to reach the D&D community and educate them on the features available on the D&D KM-IT system. There are many industry leaders who work at various DOE sites and national labs that can benefit greatly from the capabilities that the system has to offer. In many cases, these individuals are not aware of the system, so by doing outreach and marketing, the system usage can be promoted while helping the D&D community meet their knowledge management needs.

Marketing and outreach are critical for the self-sustainability of the system as it introduces the system to subject matter experts who may not be aware of its features and capabilities. This task increased the footprint of the D&D KM-IT in the community by allowing users to discover the capabilities of the D&D KM-IT.

Subtask 3.5: Methodology

This task is an ongoing process that is executed over the course of the year. When new features or content is added to the system, DOE is notified and others in the industry are reached via email to get feedback and comments. This is done not only to communicate with DOE regarding accomplishments and milestones, but also to involve other leaders in the industry in the process of spreading the word about D&D KM-IT. When sending newsletters, FIU uses the D&D KM-IT as its recipients. Currently, there are 1,117 registered users in the system. FIU has also used the public distribution list provided by the Waste Management Symposia (WMS) to make announcements about the D&D KM-IT training workshop typically held at the FIU booth during WMS.

FIU uses a third-party application/service called Mailchimp to send newsletters to a large distribution list. This service supports email stats like opened emails and read emails, and it also tracks clicks. However, for official announcement of milestones and deliverables, FIU uses a typical email system to notify its stakeholders. During the course of this year, several emails were sent to DOE notifying them about new features, such as the development of a sub-module on the KM-IT platform to highlight current EM research efforts and activities in support of D&D.

Subtask 3.5: Results and Discussion

FIU presented a poster at the 2022 Waste Management Symposia virtual conference capturing the research and efforts on D&D KM-IT during 2021. The poster was titled "*D&D KM-IT 2022 Updates*". The following, Figure 31, shows the poster prepared and presented at the virtual conference in March 2022.

Figure 31. D&D Research on KM-IT platform poster presented at WM2020.

The picture below (Figure 32) shows members of the FIU team with Jean P. Pabón from DOE-EM HQ in front of the D&D KM-IT poster at WM2022.

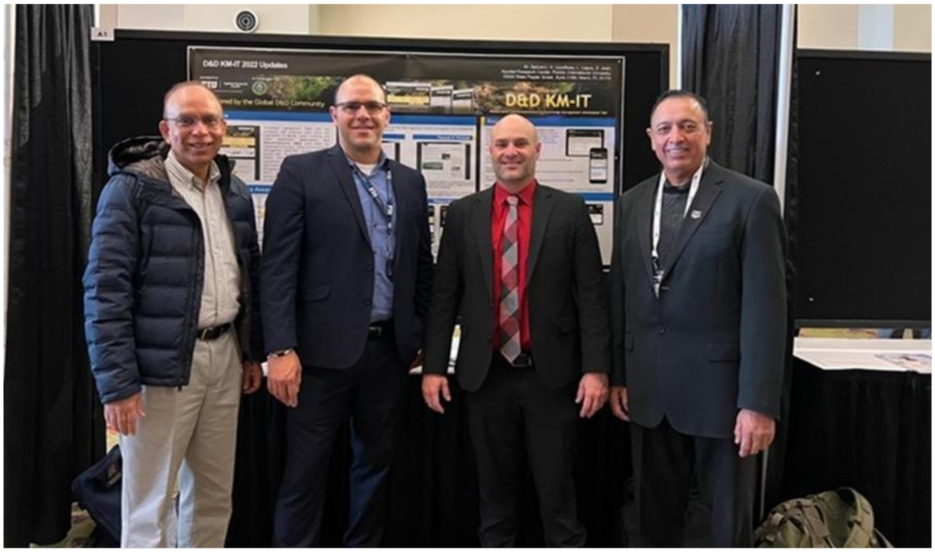

Figure 32. FIU Team with DOE HQ official (Front left to right: Himanshu Upadhyay (FIU), Walter Quintero (FIU), Jean Pabon (DOE EM), Leonel Lagos (FIU).

This subtask also included developing newsletters for mass communication via email to keep users informed of new system features and other related activities. FIU sent a newsletter to the participants of the Waste Management Symposia announcing multiple topics. Below is sample collage of some of the newsletters sent to D&D KM-IT users followed by archive newsletters that can be accessed via the URL shown (Figure 33).

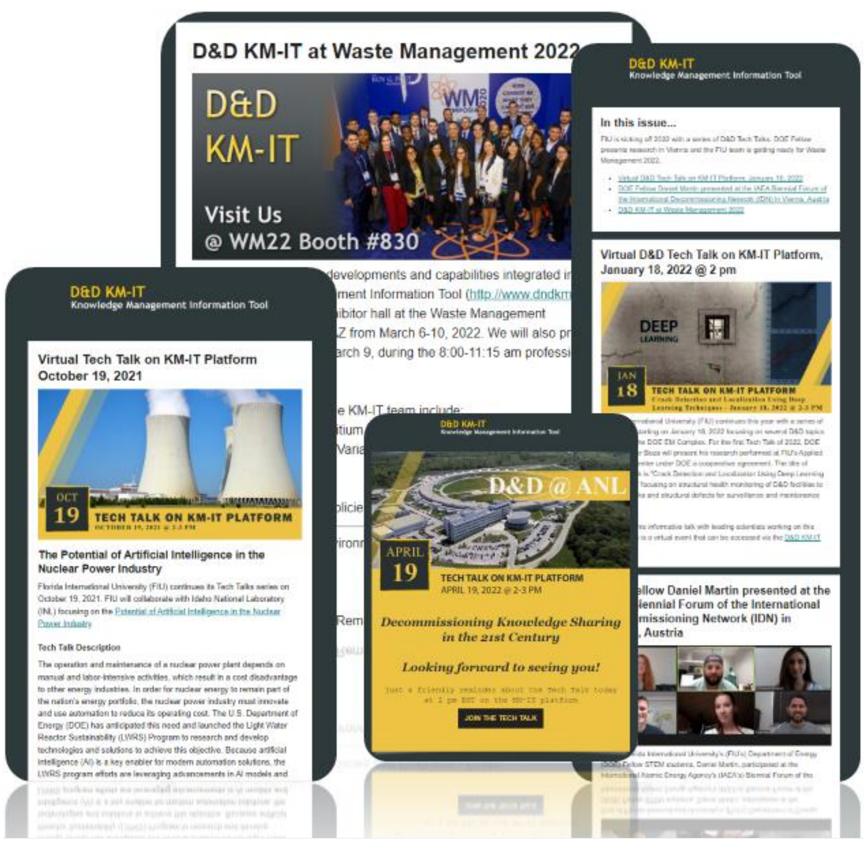

Figure 33. Sample newsletter sent to D&D KM-IT users.

Newsletter list:

- D&D KM-IT October Newsletter - https://mailchi.mp/26b9f80a3233/fiu-wms2019-4974082?e=[UNIQID]
- Tech Talk October 2021 - https://mailchi.mp/28d4f8ed5ec7/reminder-tech-talk-tuesday-1-pm-4978966
- D&D KM-IT January Newsletter - https://mailchi.mp/0aaa884f00c4/fiu-wms2019-5008598?e=[UNIQID]
- Tech Talk January 2022 - https://mailchi.mp/e85fe2315f01/reminder-tech-talk-tuesday-1-pm-6100294
- Tech Talk April 2022 - https://mailchi.mp/830292b22d8e/reminder-tech-talk-tuesday-1-pm-6200250
- D&D KM-IT May Newsletter - https://mailchi.mp/6b86331122a8/fiu-wms2019-8868777
- Tech Talk July 2022 - https://mailchi.mp/a8134dd44ccb/reminder-tech-talk-tuesday-1-pm-8918557
- D&D KM-IT October Newsletter - https://mailchi.mp/99f150f1ec54/fiu-wms2019-9443573
- Tech Talk October - https://mailchi.mp/548fcdc54364/reminder-tech-talk-tuesday-1-pm-9762977

Subtask 3.5: Conclusions

Outreach and marketing are critical elements towards the long-term sustainability of this knowledgebase and are essential for the long-term strategic vision of D&D KM-IT. Moving forward, FIU will continue to participate in industry conferences (such as Waste Management Symposia) and other workshops to demonstrate and promote the KM-IT system. This allows for collaboration with other centers, facilities, and DOE sites to increase usage and subject matter specialist participation. In addition, FIU will continue to develop newsletters for mass communication via email to keep users informed of new system features and other related activities.

Subtask 3.5: References

Deactivation and Decommissioning Knowledge Management Information Tool (D&D KM-IT), https://www.dndkm.org/, Applied Research Center, Florida International University.

Subtask 3.6: D&D KM-IT System Administration

Subtask 3.6: Introduction

D&D KM-IT system administration is an ongoing task, which involves day-to-day administration of servers that house the KM-IT databases and web applications. This task includes updating patches and OS fixes, updating antivirus engines and definitions, updating drivers and assuring that the network (firewall, routers and switches) is working properly.

Subtask 3.6: Objectives

The KM-IT infrastructure is deployed, secured, and maintained in the FIU facility. The objective of this task is for researchers and DOE Fellows to continue to test, maintain, secure, and administer the KM-IT system to keep it reliable with no down time.

Subtask 3.6: Methodology

As mentioned above, the D&D KM-IT system administration is an ongoing task that involves hardware and software upgrades. During this period, the team has been working on updating the SharePoint implementation to the collaboration tools. This is an application to host the News and Events modules of the D&D KM-IT. This application needs to be updated to support the new Secure Socket Layer (SSL) encryptions required by modern browsers. The team is creating a development environment to deploy a new version of SharePoint and then migrate the data of the production environment.

Subtask 3.6: Results and Discussion

The team worked on updating the backend application supporting the news and events module of the D&D KM-IT. This is a SharePoint application which the D&D KM-IT consumes via Really Simple Syndication (RSS) feed. The data is published via XML and the KM-IT application uses this endpoint URL to display the data. The SharePoint application had an issue which had to be resolved to get the RSS working properly. This issue was resolved by the team.

In addition, the team reapplied the SSL to the collaboration tools, a SharePoint application that hosts the KM-IT news. A new SSL certificate was issued and applied to the site. The team had to verify that no interruption to the news module was experienced by testing the news archive, news item and news on the landing page. The SSL had to be authenticated after it was renewed. Also, the administrator account access to the collaboration tools (a feature of the KM-IT that supports the news, events, and other content management) became corrupted. The team had to recreate the administrator account and link the profile to the old account manually in order to prevent data loss.

The team worked on some hardware upgrades which included hard drive replacement of the D&D KM-IT database server. It was identified that a couple of the hard drives were starting to fail and underperform. The team switched these hard drives with new ones which added more capacity and reliability. This action improved reliability and performance issues. Since the server is equipped with a RAID setup, there was no downtime experienced while the drives were being replaced.

Also, FIU focused on archiving legacy servers that were used before moving the D&D KM-IT to a virtual environment. The team is ready to take those servers offline and is going through a rigid backup process to make sure all backend code, databases and applications are properly backed up. The team also addressed security requirements made by FIU regarding public servers hosted at FIU. This included technical checkups that must be verified to be meet internal FIU compliance. The team prepared to implement some upgrades to the SharePoint application that supports the News module of the KM-IT. The version of this application needs to be upgraded so that it can be supported by the new Secure Socket Layer requirements. Finally, the team, with the help of DOE Fellows, has deployed new development machines to support the service and mobile development under Task 6.

Finally, the team continued to monitor the collaboration tools application. This application supports the KM-IT news modules along with the conference and workshop modules. There was an issue addressed during this period where the account used to read the RSS feed from the collaboration tools was not allowing anonymous access. Therefore, the KM-IT website was not able to read the feeds. The team identified the issue and updated the read access to the RSS feeds so that the KM-IT website will show the RSS feeds properly.

Subtask 3.6: Conclusions

The team has successfully kept the D&D KM-IT application and production environment running with optimal performance. After all the hardware and software updates were done, the application did not experience any outages. As a result, the application continues to be more reliable because of the routine maintenance performed on the environment where the application is running.

Subtask 3.6: References

Deactivation and Decommissioning Knowledge Management Information Tool (D&D KM-IT), https://www.dndkm.org/, Applied Research Center, Florida International University.

Subtask 3.7: Cyber Security of D&D KM-IT Infrastructure

Subtask 3.7: Introduction

Cyber security of D&D KM-IT involves securing the network infrastructure that is deployed, secured and maintained in the FIU facility. This includes administration tasks described in Subtask 3.6, but also includes conducting routine cyber security tasks to test the network's vulnerability. This involves coordination between the FIU security team and DOE Fellows who learn cyber security skills while assisting staff do penetration testing and other tasks to test the overall security of the system at the application, database, and infrastructure levels.

Subtask 3.7: Objectives

The KM-IT infrastructure is deployed, secured, and maintained in the FIU facility. The objective of this task is for researchers and DOE Fellows to continue to test, maintain, secure, and administer the KM-IT system to keep it secured and up to date with industry standards. This is done to prevent any security breaches on the system and to train DOE Fellows on security tools used in the industry.

Subtask 3.7: Methodology

The KM-IT infrastructure is deployed, secured, and maintained in the FIU facility. This is a repetitive task, as researchers and DOE Fellows continue to test, maintain, secure and administer the KM-IT system. This involves the administration and upkeep of the application server, windows server and database servers of D&D KM-IT system. Penetration testing tools, malware analysis and reverse malware engineering techniques are used in the DOE Cyber lab to test and secure the KM-IT infrastructure. To keep this infrastructure secure, the team performs various tasks. For instance, each month FIU IT security scans the D&D KM-IT website and provides a report to the team on security vulnerabilities. On a weekly basis, Symantec/Norton scans the D&D KM-IT website for vulnerabilities and malware and sends a report to the team, which is then reviewed and analyzed. If anything in the reports looks critical, the team implements counter measures to minimize the risk of the vulnerability.

In addition, other tasks are executed related to disaster recovery, such as performing backups of the D&D KM-IT environment. These backups are incremental and full backup schemes are then moved to a separate NAS device outside the network. Finally, updates to the operating system are performed which include patches and other OS updates from the vendor. Typically, these updates are performed on the staging environment to make sure that they work properly before moving the changes to the production server.

There are also other tasks that are performed to keep the application secured, but they are not necessarily done each month. For instance, the team renewed the Secure Socket Layer (SSL) certificates for the *doeresearch.fiu.edu* and *collaborationtools.fiu.edu* websites. The *doeresearch.fiu.edu* website is maintained by the FIU team and used to store documents for DOE. These documents include quarterly and yearly reports, as well as mid-year and end-of-year presentations. The *collaborationtools.fiu.edu* website is a SharePoint website used by the KM-IT for backend content management of news, events and other content. The SSLs of these two websites were renewed and the new SSL certificates were applied to the web server where these websites are running. This is a critical security task as it safeguards the information stored on the FIU servers.

Other specific tasks this period included replacing some of the machines in the cyber security lab with the help of the DOE Fellows. New machines were setup with the cyber security tools. These machines were also configured with user accounts and proper firewall settings. The environment was tested, and the team started to use it to test the duplicate D&D KM-IT infrastructure.

DOE Fellows created a private network to test for vulnerabilities on the KM-IT web server. A private network is one where none of the IPs are accessible to public networks but connects to other computers on the same physical network. Since the network is isolated, it makes it a good environment to test tools that might have some associated risk. Some of the benefits of setting up a private network include the ability to test exploits, run simulated attacks and practice in a risk-free environment (since malware and scans can be intrusive and disruptive which we would not want on FIU's network). A private network also provides an environment that can enable us to find web server vulnerabilities. The cybersecurity lab provides the perfect place to find vulnerabilities by holding a number of tools such as the ones available on Kali OS. The figure below shows the private network to test the KM-IT infrastructure.

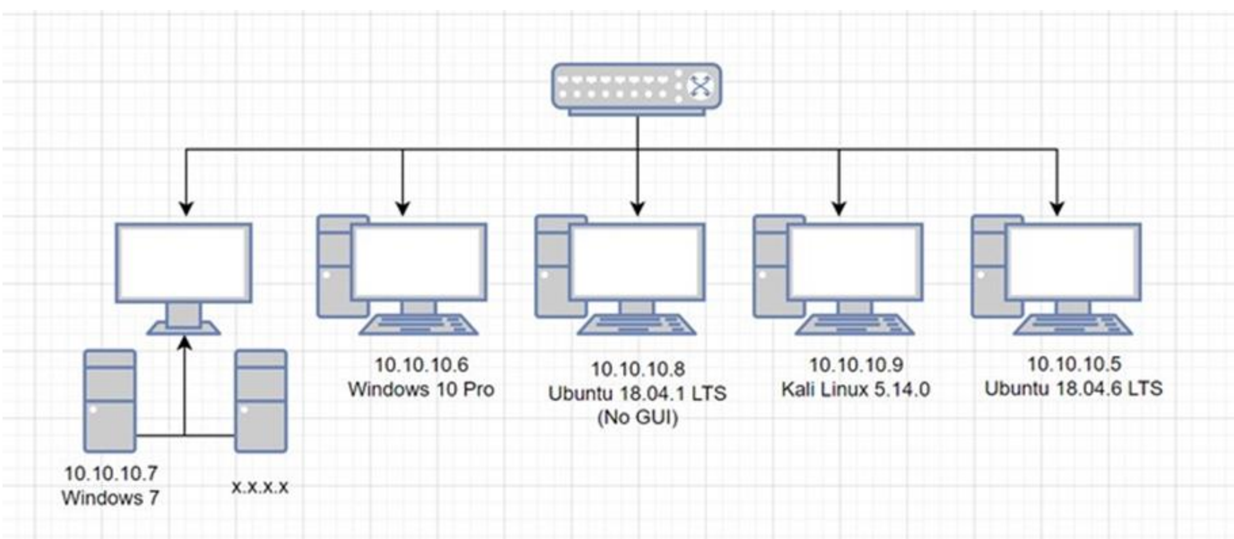

Figure 34. Diagram of Private Network used to test out cybersecurity tools.

DOE Fellows used Metasploit for testing critical vulnerabilities. Metasploit is a complete framework based on Ruby that includes a penetration testing platform to execute code. Its open-source nature makes it one of the best tools for developing, testing and using exploit code. It can be used to discover vulnerabilities in web servers and write exploits that can be used to compromise the server. Metasploit also integrates other reconnaissance tools like Nmap, SNMP scanning, Windows patch enumeration, and Nessus to find the vulnerable spot in your system. Metasploit will facilitate vulnerability assessment of the KM-IT web server and assist in finding issues that can be remedied.

```
Nmap scan report for 192.168.211.129
Host is up (0.0057s latency).
Not shown: 977 closed tcp ports (reset)
PORT     STATE SERVICE     VERSION
21/tcp   open  ftp         vsftpd 2.3.4
22/tcp   open  ssh         OpenSSH 4.7p1 Debian 8ubuntu1 (protocol 2.0)
23/tcp   open  telnet      Linux telnetd
25/tcp   open  smtp        Postfix smtpd
53/tcp   open  domain      ISC BIND 9.4.2
80/tcp   open  http        Apache httpd 2.2.8 ((Ubuntu) DAV/2)
111/tcp  open  rpcbind     2 (RPC #100000)
139/tcp  open  netbios-ssn Samba smbd 3.X - 4.X (workgroup: WORKGROUP)
445/tcp  open  netbios-ssn Samba smbd 3.X - 4.X (workgroup: WORKGROUP)
512/tcp  open  exec        netkit-rsh rexecd
513/tcp  open  login       OpenBSD or Solaris rlogind
514/tcp  open  tcpwrapped
1099/tcp open  java-rmi    GNU Classpath grmiregistry
1524/tcp open  bindshell   Metasploitable root shell
2049/tcp open  nfs         2-4 (RPC #100003)
2121/tcp open  ftp         ProFTPD 1.3.1
3306/tcp open  mysql       MySQL 5.0.51a-3ubuntu5
5432/tcp open  postgresql  PostgreSQL DB 8.3.0 - 8.3.7
5900/tcp open  vnc         VNC (protocol 3.3)
6000/tcp open  X11         (access denied)
6667/tcp open  irc         UnrealIRCd
8009/tcp open  ajp13       Apache Jserv (Protocol v1.3)
8180/tcp open  http        Apache Tomcat/Coyote JSP engine 1.1
MAC Address: 00:0C:29:A6:D1:9E (VMware)
Service Info: Hosts:  metasploitable.localdomain, irc.Metasploitable.LAN; OSs
: Unix, Linux; CPE: cpe:/o:linux:linux_kernel
```

Figure 35. Metasploit scan for open tcp ports.

The picture above shows an example of Metasploit used to conduct a scan that targets all open tcp ports on a target machine. This scan allows the services that are running to be visible along with the version of some of these services. This information is valuable to an attacker because it can be used to launch attacks targeting those services. By scanning these services, changes can be made, whether it is closing the ports that are not being used or changing the default port number so attackers have a harder time finding the services they want to target.

Overall, Metasploit brings many benefits besides the complete framework it holds, such as:

- Ease of use
- Easy to switch payloads
- Clean exit from target system
- Friendly GUI
- Open source and actively developed

In addition to Metasploit, Armitage is a powerful penetration testing tool that uses Metasploit to graphically display targets. It also allows for scanning of targets and recommends exploits. The idea was to use Armitage to scan as much information as possible on the machines. The team utilized Nmap to conduct scans on the Windows machine 10.10.10.6. The result is a list that contains the open ports, services, host name, MAC address, operating system, and other useful host information. The data scanned from the results are documented and will be used to help exploit the machines and create solutions to the issues that arise.

Subtask 3.7: Results and Discussion

The cyber security measures for the D&D KM-IT application were successfully implemented by the FIU team, and no breach of the system was detected with the procedures employed. In addition, the DOE Fellows were able to gain invaluable hands-on experience on cybersecurity and network administration, with exposure to penetration testing tools, malware analysis and reverse malware engineering techniques, to test, maintain, secure and administer the KM-IT system.

Subtask 3.7: Conclusions

Cybersecurity and administration of the D&D KM-IT application are ongoing processes to keep the application secure and reliable. The fact that there was no breach of the system detected can likely be attributed to the cyber security measures implemented, which is an indicator of the significance of this subtask and the need to maintain it as an ongoing support process for the D&D KM-IT application.

Subtask 3.7: References

Deactivation and Decommissioning Knowledge Management Information Tool (D&D KM-IT), https://www.dndkm.org/, Applied Research Center, Florida International University.

Metasploit, https://www.metasploit.com/, Metasploit, Rapid1.

Subtask 3.8: KM-IT Tech Talks (NEW)

Subtask 3.8: Introduction

The FIU team meet with DOE EM prior to the start of the period of performance to discuss opportunities to promote the D&D KM-IT across the DOE sites and facilities. Several topics were discussed, and one was the development of a Tech Talk series where scientists performing D&D-related work would present their research to the community. A couple of Tech Taks were conducted and due to their success, it was decided that a new task was needed specifically for this effort.

Subtask 3.8: Objectives

The objective of the Tech Talks is to provide a platform for scientists to share their D&D research with the community. By using the KM-IT platform, FIU can promote the KM-IT application through newsletters, flyers and event websites. The goal is to increase the engagement of DOE sites and facilities by participating on the Tech Talks as a presenter or attendees.

Subtask 3.8: Methodology

The FIU team organized D&D-focused Tech Talks every quarter on the D&D KM-IT platform. FIU collaborated with national laboratories and/or DOE sites to identify and present technical topics of interest to the community where scientists can present their research. The Tech Talks were performed virtually using an online meeting platform (Microsoft Teams). The event information, including schedule and archive of previous Tech Talks were hosted on the D&D KM-IT. The team promoted Tech Talks via newsletters, website, emails, and flyers developed by FIU. The Tech Talks were recorded, and the video was uploaded to YouTube and archived on the KM-IT platform supporting the next generation of scientists and engineers.

Subtask 3.8: Results and Discussion

FIU conducted four Tech Talks during this period where the team collaborated with national laboratories and/or DOE sites/facilities to identify and present technical topics of interest to the community. The Tech Talks were conducted virtually using an online meeting platform (Microsoft Teams) which was accessible through the KM-IT platform. The Tech Talks were promoted via newsletters sent to the registered user of the KM-IT and other recipients. The user had to register prior to attending the event using Microsoft Forms (Figure 36).

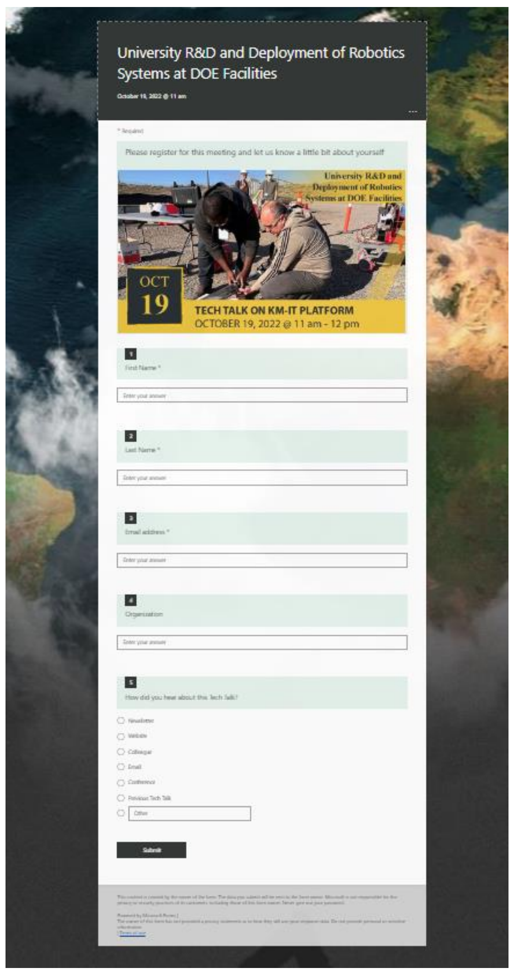

Figure 36. Tech Talk registration form using Microsoft Forms.

Flyers were also created and posted on the Tech Talk website. The flyer contained the basic event information with a QR code that will take users directly to the registration page. The image below (Figure 37) shows the flyer for the Tech Talk event held on January 18, 2022.

Figure 37. Tech Talk flyer created for the event held on January 18, 2022.

An event website was created for each Tech Talk. The website includes an archive of previous Tech Talks, links to presentations, flyers, presenter's bio, and feedback forms. Other information on the website includes a link to add the event to a calendar and a link to the Microsoft Teams application. The following image (Figure 38) shows the event website for the most recent Tech Talk.

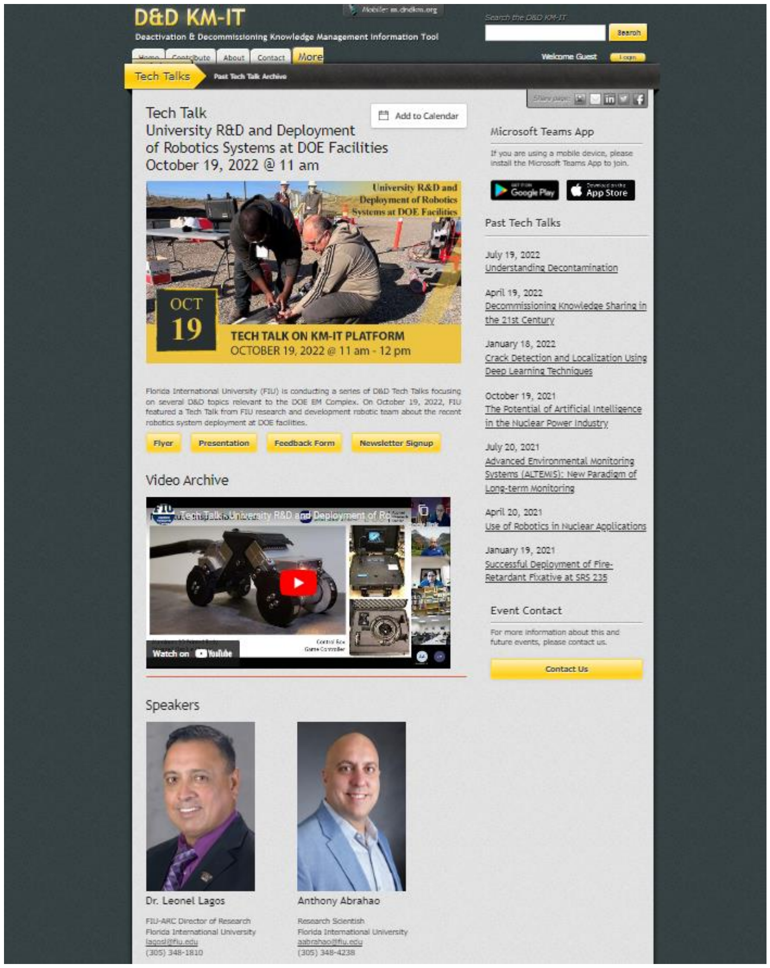

Figure 38. Tech Talk website capturing event info (title, description, presentation, speaker bio, and link to feedback form).

The following Tech Talks were conducted during this period.

- **October 19, 2021 - The Potential of Artificial Intelligence in the Nuclear Power Industry**
    - Topic – Potential of artificial intelligence in the nuclear power industry
    - Collaborator – Idaho National Laboratory (INL)
    - Speaker – Dr. Ahmad Rashdan, Senior Research and Development Scientist at INL
- **January 18, 2022 - Crack Detection and Localization Using Deep Learning Technique**
    - Topic - Using deep learning techniques to detect infrastructure cracks at DOE facilities
    - Collaborator – FIU Research
    - Speaker – Roger Boza, DOE Fellow pursuing a Ph.D. in Computer Science with focus on Machine Learning, Artificial Intelligence and Deep Learning Techniques
- **April 19, 2022 - Decommissioning Knowledge Sharing in the 21st Century**
    - Topic – Decommissioning activities and techniques, lessons learned and best practices

- Collaborator – Argonne National Laboratory (ANL)
- Speaker – Lawrence (Larry) Boing, Facility Decommissioning SME and D&D Experiences Knowledge Management Training Director

- **July 19, 2022 - Understanding Decontamination (and a dozen other lessons)**
  - Topic – Discussing how to stop worrying and learn to love engineering to get the work done
  - Collaborator – Idaho National Laboratory (INL)
  - Speaker – Dr. Rick Demmer, Retired Scientist, Project Manager and distinguished scientist from INL

The following screenshot shows the virtual environment used to conduct the Tech Talk. Each event was recorded, and video was uploaded to YouTube and then embedded on the website.

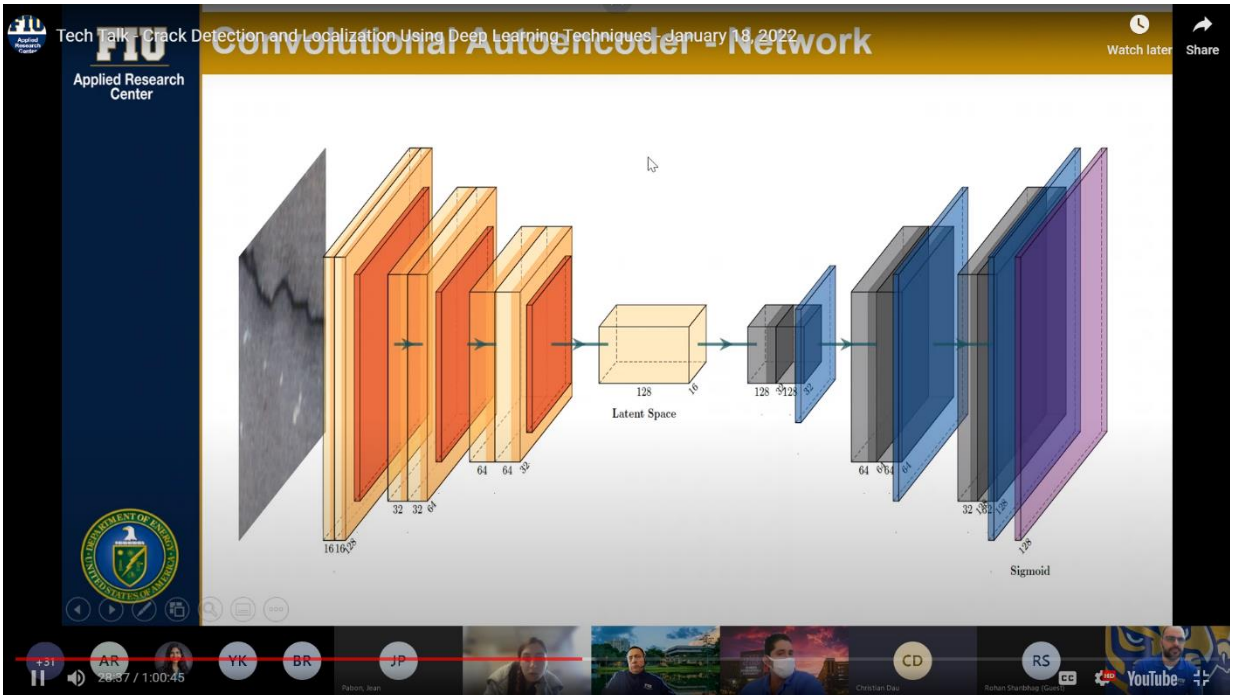

Figure 39. Tech Talk recording up.loaded to YouTube and embedded on the KM-IT website

Subtask 3.8: Conclusions

These Tech Talk events allowed subject matter experts (SMEs) to share their knowledge and experience with DOE EM sites and stakeholders. These were virtual one-hour events, which included one or two guest speakers on relevant topics of interest to the community. The events were recorded and published on D&D KM-IT along with other associated material such as the agenda, presentation slides and lessons learned for post-event viewing as well.

Subtask 3.8: References

Deactivation and Decommissioning Knowledge Management Information Tool (D&D KM-IT), https://www.dndkm.org/, Applied Research Center, Florida International University.

Microsoft Forms, https://forms.office.com/, Microsoft Form, Microsoft Corporation.

TASK 6: AI FOR EM PROBLEM SET (D&D): STRUCTURAL HEALTH MONITORING OF D&D FACILITY TO IDENTIFY CRACKS AND STRUCTURAL DEFECTS FOR SURVEILLANCE AND MAINTENANCE (SRNL)

Subtask 6.5: Design & Development of Machine Learning and Deep Learning Models to Identify and Locate Cracks in D&D Mockup Facility (Completed)

Subtask 6.5: Introduction

Research was conducted to improve the accuracy and detection rate of the previously developed machine learning/deep learning algorithms that specialize in detecting structural defects such as cracks in the D&D mockup facility located in the FIU campus. The team also built models using the state-of-the-art technology advancements in Artificial Neural Networks, Convolutional Neural Networks, Convolutional AutoEncoders, and similar emerging research. These models were tailored for anomaly detection which can detect abnormalities like cracks in the datasets of interest. The purpose was to identify outliers with high accuracy when compared to statistical or mathematical models. Other models targeted the localization problem which focuses on locating (spatially) the defects of interest in the given datasets. These models can highlight the bounding regions within an image where the objects are located. The combination of both types of models leads to the capability of identifying and locating concrete defects of interest with high precision.

Subtask 6.5: Objectives

The objective of this subtask is to improve the model architecture to fine tune predictive performance. As time passes by, new techniques are discovered which allow neural networks to extract features that are more meaningful and make better predictions.

Subtask 6.5: Methodology

The dataset used for this iteration of modeling was the open-source concrete dataset [1] composed of 20,000 images with cracks and 20,000 without cracks. The dataset was randomly down sampled to 2,000 images (50% crack, 50% without crack) to train the networks faster within the data distribution. Each image has a resolution of 128x128 pixels in RGB mode (Figure 40). The images are placed in labeled folders so that they can flow from their respective directories into the model during training.

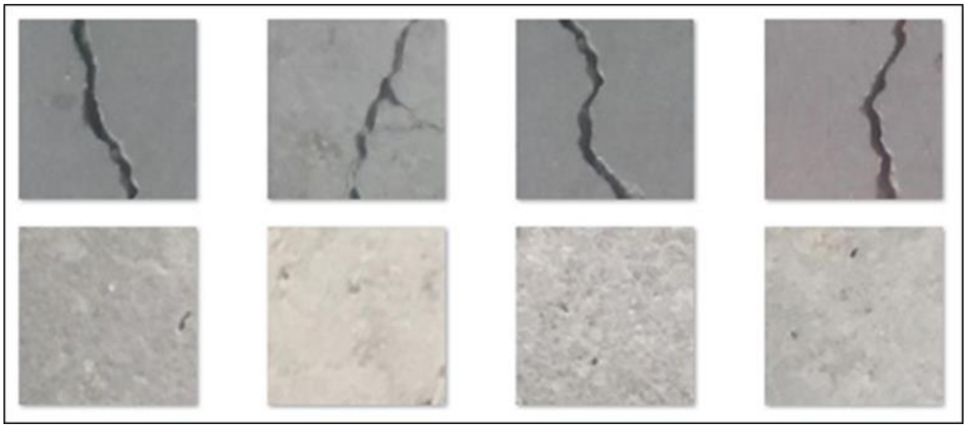

Figure 40. Top row: sample images of concrete with cracks. Bottom row: concrete images without cracks. [1]

One of the first steps in deploying neural network (NN) models on mobile devices is to find an equivalence between the computer-based trained model and the mobile-based backend that can run it. To simplify this process, it was decided to start with a small convolutional neural network (CNN) architecture that was capable of classifying images if they have a crack or not. The main considerations for the architecture of the CNN were the memory footprint and its overall accuracy. A low memory footprint will make deployment easier since the payload would be smaller. Normally there is a tradeoff between memory and accuracy. The goal is to achieve the highest accuracy with the smallest footprint possible.

The VGG16 architecture was considered as an initial model since it has been previously researched and trained to find cracks, but upon further analysis the idea was discarded as VGG16 has a large memory footprint (197MB) with over 15 million parameters. This combination is very heavy for mobile deployment and smaller networks can be designed that have comparable accuracy in their results.

To lower the memory footprint of the models, the total number of convolutional layers and filters was reduced. A total of 6 different models was investigated to see the performance as the total number of parameters was reduced (Table 1).

Table 1. Different Model Sizes and their Validation Accuracy

Model	Total number of convolutional layers	Total Parameters (Millions)	Memory Footprint (MB)	Validation accuracy
M1	4	0.01	0.23	98.1%
M2	4	0.04	0.55	98.2%
M3	3	0.10	1.26	98.4%
M4	6	0.31	3.64	98.4%
M5	6	2.32	26.6	98.8%
M6	6	10.5	121	99.1%
VGG16	16	15	197	99.4%

The M1 convolutional neural network previously trained, shown in Figure 41, was retrained to increase its accuracy. The validation accuracy went from 98.1% to 98.3%, which is a good improvement for the small network. The number of epochs (i.e., training iterations) and batch size (i.e., training samples) was not changed during this training campaign.

Layer (type)	Output Shape	Param #
conv2d_188 (Conv2D)	(None, 128, 128, 4)	112
max_pooling2d_114 (MaxPoolin	(None, 64, 64, 4)	0
conv2d_189 (Conv2D)	(None, 62, 62, 8)	296
max_pooling2d_115 (MaxPoolin	(None, 31, 31, 8)	0
conv2d_190 (Conv2D)	(None, 29, 29, 16)	1168
max_pooling2d_116 (MaxPoolin	(None, 14, 14, 16)	0
conv2d_191 (Conv2D)	(None, 12, 12, 32)	4640
max_pooling2d_117 (MaxPoolin	(None, 6, 6, 32)	0
flatten_32 (Flatten)	(None, 1152)	0
dense_73 (Dense)	(None, 8)	9224
dense_74 (Dense)	(None, 2)	18

Figure 41. M1 convolutional neural network model architecture.

It was noticed that after roughly 35 epochs out of the 100 total epochs, the convolutional neural network did not improve and only the validation accuracy fluctuated, as seen in Figure 42. This plateau in the model accuracy means that the training could be stopped earlier and thus save time.

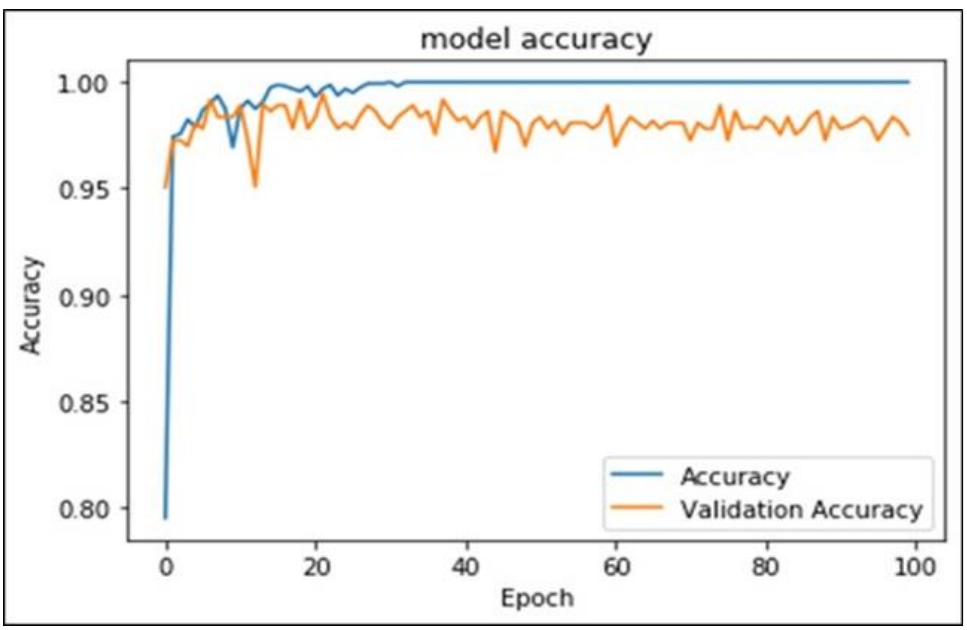

Figure 42. M1 model accuracy plot for 100 epochs.

The model loss tends to spike in cycles throughout the entire training cycle, as seen in Figure 43. This is not common since the goal is to have both the loss and validation loss converge on top of each other. There is a chance that the model found an unstable local minimum and it progressively gets better and then worse as training continues.

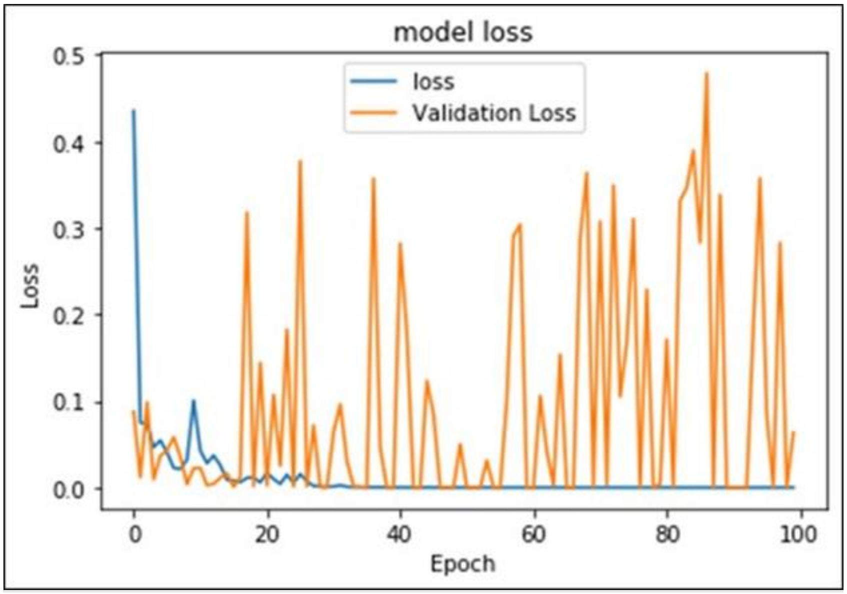

Figure 43. M1 model loss plot showing cyclical spikes in the validation set.

A new model, called M0, was created to reduce the size of the neural network architecture. The total number of parameters for M0 is 3,470 which makes it the smallest network so far. The model is composed of 4 convolutional layers, each followed by a maximum poling layer to reduce the spatial information, as shown in Figure 44.

Layer (type)	Output Shape	Param #
conv2d_9 (Conv2D)	(None, 128, 128, 4)	112
max_pooling2d_7 (MaxPooling2	(None, 64, 64, 4)	0
conv2d_10 (Conv2D)	(None, 62, 62, 4)	148
max_pooling2d_8 (MaxPooling2	(None, 31, 31, 4)	0
conv2d_11 (Conv2D)	(None, 29, 29, 8)	296
max_pooling2d_9 (MaxPooling2	(None, 14, 14, 8)	0
conv2d_12 (Conv2D)	(None, 12, 12, 8)	584
max_pooling2d_10 (MaxPooling	(None, 6, 6, 8)	0
flatten_3 (Flatten)	(None, 288)	0
dense_5 (Dense)	(None, 8)	2312
dense_6 (Dense)	(None, 2)	18

Total params: 3,470
Trainable params: 3,470
Non-trainable params: 0

Figure 44. M0 convolutional neural network model architecture.

The last two layers in the network are composed of dense layers, as shown in Figure 45, which helps the network predict the correct class for each image. The adaptive moment estimation (Adam) optimizer was selected to help the network converge rapidly. According to [2] the method is "computationally efficient, has little memory requirement, invariant to diagonal rescaling of gradients". The learning rate was set to 0.001 and the rest of the parameters were left as standard.

```
model = Sequential()
model.add(Conv2D(filters=4, input_shape=(target_image_size[0],target_image_size[1],3),
                 kernel_size=(3,3),padding="same", activation="relu"))
model.add(MaxPool2D(pool_size=(2,2)))
model.add(Conv2D(filters=8, kernel_size=(3,3), activation="relu"))
model.add(MaxPool2D(pool_size=(2,2)))
model.add(Conv2D(filters=16, kernel_size=(3,3), activation="relu"))
model.add(MaxPool2D(pool_size=(2,2)))
model.add(Conv2D(filters=32, kernel_size=(3,3), activation="relu"))
model.add(MaxPool2D(pool_size=(2,2)))
model.add(Flatten())
model.add(Dense(units=8,activation="relu"))
model.add(Dense(units=2, activation="softmax"))
model.summary()
```

Figure 45. Code snipped for the M0 model architecture.

The M0 model has a very small memory footprint, 91.5 KB as shown in Figure 46, which is 2.5 times smaller than the M1 model. The small memory size is attributed to the total number of parameters in the neural network.

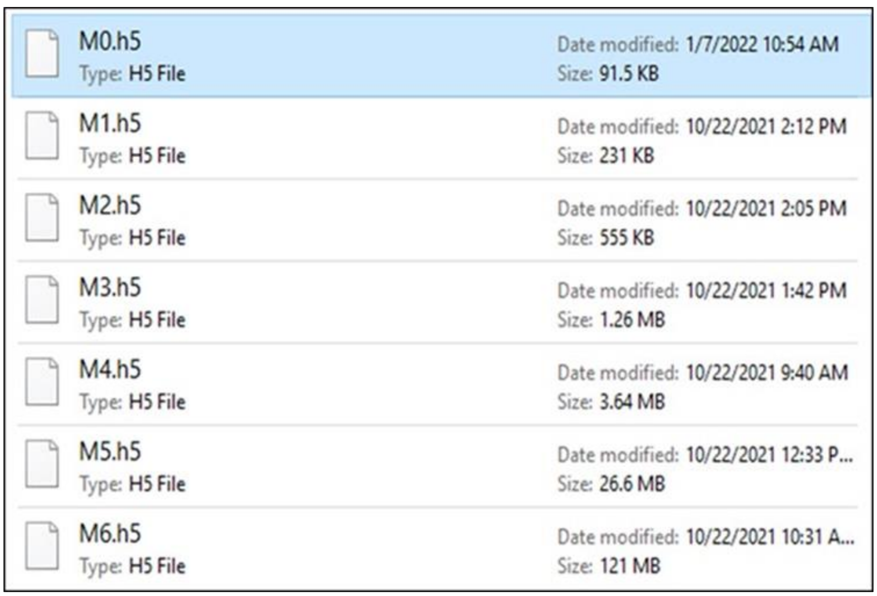

Figure 46. Model memory size for all variants.

An early stopping callback was used in the training phase of the model. The callback stops the training process before the final epoch is reached if the validation loss does not improve over a period of 20 epochs. This was done to end the training early in case the model is at a local minimum, and it cannot jump out of it in search of a better configuration.

M0 was created with a very small memory footprint (e.g., 91.5 KB) and contained 3,470 trainable parameters. The M0 model had a validation accuracy of 98.36% which made it comparable to the rest of the trained models (M1, M2, …, M6). The team use all the trained and saved models to convert them to a TensorFlow Lite version so that they can be deployed on mobile devices for on-device inferencing and prediction.

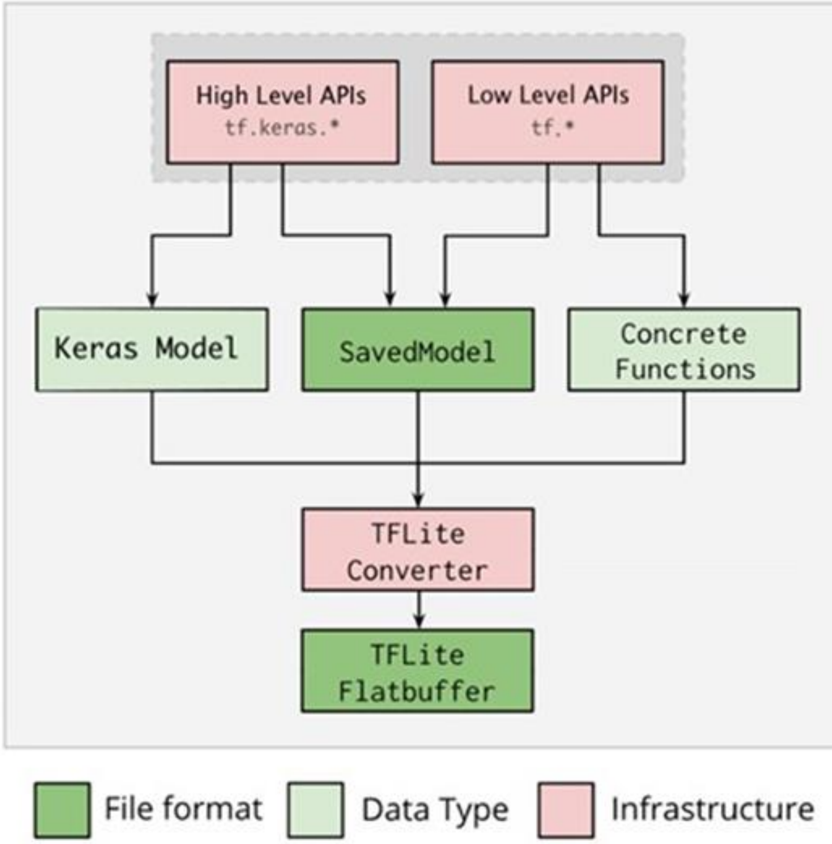

Figure 47. TensorFlow Lite converter diagram.

Source: https://www.tensorflow.org/lite/convert/

TensorFlow models can be converted into lite versions (tflite) using the TensorFlow Lite converter in three different ways as shown in Figure 47. The first and recommended way is to convert from a saved model (i.e., SavedModel). The saved model must be a TensorFlow model and not the Keras .h5 saved models. Trying to convert an .h5 saved model using the SavedModel() function will give errors. The second way is to load a Keras .h5 saved model and convert from it. This is the method used for all the models since they were saved as .h5 files. It is important to note that the TensorFlow library has a from_keras_model() function, but it only works with TF versions 2.0 and higher. If using a TF version lower than 2.0, then it is best to use the function from_keras_model_file() which works with the .h5 model file format. The last way to convert a model is from concrete functions, which are the wrappers for the graph representation of models as shown in Figure 48.

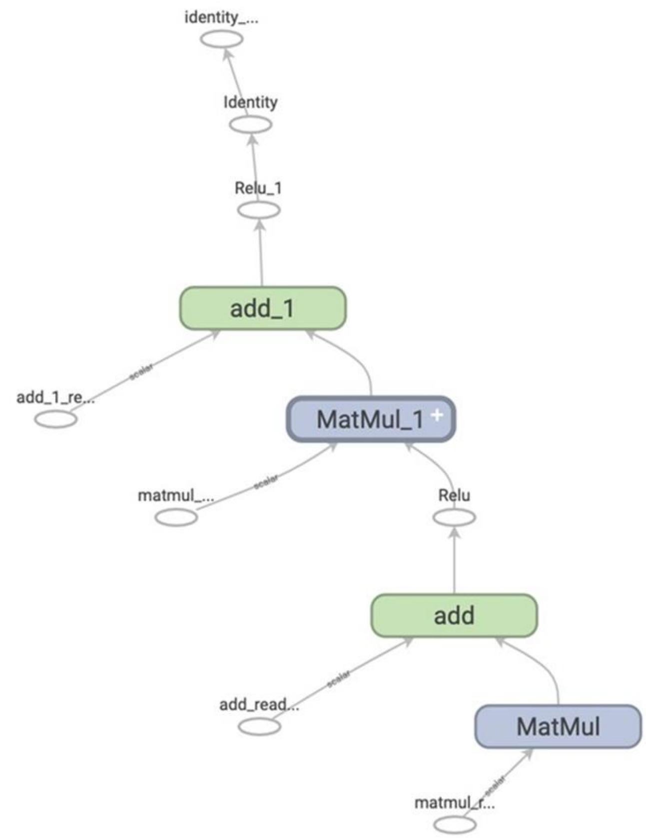

Figure 48. Example of a TensorFlow graph representing a two-layer neural network.

Source: [*https://www.tensorflow.org/guide/intro_to_graphs*](https://www.tensorflow.org/guide/intro_to_graphs)

A script was created to convert all the saved models into the tflite version with a for loop control flow structure that can be reused later. The models convert quickly, usually within 2-5 seconds, which keeps the downtime at a minimum. As the models are being converted, a printout of the number of frozen variables and converted variables are printed to the screen for verification, as shown in Figure 49. All the converted models are saved into their designated folder directories for easy access.

```
INFO:tensorflow:Froze 12 variables.
INFO:tensorflow:Converted 12 variables to const ops.
INFO:tensorflow:Froze 12 variables.
INFO:tensorflow:Converted 12 variables to const ops.
INFO:tensorflow:Froze 12 variables.
INFO:tensorflow:Converted 12 variables to const ops.
INFO:tensorflow:Froze 10 variables.
INFO:tensorflow:Converted 10 variables to const ops.
INFO:tensorflow:Froze 16 variables.
INFO:tensorflow:Converted 16 variables to const ops.
INFO:tensorflow:Froze 18 variables.
INFO:tensorflow:Converted 18 variables to const ops.
INFO:tensorflow:Froze 16 variables.
INFO:tensorflow:Converted 16 variables to const ops.
```

Figure 49. Information printed by the TensorFlow converter for all the Keras .h5 saved models.

The Tensorflow lite models can now be deployed on mobile devices and used for making predictions. One thing to note is that the size of the converted models, as shown in Figure 50, are much smaller than the original files. This is due to the reduction in floating point precision as well as other factors.

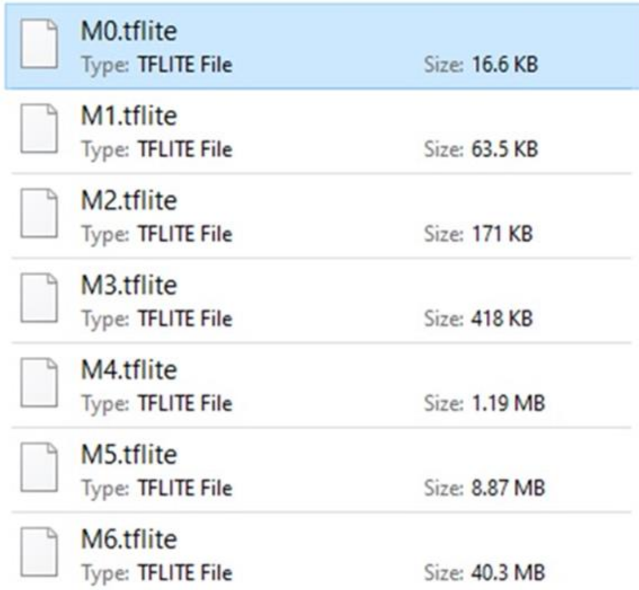

Figure 50. TensorFlow lite model variants memory footprint size.

The YOLOv3 crack detection model that was previously trained was retrained to increase the detection rate and the accuracy of the bounding regions. The new model was trained on the same dataset as the old model, but the epoch count was increased to 1,000 iterations with an early stopping callback function that would terminate the training session if the validation loss did not improve over a period of 100 consecutive epochs. If the early stopping executes and terminates the training session, the best weights from its history are preserved and saved. For the current training effort, the model was trained for 584 epochs before it stopped due to the early stopping condition, as shown in Figure 51.

```
Epoch 577/1000
5/5 [==============================] - 4s 801ms/step - loss: 25.7063 - val_loss: 23.5676
Epoch 578/1000
5/5 [==============================] - 4s 847ms/step - loss: 28.8526 - val_loss: 27.2604
Epoch 579/1000
5/5 [==============================] - 4s 808ms/step - loss: 27.8816 - val_loss: 25.3630
Epoch 580/1000
5/5 [==============================] - 4s 828ms/step - loss: 31.7066 - val_loss: 20.1554
Epoch 581/1000
5/5 [==============================] - 4s 809ms/step - loss: 29.9588 - val_loss: 28.0598
Epoch 582/1000
5/5 [==============================] - 4s 826ms/step - loss: 27.6605 - val_loss: 21.4318
Epoch 583/1000
5/5 [==============================] - 4s 824ms/step - loss: 28.2139 - val_loss: 21.6117
Epoch 584/1000
5/5 [==============================] - 4s 819ms/step - loss: 26.9793 - val_loss: 22.5110
Epoch 00584: early stopping
```

Figure 51. Keras early stopping callback executing at epoch 584 and successfully stopping the training.

After the model finished its coarse training, all the frozen layers in the network were unfrozen and fine-tuning was done for a maximum of 500 epochs. The same early stopping conditions were applied on the fine-tuning as the coarse training. Additionally, a reduced learning rate on the plateau callback function was used to lower the learning rate on the network when a plateau was reached, as shown in Figure 52.

```
Epoch 1/500
11/11 [==============================] - 18s 2s/step - loss: 29.0725 - val_loss: 24.2684
Epoch 2/500
11/11 [==============================] - 5s 409ms/step - loss: 27.8082 - val_loss: 19.8900
Epoch 3/500
11/11 [==============================] - 5s 411ms/step - loss: 24.2520 - val_loss: 23.9511
Epoch 4/500
11/11 [==============================] - 5s 411ms/step - loss: 27.1248 - val_loss: 22.2905
Epoch 5/500
11/11 [==============================] - 5s 410ms/step - loss: 25.4978 - val_loss: 23.2085

Epoch 00005: ReduceLROnPlateau reducing learning rate to 9.999999747378752e-06.
Epoch 6/500
11/11 [==============================] - 5s 410ms/step - loss: 21.8535 - val_loss: 20.6856
Epoch 7/500
11/11 [==============================] - 5s 410ms/step - loss: 22.4398 - val_loss: 20.4571
Epoch 8/500
11/11 [==============================] - 5s 412ms/step - loss: 23.2671 - val_loss: 18.3584
Epoch 9/500
11/11 [==============================] - 5s 410ms/step - loss: 23.5325 - val_loss: 27.1515
Epoch 10/500
11/11 [==============================] - 5s 410ms/step - loss: 21.8174 - val_loss: 18.8141
Epoch 11/500
11/11 [==============================] - 5s 411ms/step - loss: 21.0029 - val_loss: 14.7823
Epoch 12/500
11/11 [==============================] - 5s 411ms/step - loss: 22.0426 - val_loss: 17.3443
Epoch 13/500
11/11 [==============================] - 5s 411ms/step - loss: 20.9737 - val_loss: 23.8583
Epoch 14/500
11/11 [==============================] - 5s 411ms/step - loss: 23.1780 - val_loss: 20.5444

Epoch 00014: ReduceLROnPlateau reducing learning rate to 9.999999747378752e-07.
```

Figure 52. Learning rate being reduced when a plateau is reached by using the ReduceLROnPlateau() function.

The early stopping in the fine-tuning model stopped the training session at epoch 304 and restored the current best weights as shown in Figure 53.

```
Epoch 298/500
11/11 [==============================] - 5s 444ms/step - loss: 22.3398 - val_loss: 14.4362
Epoch 299/500
11/11 [==============================] - 5s 448ms/step - loss: 22.8201 - val_loss: 25.8203
Epoch 300/500
11/11 [==============================] - 5s 434ms/step - loss: 20.5980 - val_loss: 16.1418
Epoch 301/500
11/11 [==============================] - 5s 433ms/step - loss: 20.4753 - val_loss: 22.5539
Epoch 302/500
11/11 [==============================] - 5s 437ms/step - loss: 19.9402 - val_loss: 21.5494
Epoch 303/500
11/11 [==============================] - 5s 453ms/step - loss: 21.3147 - val_loss: 17.6832
Epoch 304/500
11/11 [==============================] - 5s 442ms/step - loss: 19.2678 - val_loss: 20.8502
Epoch 00304: early stopping
```

Figure 53. Keras early stopping executing at epoch 304 during fine-tuning.

The fine-tuned model usually has a lower loss value at the end of training, which means on average the model will perform better at detection of the objects of interest. In Figure 54 it can be seen that the fine-tuned model oscillates between 15 and 24 in the loss value while it tries to find a local minimum.

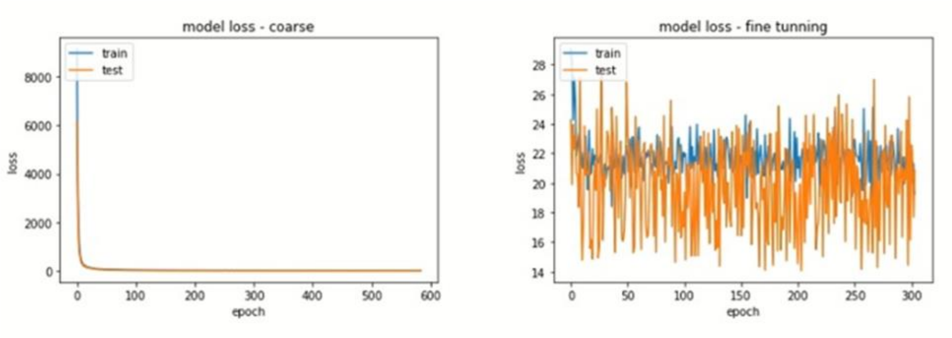

Figure 54. Model loss plot for coarse and fine-tuned training.

Subtask 6.5: Results and Discussion

Overall, the M1-M6 models performed very well. As expected, the validation accuracy was reduced as the model size (total parameters and memory footprint) was decreased. The current analysis showed that the accuracy does not decrease linearly with the reduction of the network size. Even the smallest network analyzed in this iteration was able to correctly classify over 98% of the images (Figure 55).

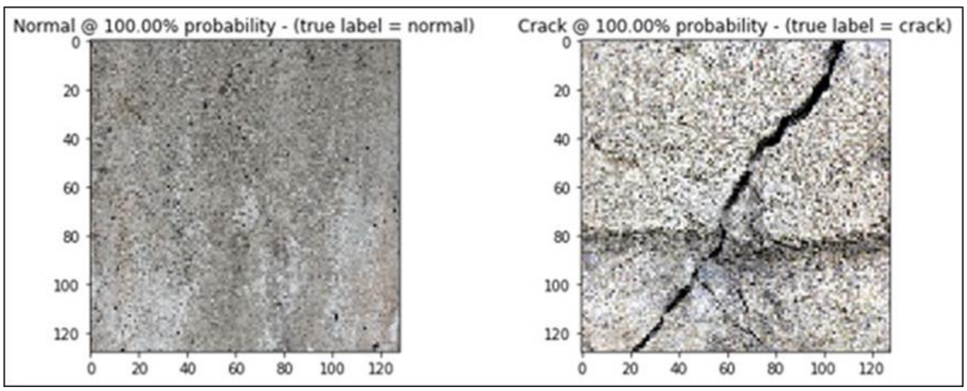

Figure 55. Left: correct classification of normal image. Right: correct classification of crack image.

The small network does fail occasionally, as shown in Figure 56, with a high probability.

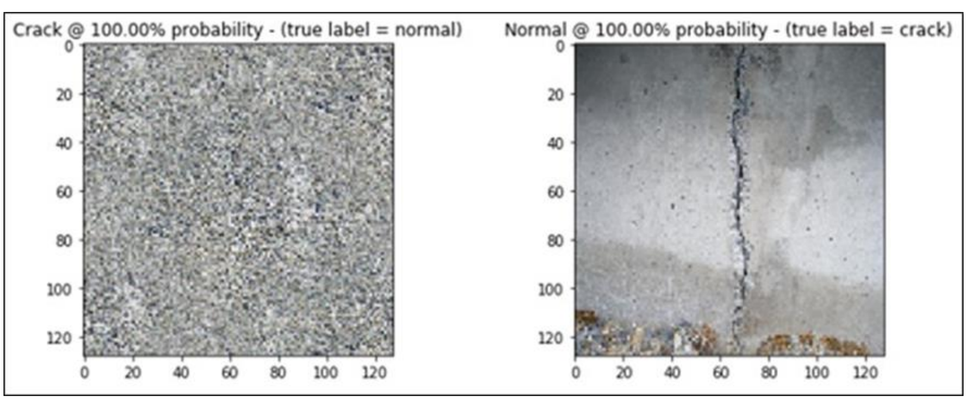

Figure 56. Left: incorrect classification of normal image. Right: incorrect classification of crack image.

The tradeoff between size and accuracy for the classification task of cracks shows that within the current data distribution, the small model ("M1") with approximately 10,000 parameters and a memory footprint of 0.23MB can perform on par with the larger models. The retrained M1 model was able to correctly classify images as "crack" that it previously had misclassified. All the previously correctly classified images were still correctly classified. The small sized networks will be easier to deploy on mobile devices.

The early stopping callback for the M0 model executed correctly and stopped the model after 35 epochs of training as shown (Figure 57). This was expected since after visual inspection of the training previously done, the models do not progress past about 30 epochs. The validation accuracy for this model was 98.36%, which is comparable to the M1 model tuned previously at 98.38%.

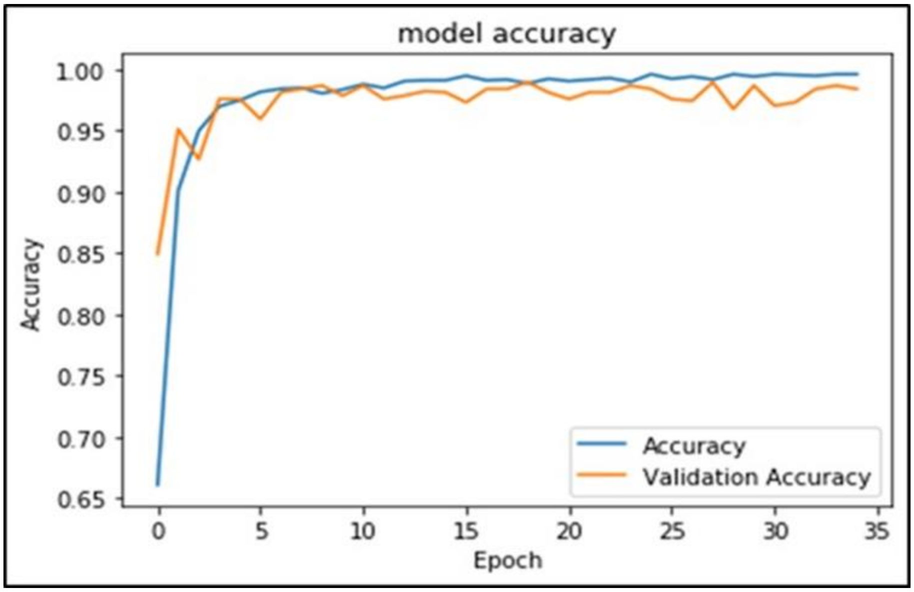

Figure 57. M0 training stopped after 35 epochs by the early stopping callback.

The validation loss also shows that it closely follows the training loss, as seen in Figure 58, which is desirable when training the model. Both the validation loss and training loss converged.

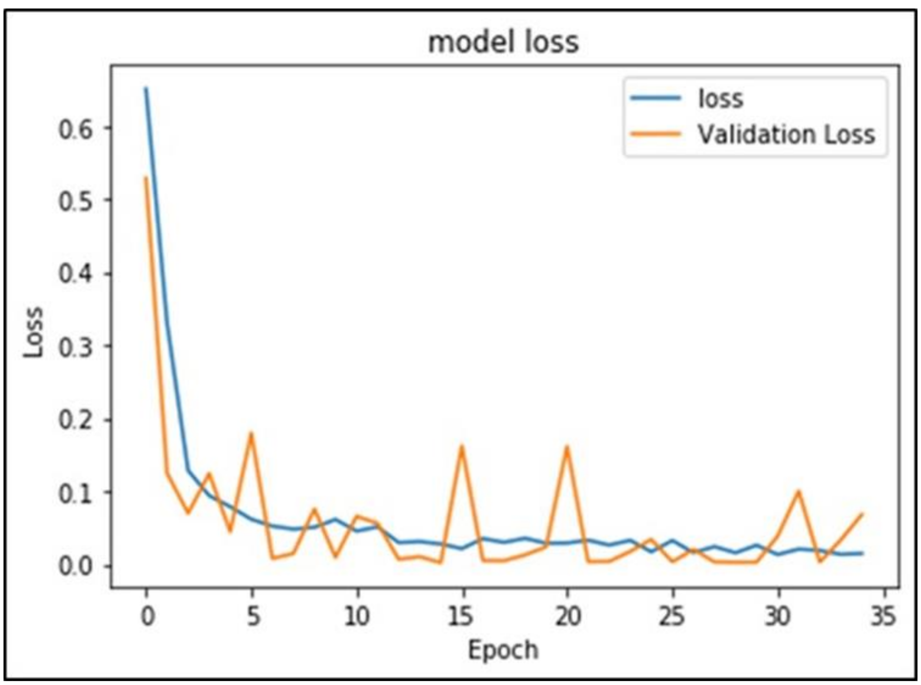

Figure 58. M0 validation loss converging with the training loss.

Converting the models to their tflite counterparts was successful. Their reduction factor is not linear and affects smaller networks more than larger networks. In Table 12 one can see that the M0 model, saved as a Keras .h5, has a file size of 91.5 KB, but after the conversion it is only 16.6 KB which is a reduction of 5.51. The rest of the models experienced a similar reduction but seem to approach a factor of 3.0.

Table 12. File Size of Model Variants in their Keras and TF Lite Versions

Model Name	Keras Model – File Size	TF Lite Model – File Size	Reduction
M0	91.5 KB	16.6 KB	5.51
M1	231 KB	63.5 KB	3.64
M2	555 KB	171 KB	3.25
M3	1.26 MB	418 KB	3.01
M4	3.64 MB	1.19 MB	3.05
M5	26.6 MB	8.87 MB	3.00
M6	121 MB	40.3 MB	3.00

The newly trained YOLOv3 model was able to detect the cracks on images with higher accuracy as shown in Figure 59.

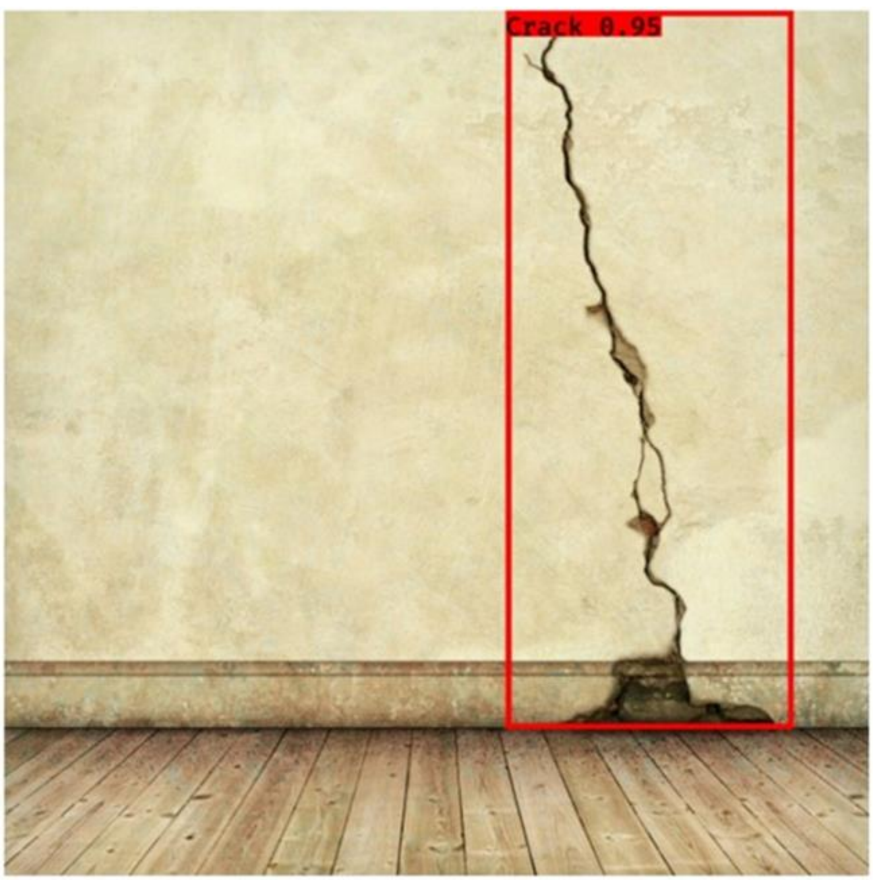

Figure 59. YOLOv3 fine-tuned model detection of a crack at 0.95 confidence.

The inferencing speed of the model was tested on a laptop using an Intel i7 CPU and a desktop using a NVidia 1070 GPU. The laptop was able to process 2-3 images per second while the desktop was able to process 22-30 images per second, as shown in Figure 60.

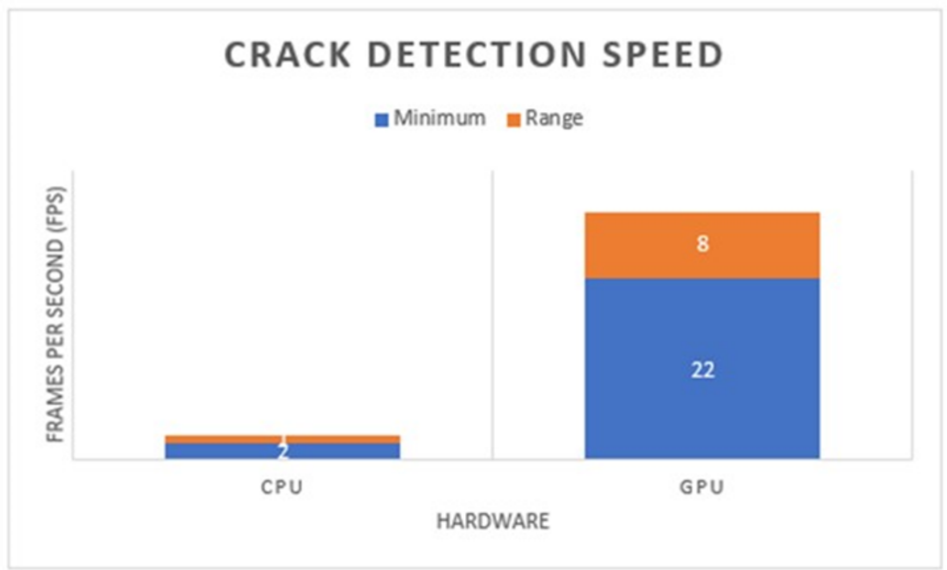

Figure 60. Inferencing speed of trained YOLOv3 crack detection network.

Subtask 6.5: Conclusions

The small memory footprint shows signs that it can still be improved through training and hyper parameter tuning. There is also a possibility to construct even smaller networks and possibly achieve similar testing accuracy.

The M0 model can perform similarly to the M1 model previously tuned. They both have the same accuracy despite having different convolutional layers. The M0 is 2.5 times smaller than the M1 architecture which allowed the model to have a smaller memory footprint when saved. This will be beneficial when moving this model to the cloud. The model M0 was created to reduce the size of the neural network architecture. The total number of parameters for M0 is 3,470 which makes it the smallest network so far. The model is composed of 4 convolutional layers each followed by a maximum poling layer to reduce the spatial information as shown in Figure 6.

To deploy the trained TensorFlow models which are saved as Keras .h5 files, it is necessary to use the TensorFlow Converter and generate the TensorFlow Lite model file. The TF Lite model can then be deployed to mobile devices as shown in Figure 61.

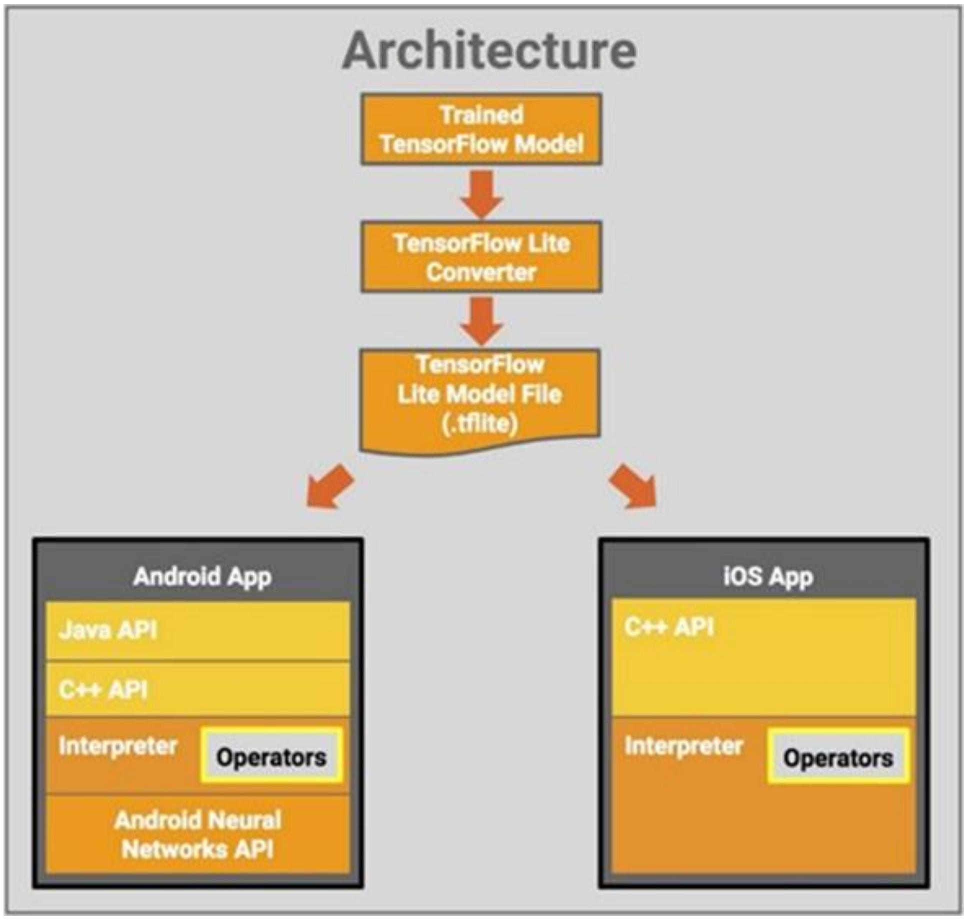

Figure 61. Flow diagram for the conversion of TensorFlow models.

Source: https://developers.googleblog.com/2017/11/announcing-tensorflow-lite.html

Subtask 6.5: References

[1] Kingma, D.P., & Ba, J. (2015) Adam: A Method for Stochastic Optimization. *Proceedings of the 3rd International Conference for Learning Representations (ICLR)*, San Diego, CA.

[2] D. P. Kingma, J. Ba., "Adam: A Method for Stochastic Optimization," 2017

Subtask 6.6: Design & Development of a Mobile Application to Deploy Machine Learning and Deep Learning Models on the iOS Devices in collaboration with SRS (Completed)

Subtask 6.6: Introduction

This subtask was focused on the design & development of a mobile application to deploy trained machine learning and deep learning models on the handheld devices, such as smart phones and tablets. Due to the limitation of the resources on the mobile devices, research focused on the overall memory size of the trained machine learning models. A lightweight version of the neural network backend libraries could be installed on the mobile devices to run the trained models to perform prediction in real time. A mobile app needed to be developed to interact with the neural network backend libraries to run the models and perform predictions. The mobile app will have the capability to load models into memory, select input source, perform predictions, and visualize results.

Subtask 6.6: Objectives

The aim of this subtask is to research and explore deployment of trained models on mobile devices for use in real-time around the DOE complex by operators.

Subtask 6.6: Methodology

The team set up a mobile development environment. This included downloading the latest version of Microsoft Visual Studio with Xamarin and experimenting with its new features. The initial research focused on finding a suitable framework that would allow the FIU team to be able to easily create an application that would be able to work properly on a mobile device. A framework was needed that would allow developer apps to be published on multiple platforms.

The team decided on using Windows Visual Studio 2022 along with the Xamarin.Forms framework, an open-source cross-platform framework for building iOS, Android, & Windows apps with .NET from a single shared codebase. The team downloaded the latest version of Microsoft Visual Studio with Xamirin to experiment with its new features. With MS Visual Studio's Xamarin.Forms the team was able to find the capabilities needed to make an application that would be available to publish on a mobile device running iOS.

The team also downloaded a light version of TensorFlow on a mobile device to see what features were available out of the box. TensorFlow Lite backend was used to package a sample project demonstrating the capabilities. The repository, located online at GitHub [3], was downloaded and configured on a mobile device. The project was created by TensorFlow and offers a sample user interface that is very user friendly, as seen in Figure 62.

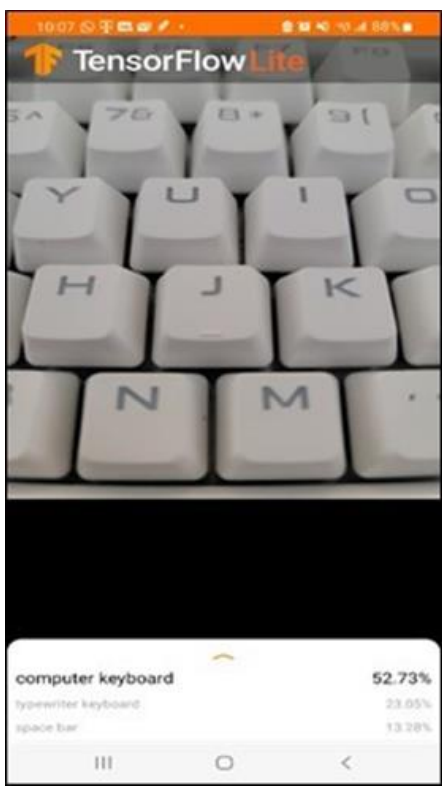

Figure 62. TensorFlow Lite sample mobile application for classification.

When the user opens the mobile app, the camera immediately activates and begins collecting images as a video stream. The images are fed one at a time to one of the 4 available classification models, as seen in Figure 63, for predictions. The top three predictions are displayed on the screen in real-time for the user to see. The available models are pre-trained and offered just for demonstration purposes.

Figure 63. Mobile app showing available models to choose from.

The TensorFlow Lite mobile app also has a pulldown menu that shows the frame size, crop size, view size, rotation, inference time, threads, model and device. Detailed information about these parameters is shown in Table 13. The predictive models can be changed without having to close the mobile app.

Table 13. Description of Parameters Available in the Mobile App

Parameter	Description
Frame Size	Size of image being captured by camera.
Crop Size	Size of cropped image passed to model.
View Size	Size of image displayed on screen for user.
Rotation	Rotation of image.

Inference Time	Time take for the selected model to make a prediction.
Threads	Number of threads used by the app to execute.
Model	Trained model.
Device	To execute on CPU or GPU.

Multiple UIs were created with different individual functions that will be going into the final product. These rough drafts included a UI feature for a splash screen that shows the D&D KM-IT Logo, one to use the phone camera within the application to take a picture, and another to bound one or multiple items in a picture in a box after being passed through coordinates upon which to draw the box or boxes.

The following pictures are screenshots of the splash screen application and the camera application on a mobile device. These screenshots show the progression toward the final product using Visual Studio. Figure 64 shows a screenshot of the splash screen UI feature that is being developed. The splash screen works by simply flashing a desired image on the screen of the mobile device for a certain amount of time upon opening the application; after a certain time, the splash screen fades away and the user is given control of the application. Currently the splash screen is a simple gray screen with the KM-IT logo as the aim is to keep a singular color scheme between the KM-IT projects.

Figure 64. Screenshot of the splash screen UI feature.

The next screenshots show the base camera function application. Figure 65 shows the start screen upon opening the application, asking the user if they would like to capture or upload an image. However, uploading an image is not our current goal and something that is not currently intended to be part of the application. Upon clicking “Capture Image”, the user will see the screen in Figure 66. The background of this image is given in the coding, as the camera is currently being run on a simulator.

Both of these functions are still being worked on and improved and will eventually be introduced into the main project so that the functions are included in the final application.

Figure 65. Start screen upon opening the application, asking the user if they would like to capture or upload an image.

Figure 66. Screen showing the camera capture feature after user selects "Capture Image".

A client-server model is a distributed application structure that partitions certain workloads between the providers of services (e.g., server) and the requesters (e.g., client). The client-server architecture, which is commonly referred to as distributed applications, was chosen to test the mobile deployment of deep learning models.

The integrated development environment (IDE) has a drag and drop approach for designing the application layout which makes it intuitive and user friendly, as seen on Figure 67. Widgets can be created and placed using code as well, but is not as easy as the drag and drop. Each widget placed on the application has a unique ID which is then referenced from the code to create an object and control the functionality.

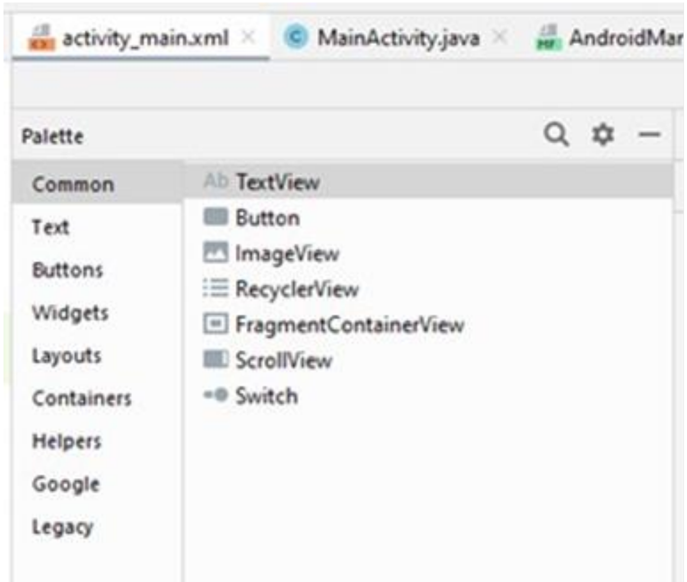

Figure 67. Drag and drop menu for placing common widgets (i.e., buttons, image views, etc.) on the application.

The IDE has options to view the code and design individually or to split the screen and display both the code and design side by side as shown in Figure 68.

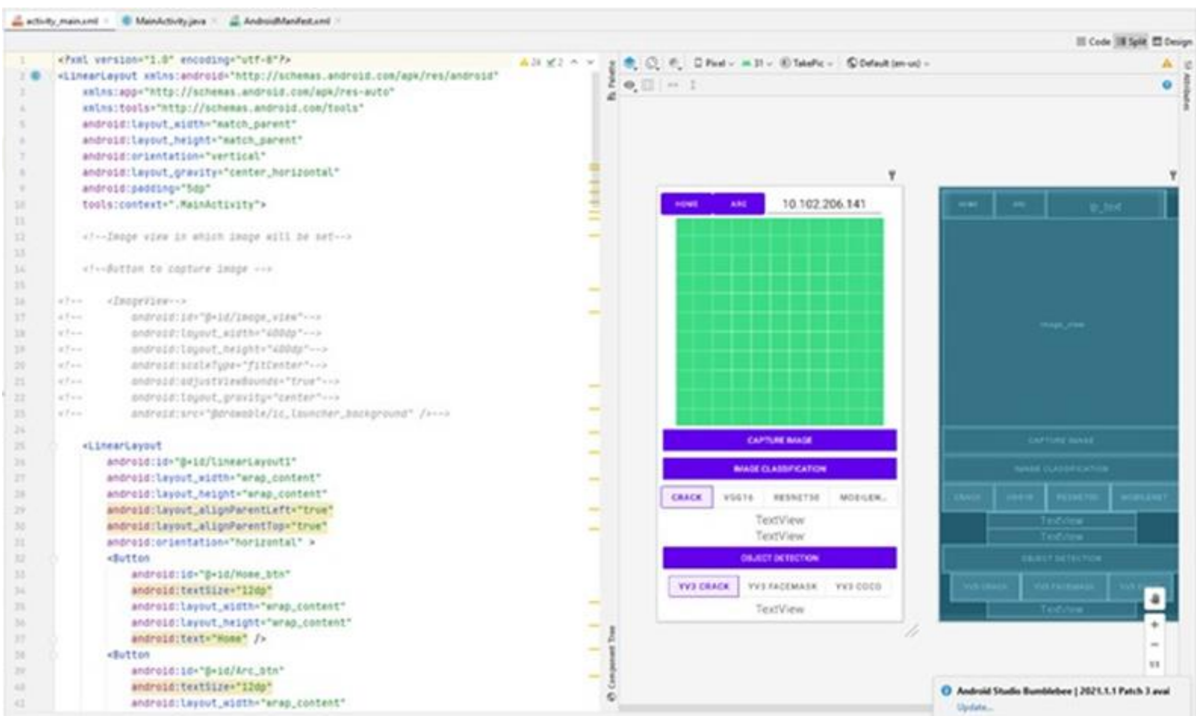

Figure 68. Split view of the code and design windows.

The split view is great for verifying that the screen layout looks exactly as intended while writing the design code for the application. It is also very useful for locating sections of the code since clicking on a widget on the design view will select the code relevant to it in the code window.

The application was designed with both image classification and object detection in mind, as shown in Figure 69. At the top of the application window there are buttons to preselect the location of the deep learning server. There is also a text area where an IP address can be specified to direct the application to a different server.

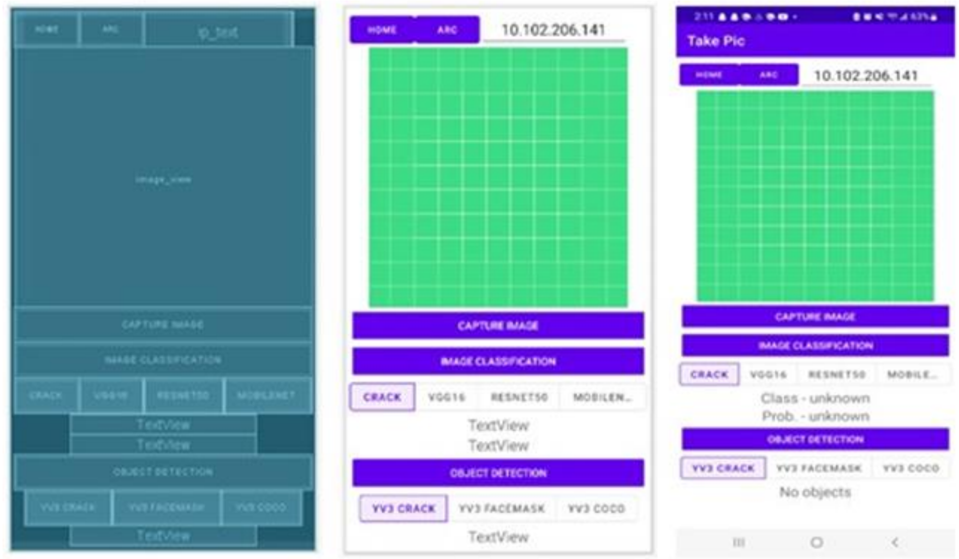

Figure 69. Application screen concept (left), design view in IDE (middle), and deployed on a mobile device.

Once a server location is selected or specified, the “capture image” button can be pressed to access the phone camera and take a picture. The image taken can be sent to the selected server to do either image classification or object detection with the trained models. To perform image classification, one of the four models available must be selected (i.e., crack, VGG16, RestNET50, and MobileNet) and the “image classification” button clicked as shown in Figure 70. The crack model was trained under Subtask 6.5 and completed last year, while VGG16, RestNET50, and MobileNet were loaded with pretrained weights from the ImageNet open-source dataset. ImageNet has 1,000 classes including common objects such as stop lights, airplanes, cars, and teddy bears. Once the “image classification” button is pressed, the image is converted to a byte stream and sent over a TCP/IP connection to the server.

Figure 70. Image classification models available on the server.

Similarly, to perform object detection, one of the three models available must be selected (i.e., YV3 crack, YV3 facemask, and YV3 COCO) and the “object detection” clicked as shown in Figure 71. All three models use the YoloV3 architecture. YV3 crack was trained under Subtask 6.5. YV3 facemask was quickly trained using knowledge transfer and a small dataset for demonstration purposes. YV3 COCO was loaded using pretrained weights trained on the open-source COCO dataset capable of detecting 80 different types of objects. Once the model has been selected. the “object detection” button can then be clicked and the data is sent to the server for processing.

Figure 71. Object detection models available on the server.

The byte stream is converted back to an image when the server receives data. The image is then passed through the selected model and the predictions are sent back to the client. Once the app receives the predictions they are displayed on the screen as shown in Figure 72.

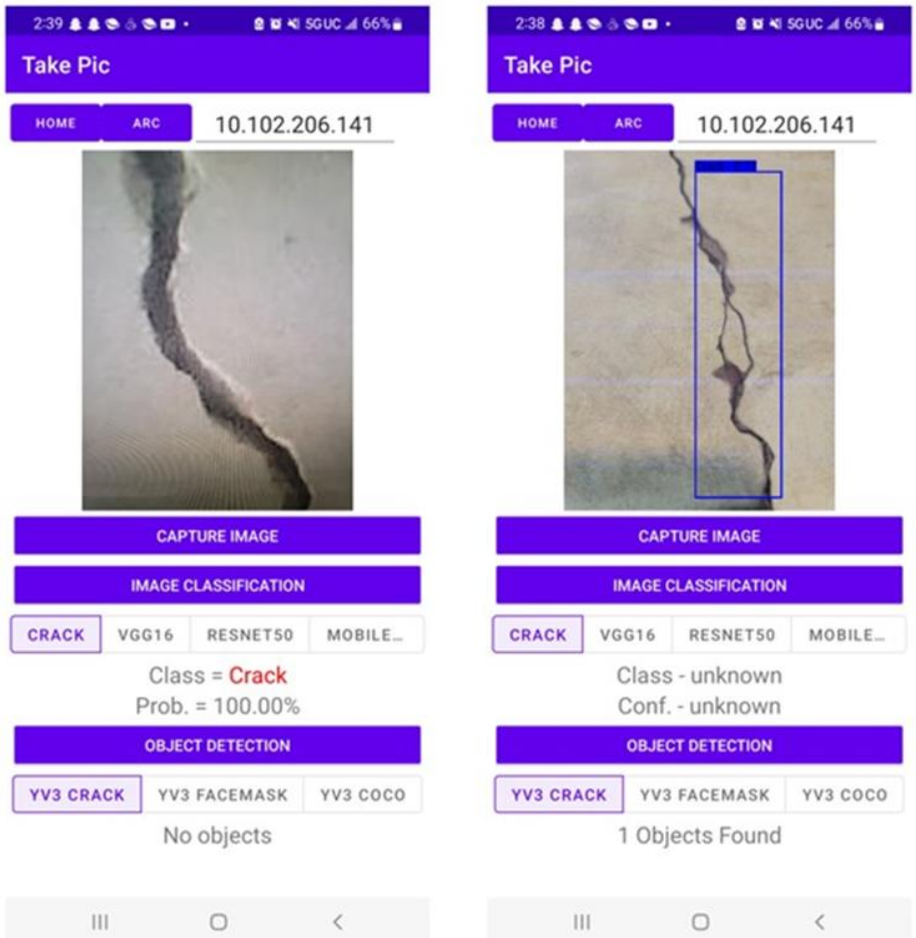

Figure 72. Image classification results (left) and object detection bounding box (right).

The server side of the client-server architecture was written in Python using socket programming. The main reason Python was used as the programming language was because all the models were trained, and their architectures were developed in Python with the help of TensorFlow and Keras. TensorFlow is the neural backend library and Keras is a wrapper class that facilitates interactions with TensorFlow, as shown in Figure 73.

```python
import tensorflow as tf

from tensorflow import keras, Graph, Session

from YOLOv3Facemask.yolo import YOLO as YOLO_Facemask
from YOLOv3COCO.yolo import YOLO as YOLO_COCO
from YOLOv3Crack.yolo import YOLO as YOLO_Crack

import PIL.Image as Image
```

```
Using TensorFlow backend.
```

Figure 73. Import statements for TensorFlow and Keras in Jupyter Notebook.

The first step in the server is to load all dependencies and libraries for the project (e.g., TensorFlow, Keras, Matplotlib, Pillow, Socket, Threading, IO, and Numpy). Each deep learning model is loaded into memory individually in a different TensorFlow session so that multiple models can be used simultaneously. After the models are loaded, a sample picture is used to make testing predictions and ensure that everything is working as expected, as shown in Figure 74.

Testing YOLOv3 Crack

In [4]:

```python
thread_graph = Graph()
with thread_graph.as_default():
    thread_session = Session()
    with thread_session.as_default():
        yolo_crack = YOLO_Crack()

        graph = tf.get_default_graph()

models["yolov3 cr"] = [graph, thread_session]
```

```
WARNING:tensorflow:From C:\Users\Roger Boza\AppData\Local\conda\conda\envs\Tensorflow\lib\site-packages\tensorflow_core\python
\ops\resource_variable_ops.py:1630: calling BaseResourceVariable.__init__ (from tensorflow.python.ops.resource_variable_ops) wi
th constraint is deprecated and will be removed in a future version.
Instructions for updating:
If using Keras pass *_constraint arguments to layers.
YOLOv3Crack/crack-ft-4.h5 model, anchors, and classes loaded.
WARNING:tensorflow:From C:\Users\Roger Boza\AppData\Local\conda\conda\envs\Tensorflow\lib\site-packages\tensorflow_core\python
\ops\array_ops.py:1475: where (from tensorflow.python.ops.array_ops) is deprecated and will be removed in a future version.
Instructions for updating:
Use tf.where in 2.0, which has the same broadcast rule as np.where
```

In [5]:

```python
image_path = "YOLOv3Crack/data/testing/wall-crack-2.jpg"
image = Image.open(image_path)

g, ts = models["yolov3 cr"]
with g.as_default():
    with ts.as_default():
        detection = yolo_crack.detect_image(image)
```

```
(416, 416, 3)
Found 1 boxes for img
Crack 0.95 (1450, 0) (2281, 2076)
3.7048
```

Figure 74. Python code to create, load and test YOLOv3 models.

Once all models have been loaded into memory, the server starts listening on the desired port for incoming connections. When a connection is established from a client, the server hands off the request to a thread and begins making predictions. While the thread is making predictions, the server continues listening for additional requests. When a thread is finished making predictions, the results are converted to a byte stream and sent back to the client via the TCP/IP connection, as shown in Figure 75.

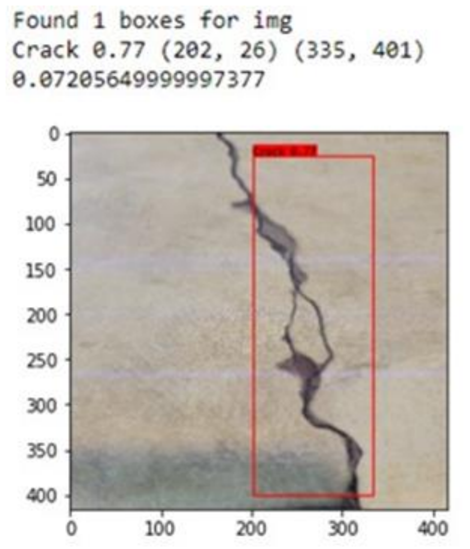

Figure 75. Server receiving request, making a prediction, and sending response back to client.

A mock-up demo was created and showcased at the Waste Management Symposia 2022 for the client-server. In this case, an additional client was created to run in real-time from a laptop. The laptop frontend was created using OpenCV to capture real-time images from the camera sensor and pass it through the YOLOv3 COCO model. The results were displayed in real-time onscreen for everyone to see as shown in Figure 76.

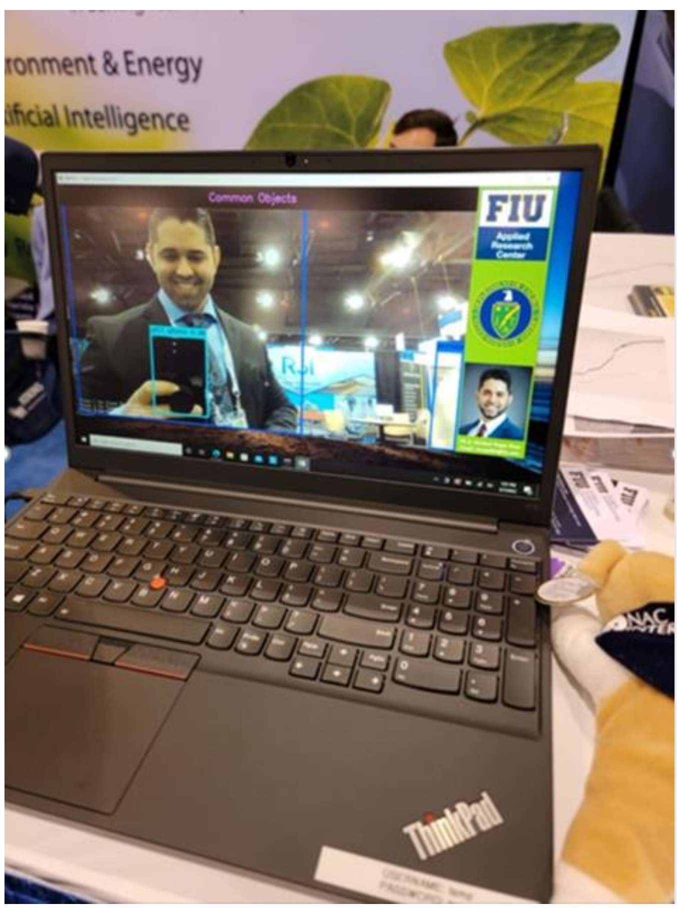

Figure 76. Laptop client running in real-time doing predictions for common objects.

The back-end socket server was also modified to handle JSON objects in the requests. This modification was done to have an unambiguous data transfer scheme between the mobile app, Web API, and the server socket. JSON objects are lightweight and self-describing. They are formatted hierarchically and can be parsed quickly as seen in Figure 77.

```python
        if result == "":
            self.csocket.sendall(bytes('{"Result":"None"}','UTF-8'))
        else:
            self.csocket.sendall(bytes(json.dumps(result),'UTF-8'))
```

Figure 77. Python code snippet for converting results into a JSON format.

Subtask 6.6: Results and Discussion

For the sample app provided by TensorFlow, Increasing the number of threads increases the speed at which the models make predictions. Some models do, however, experience a slow response time when a high number of threads is selected. The reason for this is that the input/output operations as well as the data parallelism overhead, incur a higher processing cost. Changing the device from CPU to GPU also speeds up the predictions, but not all models can be executed on the GPU at the moment.

The final front-end graphical user interface (GUI) for the mobile application was developed in Visual Studio using Xamarin. Xamarin, shown on Figure 78, is a Microsoft-owned software that provides cross-platform implementation of the common language infrastructure (CLI).

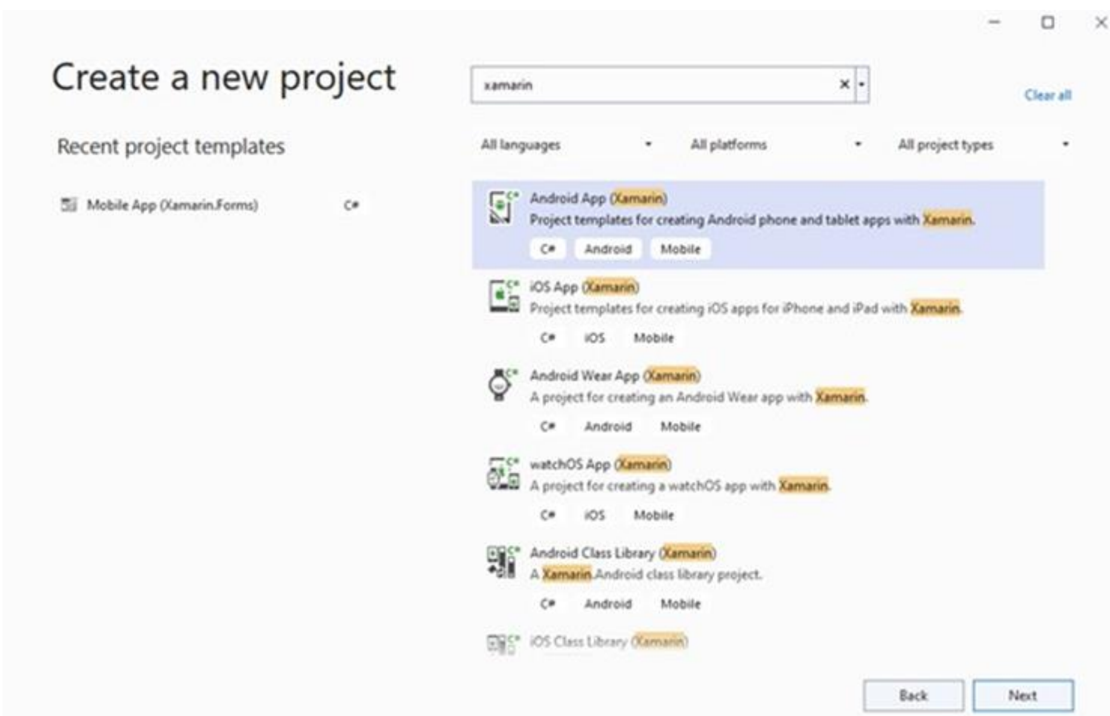

Figure 78. Microsoft Visual Studio new project window with Xamarin projects.

The following screenshot shows the interface of the current application. Figure 79 shows the mobile app sliding menu. Here the user can select what machine learning functionality they want to use.

- Image Classification (Crack Classifier) – This feature will use an image as an input and determine if there is a crack detected on the image and show the probability percentage of the crack classification. The result of this computation will return back the image, with the label “Crack” or “Normal” and the probability percent (Figure 81).
- Object Detection (Crack Detection) – This feature also uses an image as an input. The AI machine learning algorithm will return the image with all the information necessary for the mobile app to draw a box around a crack (if found) on the original image (Figure 82).

Figure 80 simple shows a picture captured via the mobile app. This image is then sent to the Web API with the requested functionality above. The Web API forwards this information to the AI machine learning server who does the computation and returns back the results shown on Figure 81 or Figure 82 depending on the user selection.

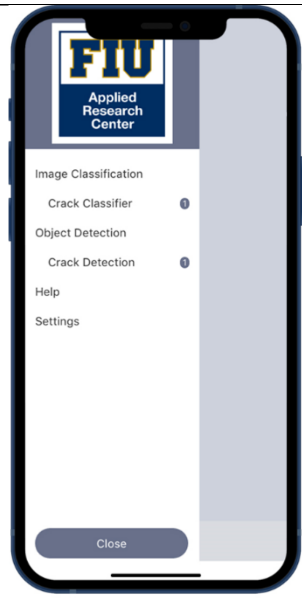

Figure 79. mobile app menu.

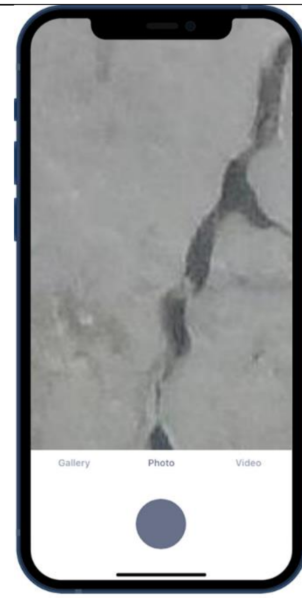

Figure 80. mobile app showing image capture.

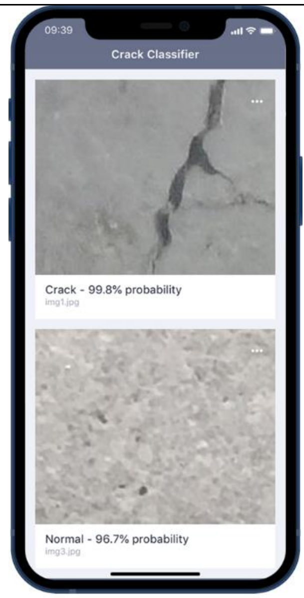

Figure 81. mobile app crack classifier feature.

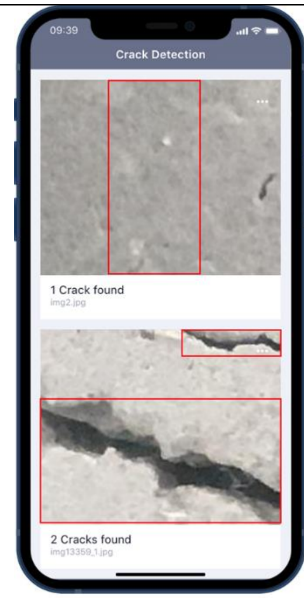

Figure 82. mobile app crack detection feature.

Subtask 6.6: Conclusions

The successful deployment of the mobile app provided by TensorFlow using TensorFlow Lite allowed the team to explore the possibility of deploying the custom-made model.

Subtask 6.6: References

[3] Android image classification example. Source:

https://github.com/tensorflow/examples/tree/master/lite/examples/image_classification/android.

Subtask 6.7: Research and Prototype Deployment of a Web Service API framework for AI Deep Learning Model (Completed)

Subtask 6.7: Introduction

FIU researched the development and deployment of the prototype of an AI Deep Learning model on a Web Service API framework for crack detection in a D&D facility. The idea was to expose the already built AI Deep Learning model as a service so that it can be consumed by multiple clients to perform predictions. In theory, the structure images can be collected (possibly using a mobile device) and sent to the web service which in turn will communicate with the AI model running on the cloud. The model processes the image(s) using prebuilt machine learning and deep learning models to determine the crack that exists in the image (crack detection). This AI model service prototype was deployed on the web so that it could be access by the mobile application.

Subtask 6.7: Objectives

The objective is to design and develop a Web API service that will be used by the mobile app to deploy AI models.

Subtask 6.7: Methodology

FIU researched the development and deployment of the prototype of an AI Deep Learning model on a Web Service API framework for crack detection in a D&D facility. The objective was to expose the already built AI Deep Learning model as a service so that it can be consumed by multiple clients to perform predictions. In theory, the structure images can be collected (possibly using a mobile device) and sent to the web service which in turn will communicate with the AI model running on the cloud. The model processes the image(s) using prebuilt machine learning and deep learning models to determine the crack that exists in the image (crack detection). This AI model service prototype was deployed on the web so that it could be accessed by the mobile application.

A Web API [5] was created to expose the deep learning models to the mobile app. The API runs in a local server now and functions as a communication point between the front-end GUI and back-end process. The API can handle different kinds of requests from the mobile app. It can provide a list of all available deep learning models, do image classification, and perform object detection. Each request has a different signature, shown in Figure 83, which allows the API to correctly execute the appropriate functions.

```
Examples:
To do object detection using a model called "yolov3_crack":
'{"Action": "Object Detection", "ModelName": "yolov3_crack", "ImageData": "/9j/4AAQSkZJRgABAgAAZ........."}'

To do image classification using a model called "crack_flassifier":
'{"Action": "Image Classification", "ModelName": "crack_classifier", "ImageData": "/9j/4AAQSkZJRgABAgAAZ........."}'

To get a list of all models available for object detection:
'{"Action": "Model Names", "Type" : "Object Detection"}'

To get a list of all models available for image classification:
'{"Action": "Model Names", "Type" : "Image Classification"}'
```

Figure 83. JSON request format for the Web API.

Once the Web API receives a request, it dispatches it to a socket server listening on a specific port. The socket server has all the available models loaded in memory waiting to do inferencing on the imagery data received as shown in Figure 84.

```python
        global model_locks
        if action == "Object Detection":
            model_name = json_object["ModelName"]
            image_data_base64 = json_object["ImageData"]

            model_locks[model_name].acquire()
            result = cps.predict_base64(model_name, image_data_base64)
            model_locks[model_name].release()
        elif action == "Image Classification":
            model_name = json_object["ModelName"]
            image_data_base64 = json_object["ImageData"]

            model_locks[model_name].acquire()
            result = ccs.predict_base64(model_name, image_data_base64)
            model_locks[model_name].release()
        elif action == "Model Names":
            model_type = json_object["Type"]
            model_name_list = []
            if model_type == "Object Detection":
                model_name_list = object_detection_model_names
            elif model_type == "Image Classification":
                model_name_list = image_classification_model_names
```

Figure 84. Python code snippet for executing the desired deep learning model.

The imagery data in the JSON object is expressed as a Base64 value encoding. The socket server first decodes the imagery data and converts it into an RGB image. It then passes the image to the desired model and responds with the results in a JSON file as shown in Figure 85.

```python
In [*]:
LOCALHOST = ""
PORT = 22223
server = socket.socket(socket.AF_INET, socket.SOCK_STREAM)
server.setsockopt(socket.SOL_SOCKET, socket.SO_REUSEADDR, 1)
server.bind((LOCALHOST, PORT))
print("Server started")
print("Waiting for client request..")
while True:
    server.listen(1)
    clientsock, clientAddress = server.accept()
    newthread = ClientThread(clientAddress, clientsock)
    newthread.start()
    #break
```

```
Server started
Waiting for client request..
Connection from :  ('192.168.211.1', 60877)
exit = ends with done
(416, 416, 3)
Found 2 boxes for img
tie 1.00 (69, 254) (171, 416)
person 1.00 (17, 34) (402, 396)
0.11127810000000693
{'Result': {'Object 1': {'Class': 'tie', 'xPosition': 69, 'yPosition': 254, 'Wi
dth': 171, 'Height': 420, 'Probability': '0.99802226'}, 'Object 2': {'Class':
'person', 'xPosition': 17, 'yPosition': 34, 'Width': 402, 'Height': 395, 'Proba
bility': '0.9999268'}}}
Client at  ('192.168.211.1', 60877)  disconnected...
```

Figure 85. Socket server responding to request.

In addition, the team developed the Web Service API that allowed the mobile application to communicate with the machine learning server where the algorithms will be available. The screenshot below (Figure 86) shows the API Help page where all the methods available on the API will be exposed. This Help page will provide documentation for users/developers, so they can use the available methods.

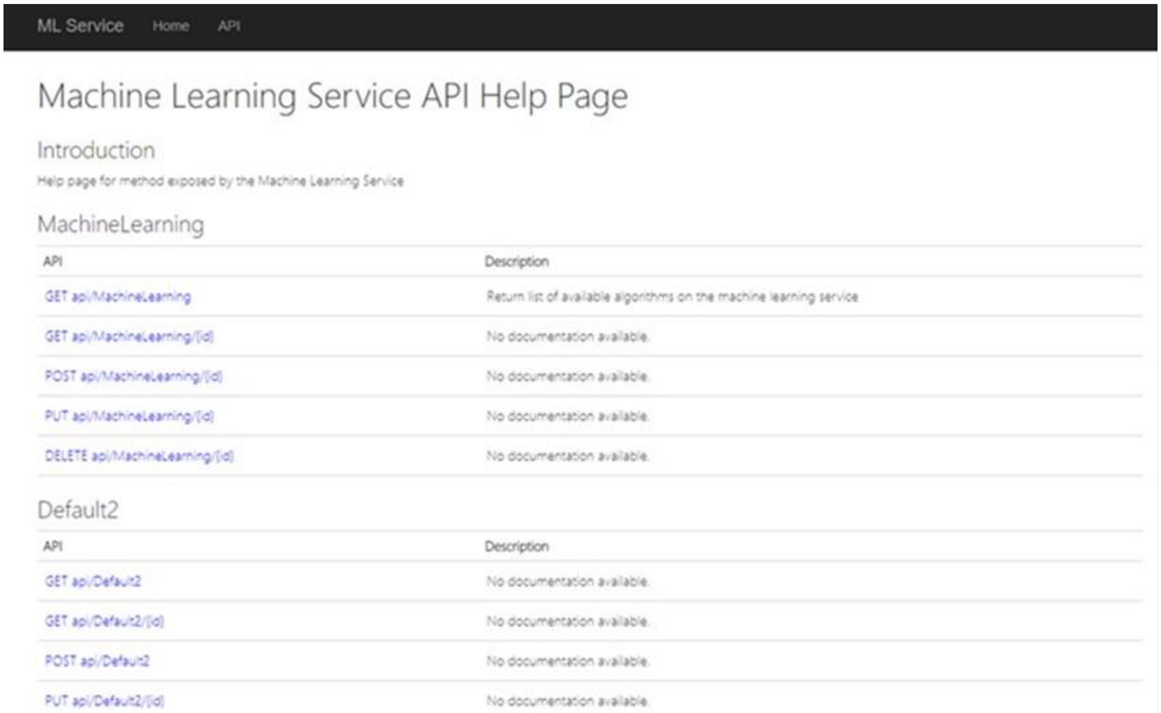

Figure 86. Machine Learning Web Service API Help page.

The team made substantial progress on the Web Application Programming Interface (API) and Object detection and image classification. Communication between the public Web API and the machine learning server happens using socket programming. Data is transmitted between them using JavaScript Object Notation (JSON) expressed as a string. The Python built in library “json” is used to decode the messages and execute the intended commands. During a testing phase, it was noticed that an exception was being thrown by the machine learning server when decoding a JSON file. The exception, shown in Figure 49, is thrown when the byte order marker (BOM) is present at the beginning of the file.

```
json.decoder.JSONDecodeError: Unexpected UTF-8 BOM (decode using utf-8-sig):
```

Figure 49. JSON decoder error when the file contains the byte order marker (BOM).

BOM is a magic number (e.g., U+FEFF) at the beginning of a text stream that can signal several things to a program. It is common to use BOM to communicate the endianness of the text, whether the text is encoded using Unicode, or which Unicode character encoding was used. BOM use is optional, and a JSON implementation is not required to accept it. Since it is not required to be accepted, the unexpected presence of the marker interferes with the use of UTF-8 encoding. One way to mitigate the error is to decode the text message using a Python built in library named “codecs” with the encoding flag set to “utf-8-sig”. Using this approach, shown in Figure 50, the text stream is decoded correctly and BOM is removed. After BOM is removed, it can be decoded into a JSON object using the “json” library.

```
decoded_content = codecs.decode(content, 'utf-8-sig')
```

Figure 50. Using the built in Python “codecs” library to remove BOM from a text stream.

Postman [4], an API platform for building and using APIs, was used to send messages between the Web API and the machine learning server. Currently, there are four actions/commands that can be given to the API. The commands and their description are described in Table 14.

Table 14. API Commands and their Description

Command	Description
Model Names: Object Detection	Returns a list of all models for object detection.
Model Names: Image Classification	Returns a list of all models for image classification.
Object Detection	Predicts the objects and their location in an image.
Image Classification	Predicts the image category.

All four commands were successfully tested using Postman. The first command, using the API called GetImageResult, executes the object detection command (Figure 51) on the machine learning server. The top part of Figure 51 shows the text string which is sent to the server containing the action desired, the model to use, and the byte-encoded image to predict on. The bottom part of Figure 87 shows the result sent back from the server formatted as a JSON file.

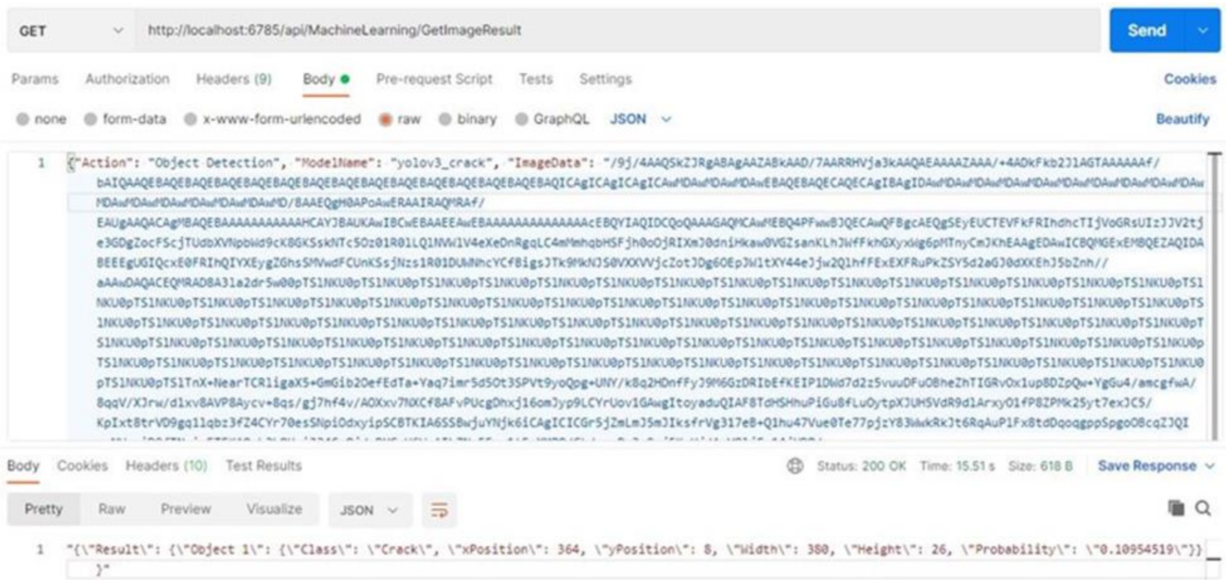

Figure 87. Postman executing the object detection command.

The second command, also using the GetImageResult API, executes the image classification command (Figure 88) on the machine learning server. The layout of the image is the same as mentioned above. The difference is in the response from the server where it contains the image category and the probability of prediction.

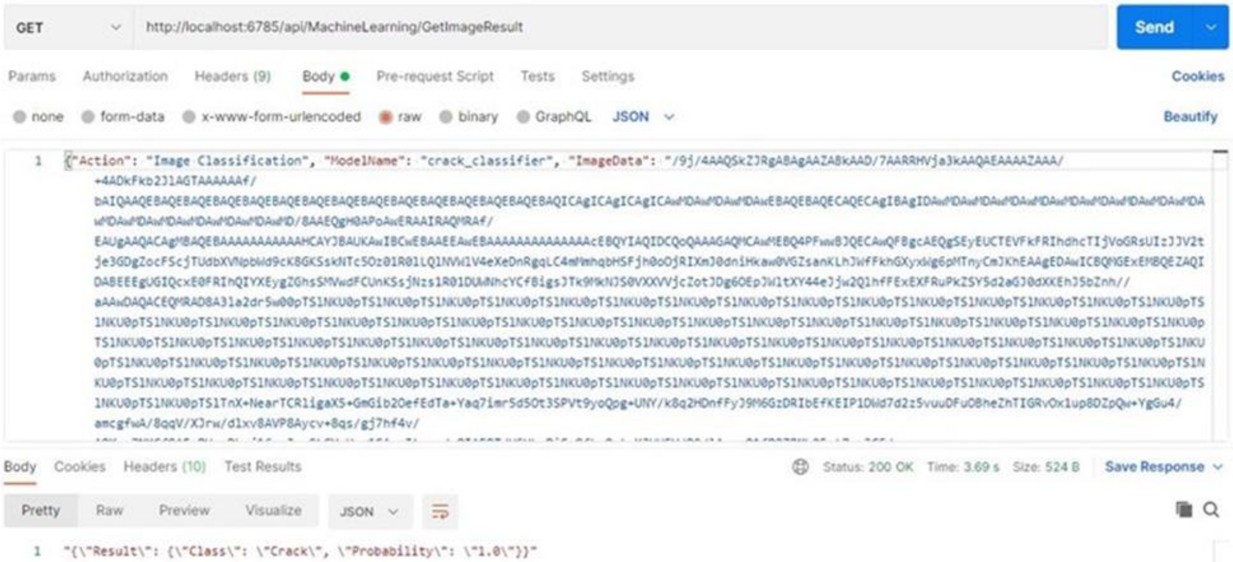

Figure 88. Postman executing the image classification command.

The other two commands, used for retrieving a list of model names available to do object detection and image classification, are shown in Figure 89 and Figure 90 respectively

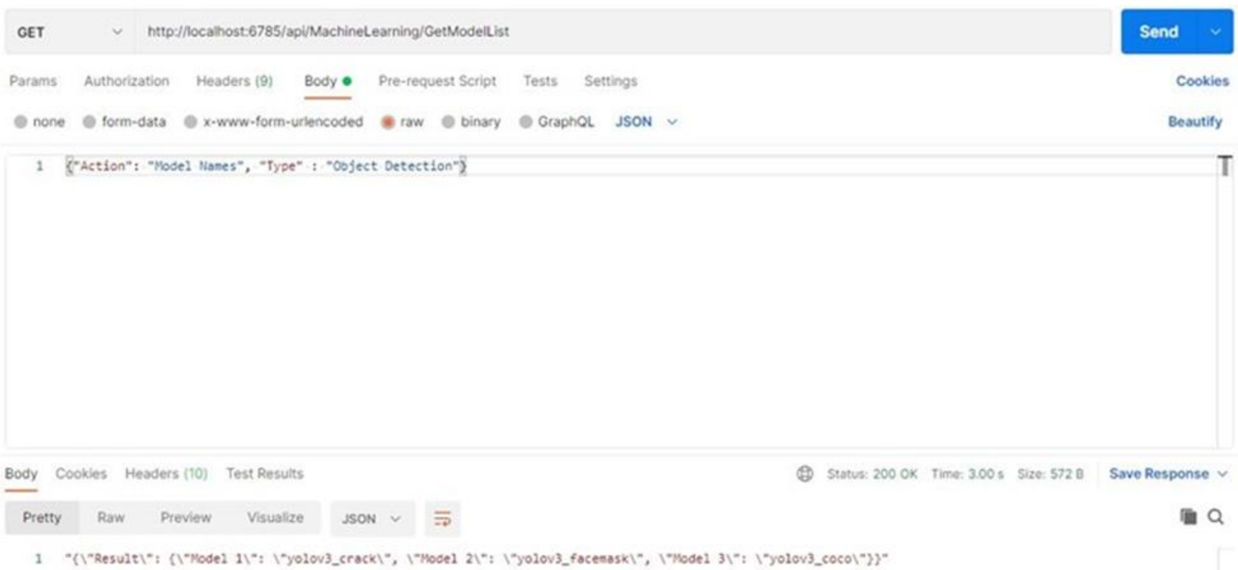

Figure 89. Postman executing the command to get a list of all object detection models available.

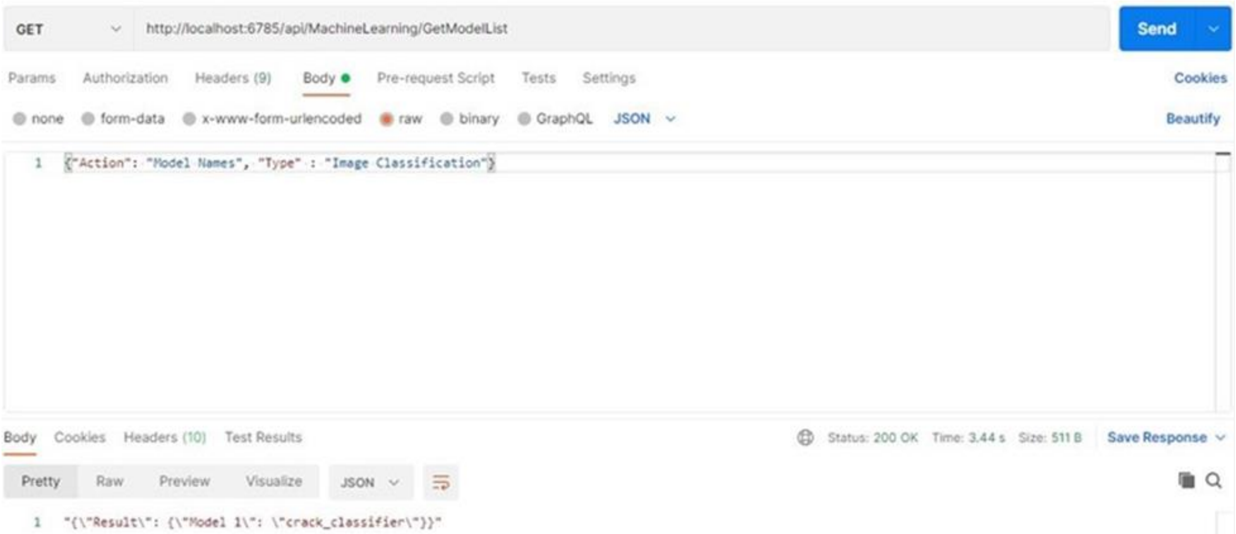

Figure 90. Postman executing the command to get a list of all image classification models available.

Subtask 6.7: Results and Discussion

The Application Program Interface (API) was completed and running on the stage server. The welcome page for the API, shown in Figure 91, shows the navigation options which users can use.

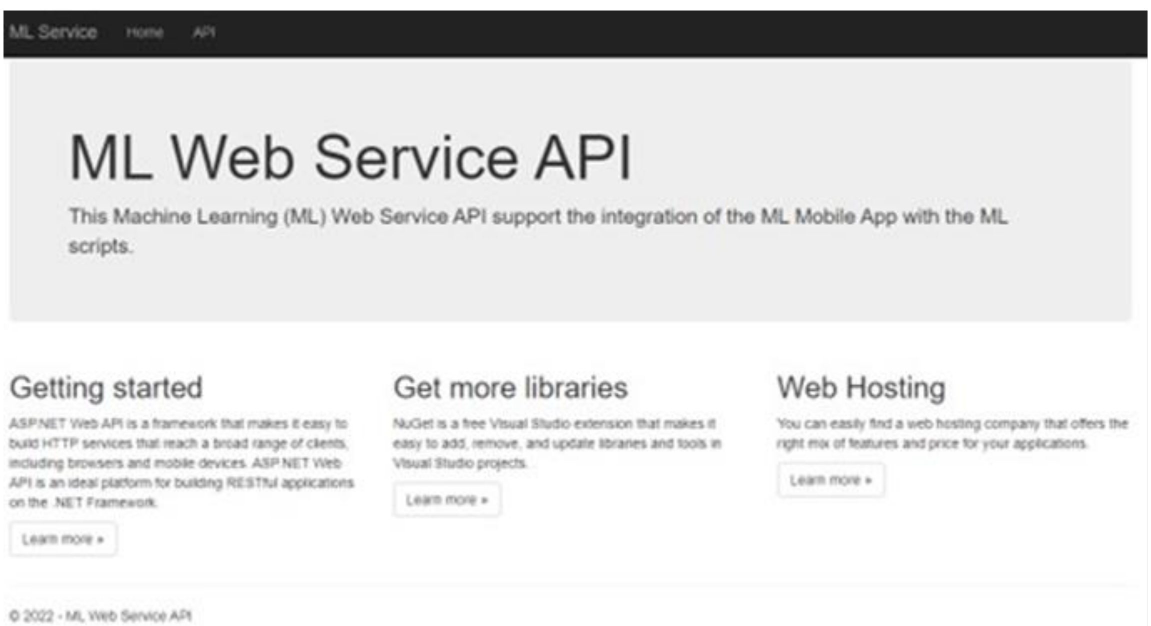

Figure 91. Machine Learning Web API welcome page.

Navigating to the API tab shows the available methods which are currently implemented and in use as shown in Figure 92. Clicking on each API method opens a page with specific information and details on how to use it. The page contains the end point location, whether it is a PUT or GET hyper-text transfer protocol (HTTP) command, any unique resource identifiers (URI), the body parameters (e.g., Action and Type), a sample request format, and example response information, as shown in Figure 93.

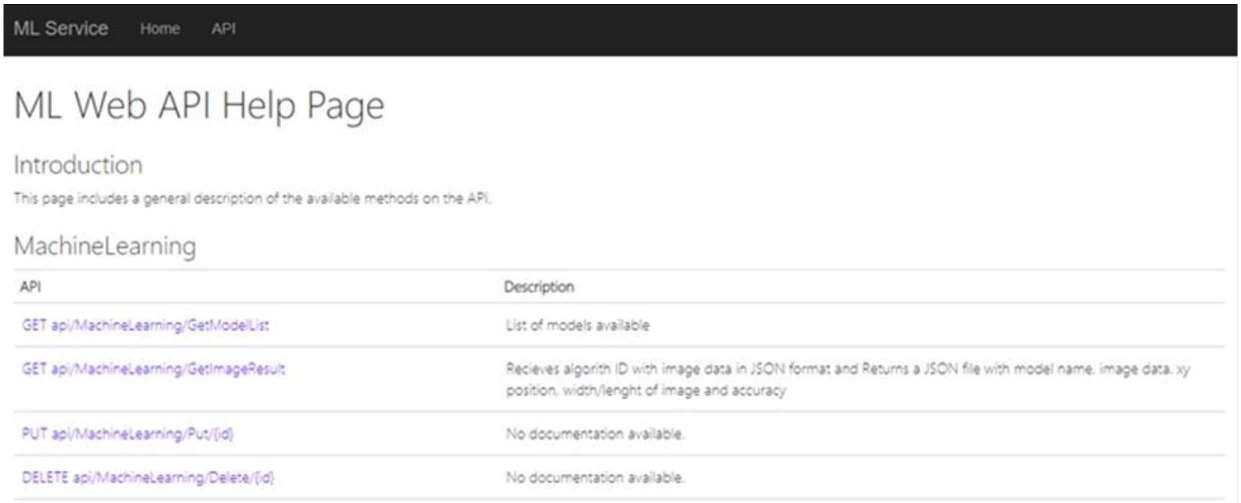

Figure 92. Current methods available in the Machine Learning Web API.

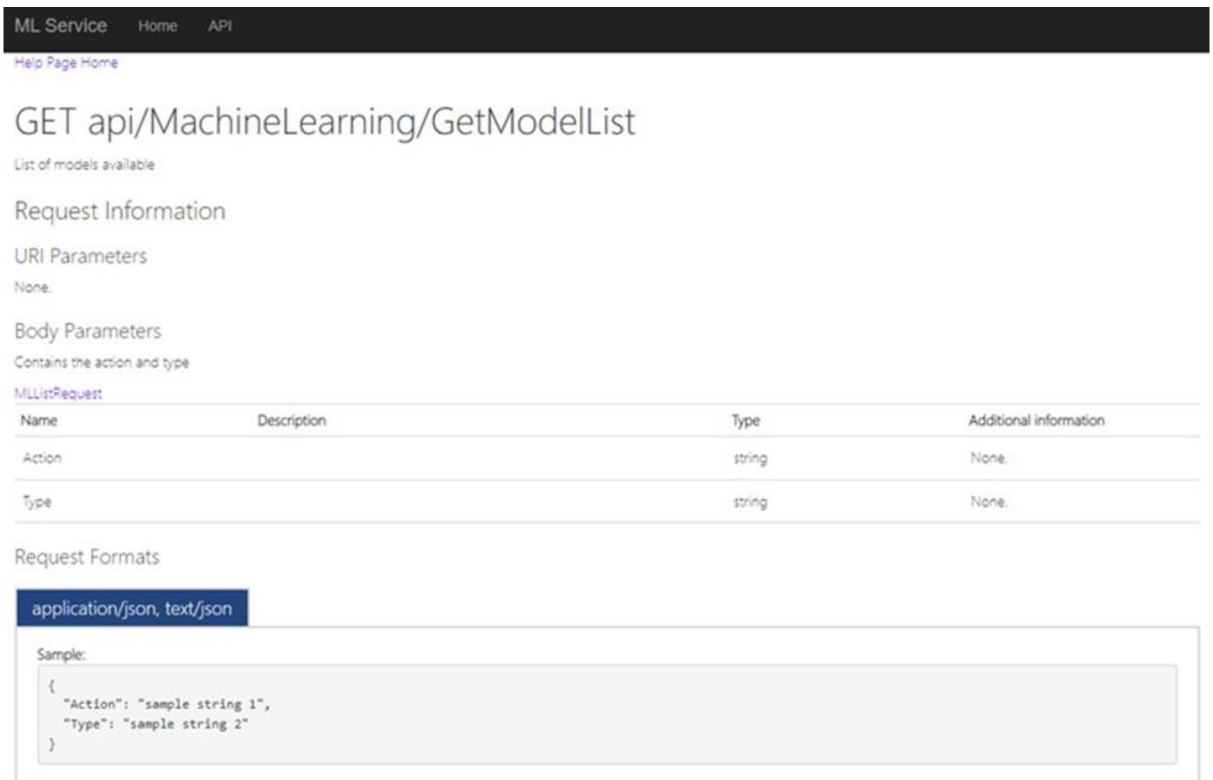

Figure 93. Information and usage page for the GetModelList.

The first method, GetModelList, is used to retrieve a list of all available models. To use it, two parameters are required. The first parameter is the "Action", and the second parameter is the "Type". In this example the "Action" is "Model Names", and the "Type" is either "Image Classification" or "Object Detection". The second method, GetImageResult (Figure 94), is used to make predictions on an image. This method has three parameters (e.g., Action, ModelName, and ImageData). The "Action" here refers to whether object detection or image classification is requested. The "ModelName" is one of the returned model names from the GetModelList method. Lastly, "ImageData" is a byte representation of the raw image that needs to be processed.

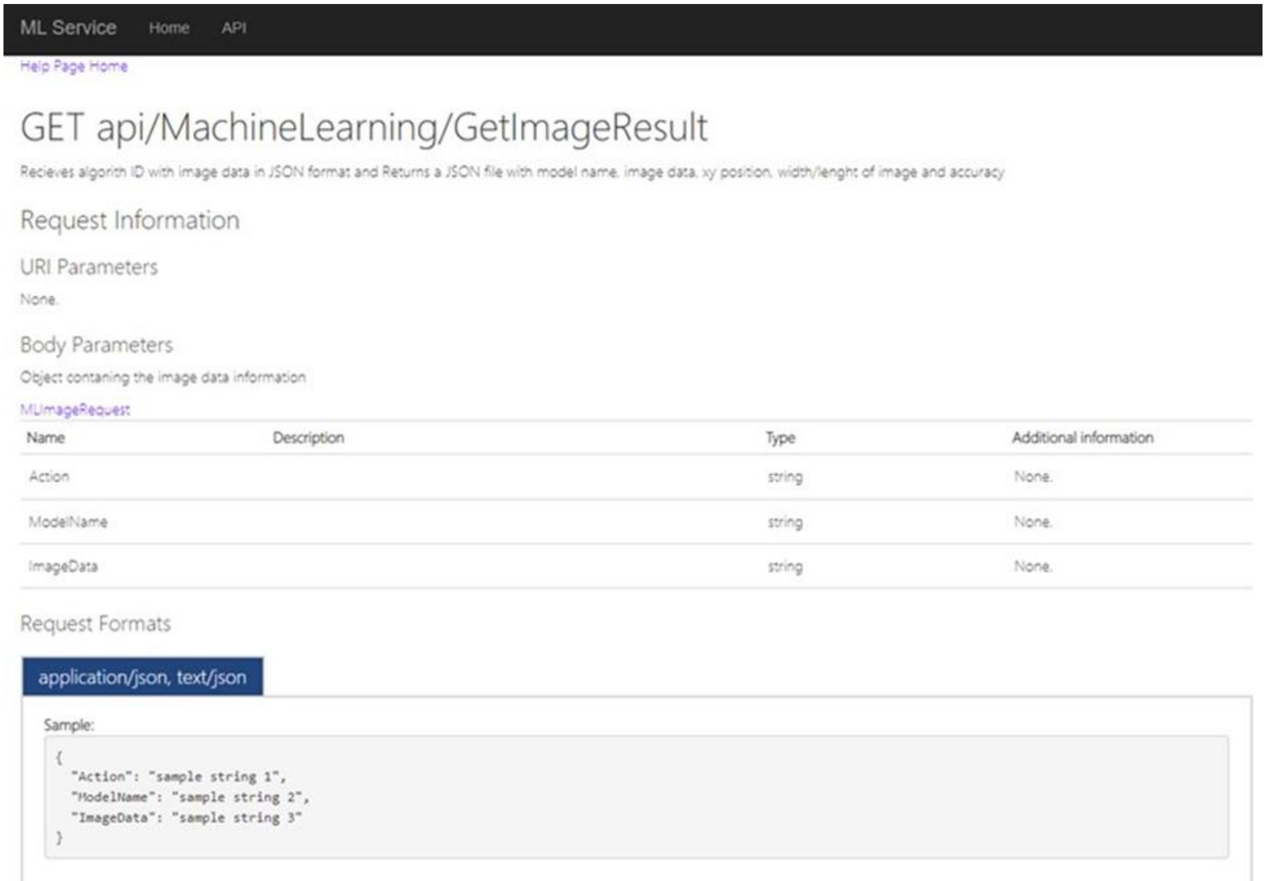

Figure 94. Information and usage page for the GetImageResult.

Subtask 6.7: Conclusions

To make the models available on the mobile device, the team had to design a Web API service, so the mobile app could communicate with the machine learning server to perform the predictions. The following figure (Figure 95) shows how each of the technologies work together. The mobile application snaps a picture of an infrastructure and sends the image data and command inside a message formatted using JSON to the Web API using HTTP GET protocol. The Web API forwards the message to the Machine Learning platform where the convolutional neural network determines if the image contains a crack. The results are sent back to the mobile app via the Web API using JSON, which uses the data to display the results to the user.

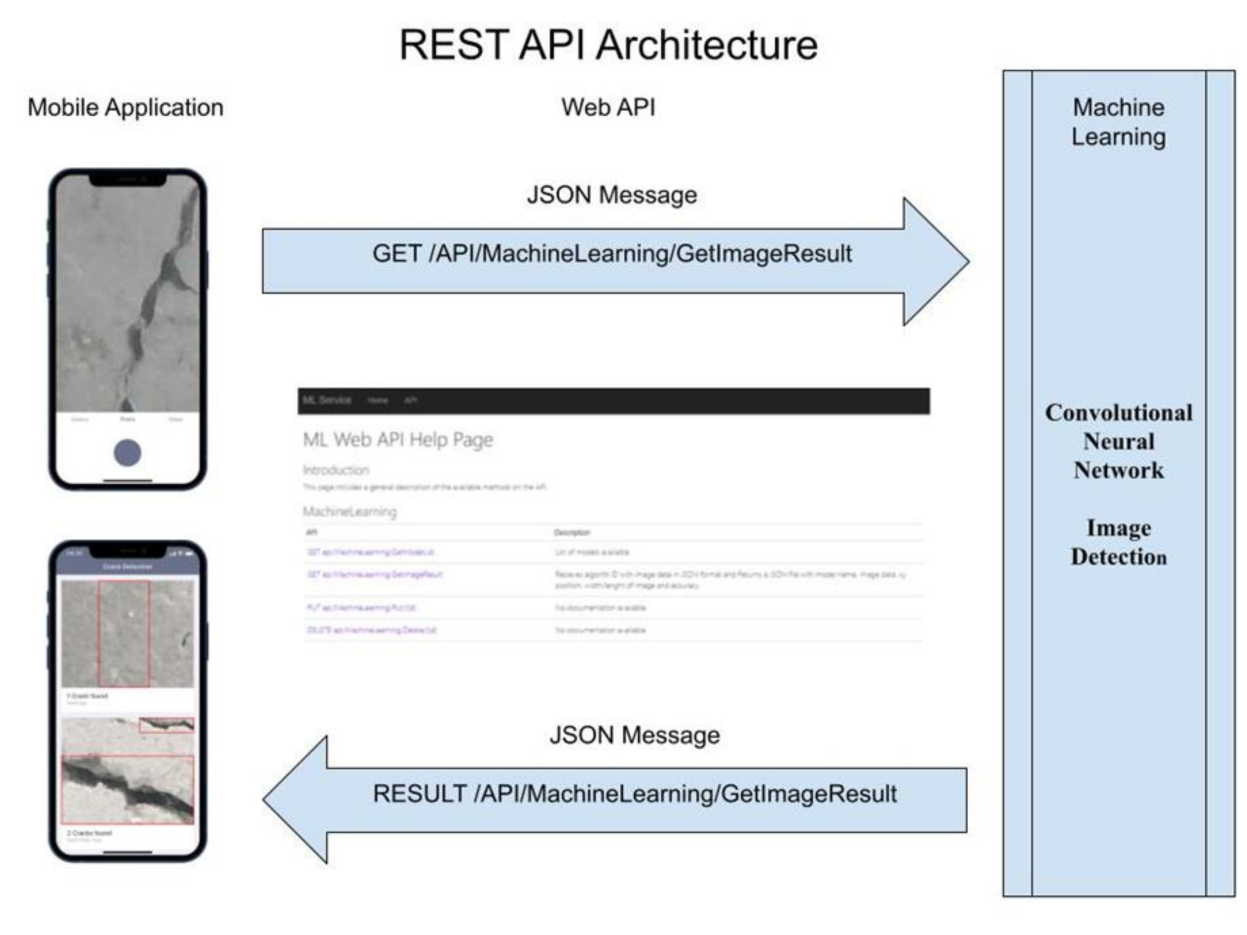

Figure 95. REST API architecture.

Overall Conclusion:

Task 6 was successfully completed (Deliverable 2021-P3-D7) on September 9, 2022. Under Task 6 specific applications of AI and machine learning algorithms to solve DOE-EM problem sets and challenge areas. These algorithms and models were investigated for their ability to assess the structural integrity of aging facilities in support of ongoing surveillance and maintenance (S&M) across the DOE complex.

These technologies were all effectively implemented for object detection to solve EM challenges in surveillance and maintenance of the D&D facilities. Together, they can serve as an early notification to facility maintenance personnel to pay attention to the identified cracks of D&D structure and deployed on mobile devices.

All the algorithms and models developed under Task 6 for crack detection will be used in proposed Task 9, Waste Processing-Waste Identification & Segregation in FIU Year 3.

Subtask 6.7: References

[4] Postman. (n.d.). Retrieved December 9, 2022, from https://www.postman.com/postman/

[5] Wikimedia Foundation. (2022, November 16). *Web api*. Wikipedia. Retrieved December 9, 2022, from https://en.wikipedia.org/wiki/Web_API

TASK 7: AI FOR EM PROBLEM SET (SOIL AND GROUNDWATER) - EXPLORATORY DATA ANALYSIS AND MACHINE LEARNING MODEL FOR HEXAVALENT CHROMIUM [CR (VI)] CONCENTRATION IN 100-H AREA (PNNL)

Subtask 7.2: Data Pre-Processing and Exploratory Data Analysis to Evaluate the Chromium Concentration in the Samples

Subtask 7.2: Introduction

The northcentral part of the U.S. Department of Energy (DOE) Hanford Site contains the 100-HR-3 Groundwater Operable Unit (OU). Historical operations in this OU resulted in the contamination of soil and groundwater with various contaminants [1]. Hexavalent chromium Cr(VI) is one of the primary contaminants at the Hanford Site 100-Area. This site is adjacent to the Columbia River which makes the associated groundwater and surface water vulnerable to Cr(VI) contamination. To monitor the Cr(VI) level in the surface water and groundwater, aquifer tubes were installed on the Columbia River shoreline and groundwater monitoring wells were installed in the inland area respectively. For effective sampling based on the nature of the water table in the site and other influential geophysical processes in the area, the groundwater monitoring wells are frequently sampled whereas the aquifer tubes are sampled once a year in the Fall. Thus, the resulting dataset entails exploratory analysis and pre-processing to address such imbalanced sampling for the dataset to be used in the Artificial Intelligence/Machine Learning (AI/ML) modeling. In addition, the manual sample collections from the site and lab analyses to create the samples in the dataset, introduce irregularities in the sample-to-sample time interval in the dataset. Moreover, this manual sampling may also create missing value problems in the dataset. These missing value problems and temporal irregularities also require special steps in the pre-processing and exploratory data analysis stage to make the dataset usable for AI/ML modeling [2]. The Pacific Northwest National Lab curates the dataset for the Hanford Site and archives it online for public access in the database named PHOENIX. The demonstration dataset used in this research was collected from the above database

Subtask 7.2: Objectives

The main object of this subtask is to examine the dataset to explore its properties and irregularities by applying AI/ML algorithms on it. It is an essential step for machine learning modeling since it ensures that the dataset does not have any missing values, NAN values, outliers or other erroneous values which is also applicable to the Hanford site dataset.

Subtask 7.2: Methodology

The major steps for data preprocessing can be broken down into 4 primary steps. As depicted by Figure 96, the steps are data points segregation, statistical analysis and dataset cleansing, interpolation to handle missing value problems, aquifer tube adjacent groundwater monitoring well identification and finally smoothing the time series with rolling mean. The collected dataset for the Hanford site contains a lot of different types of contaminants sampling data. However, for the Cr(VI) spatiotemporal relationship exploration between surface water and groundwater, this analysis was focused on aquifer tube and groundwater monitoring samples in the dataset. Thus, the data points were filtered from the dataset based on their type of “groundwater” or type of "aquifer tube" and then segregated them into individual time series. Afterward, statistical analysis was performed to get an insight into the dataset. The missing value problem in the dataset was handled using linear interpolation. In the subsequent AI/ML modeling, shoreline or aquifer tube adjacent groundwater monitoring wells were used as the proxy due to the higher data density of the groundwater monitoring wells. Thus, the aquifer tube to groundwater monitoring wells adjacency relations were identified as the next step in the pre-processing process using the spatial information about the time series. Finally, each timeseries was smoothed using a rolling mean window of 90 days.

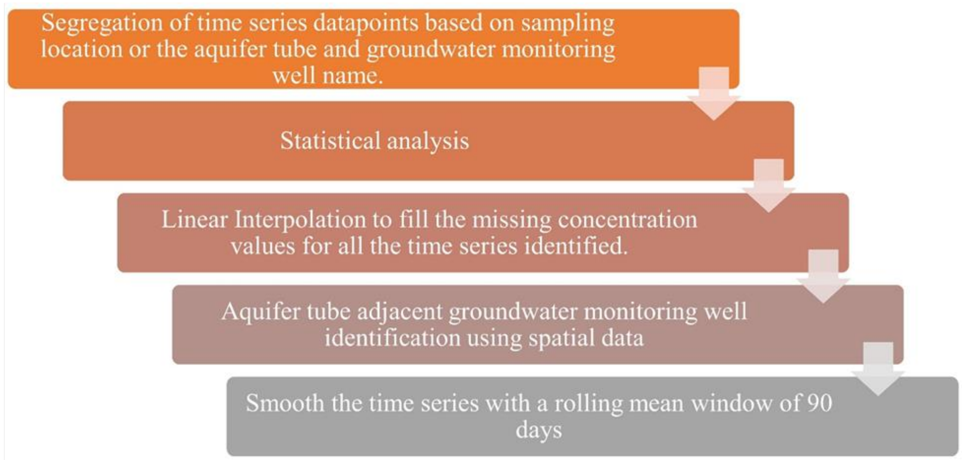

Figure 96. Steps of data pre-processing and exploratory data analysis.

Subtask 7.2: Results and Discussion

The data pre-processing and data exploration algorithm researched and developed for the Hanford site dataset identified 87 well locations that have sufficient data points to be used in the AI/ML modeling. However, four of them, specifically 699-97-48C, 199-D8-54B, 199-D5-141, and 699-97-61, were eliminated from the chosen subset as those four groundwater wells reside in the Ringold Upper Mud (RUM) and the concentrations in the RUM wells and the ones in the unconfined aquifer tubes were not supposed to be related. Through additional preprocessing, out of the 83 wells, 41 wells were left that were of type "groundwater sample" and the other wells removed were all wells of type "extraction well". The dataset timeseries spanned through the year 2015 to 2019 inclusive and resulted in 1,826 dates that were then divided into 50 date ranges, each of which lasted one month and six days. Each date range contained the mean of the hexavalent chromium concentration values for all the groundwater wells that were being analyzed. In Figure 97 and Figure 98 below respectively, a boxplot and histogram show the concentration distributions of the 41 wells used in the modeling.

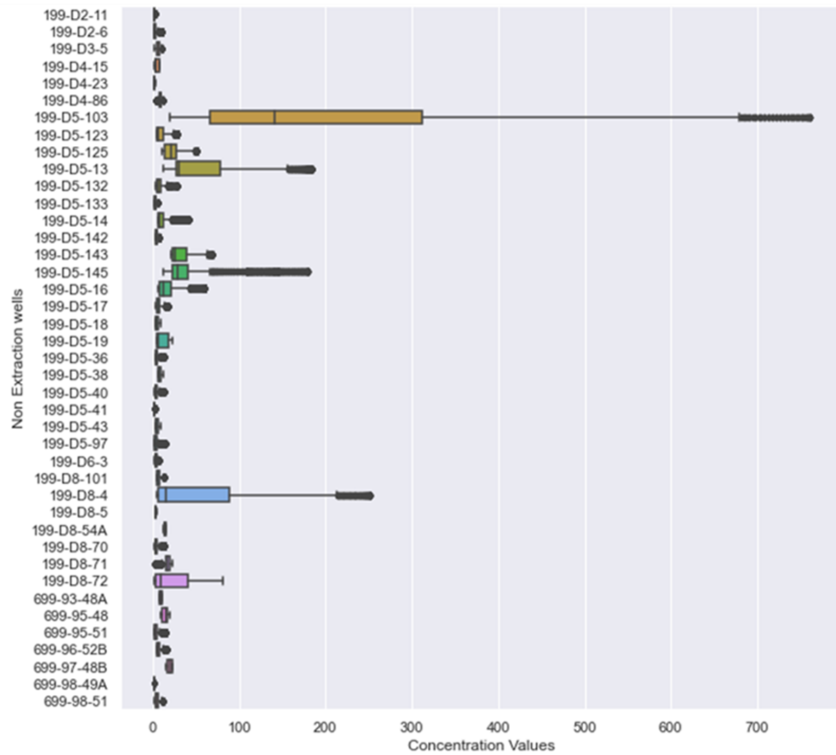

Figure 97. Boxplot for 41 non-extraction wells used in AI/ML modeling.

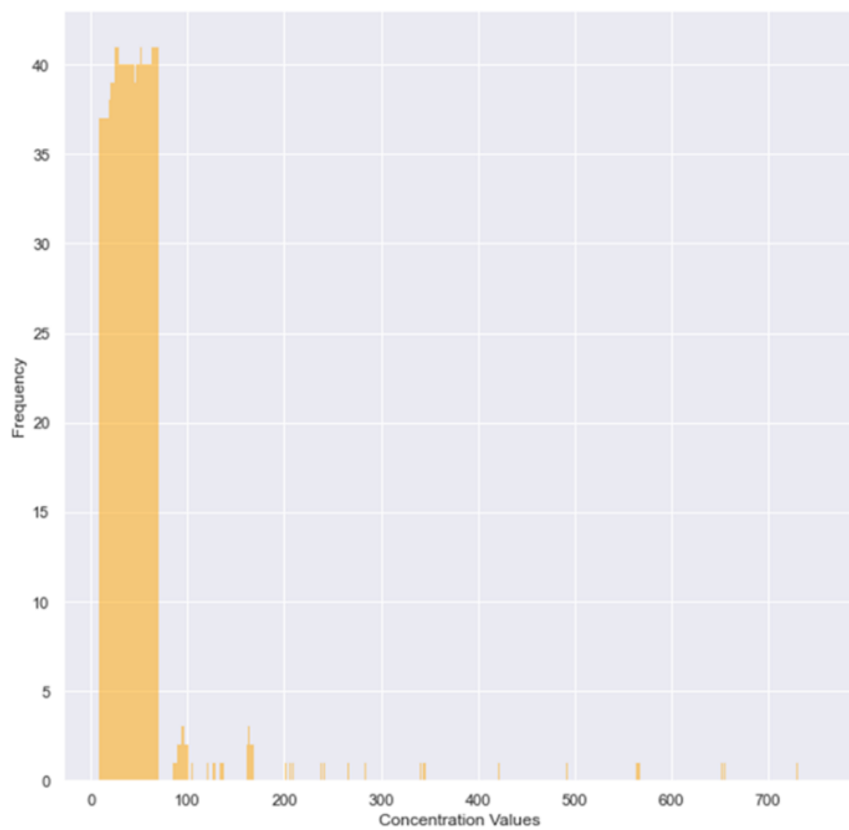

Figure 98. Histogram visualization for 41 non-extraction wells used in AI/ML modeling. It is noticeable that most wells of type "non-extraction" have concentration values centered around 0 to 80.

Aquifer tubes timeseries were used as the target variables in the AI/ML approach for spatiotemporal relationship exploration between inland monitoring wells and shoreline hexavalent chromium [Cr(VI)] concentrations. However, the aquifer tubes at the DOE Hanford Site 100 Areas are usually sampled once a year during Fall whereas the groundwater wells are sampled more frequently as depicted by Figure 99. The aquifer tube interpolated timeseries presented by the red bold line has far fewer original data points, depicted by the red dots, than the number of original data points available for each groundwater well's timeseries, depicted by the black dots. To mitigate this skewed dataset issue, the nearest corresponding groundwater well of each aquifer tube is considered as a proxy target variable in the AI/ML model which is expected to better represent the actual phenomenon of the spatiotemporal relationship. As an instance, the proxy groundwater well 199-D8-68's time series for the representative aquifer tube DD-16-4, is also plotted in Figure 99. It is apparent that there is a better subjective similarity in this representative predictor/target combination when the nearest groundwater water well's time series is considered as a proxy target variable.

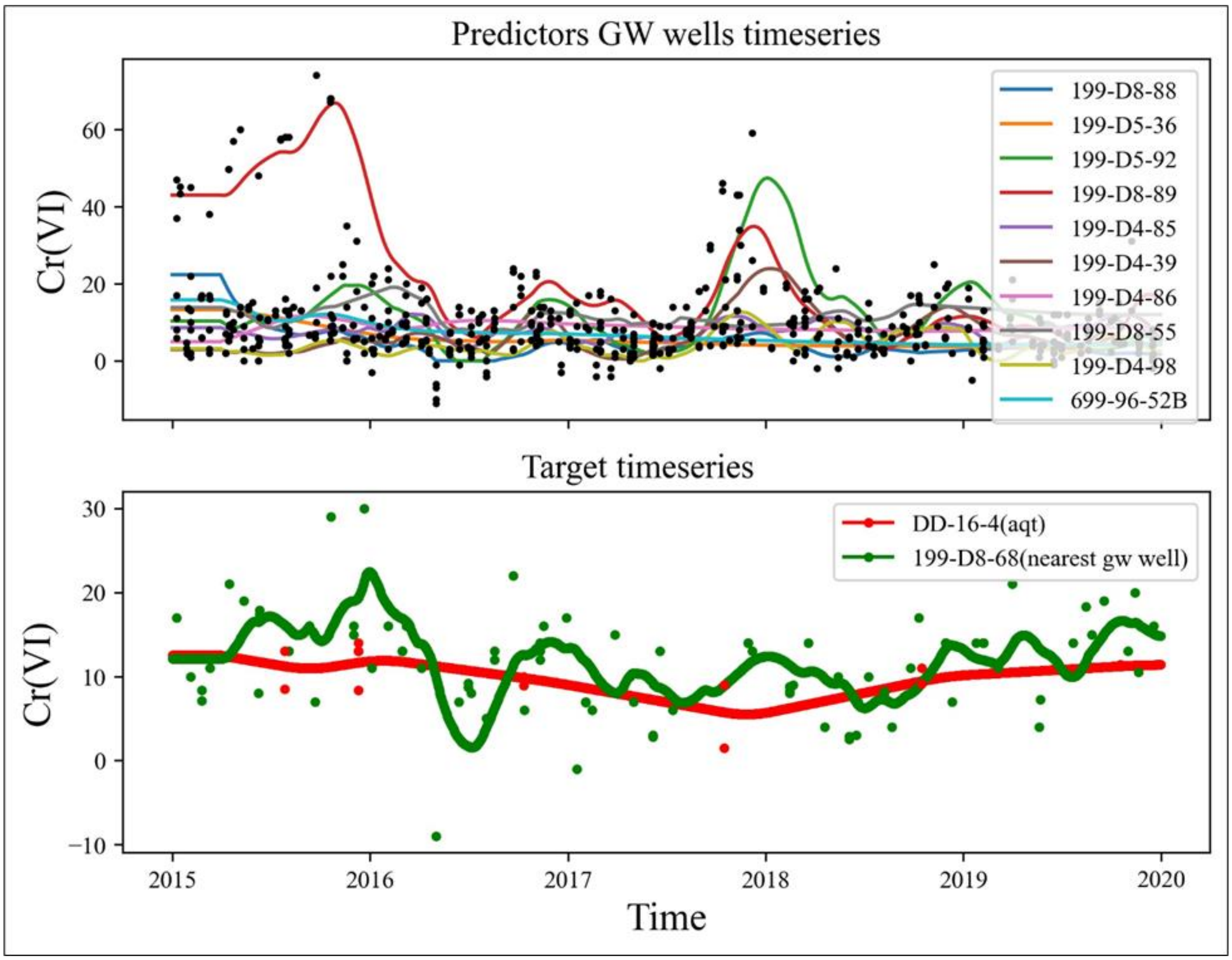

Figure 99. The nearest groundwater wells as the proxy target variable for the AI/ML modeling.

The identified nearest groundwater wells corresponding to the shoreline aquifer tubes based on the shortest Euclidean distances are presented in Figure 100 for a representative operable unit. It has been observed that for some groups of aquifer tubes, the nearest corresponding groundwater wells coincide.

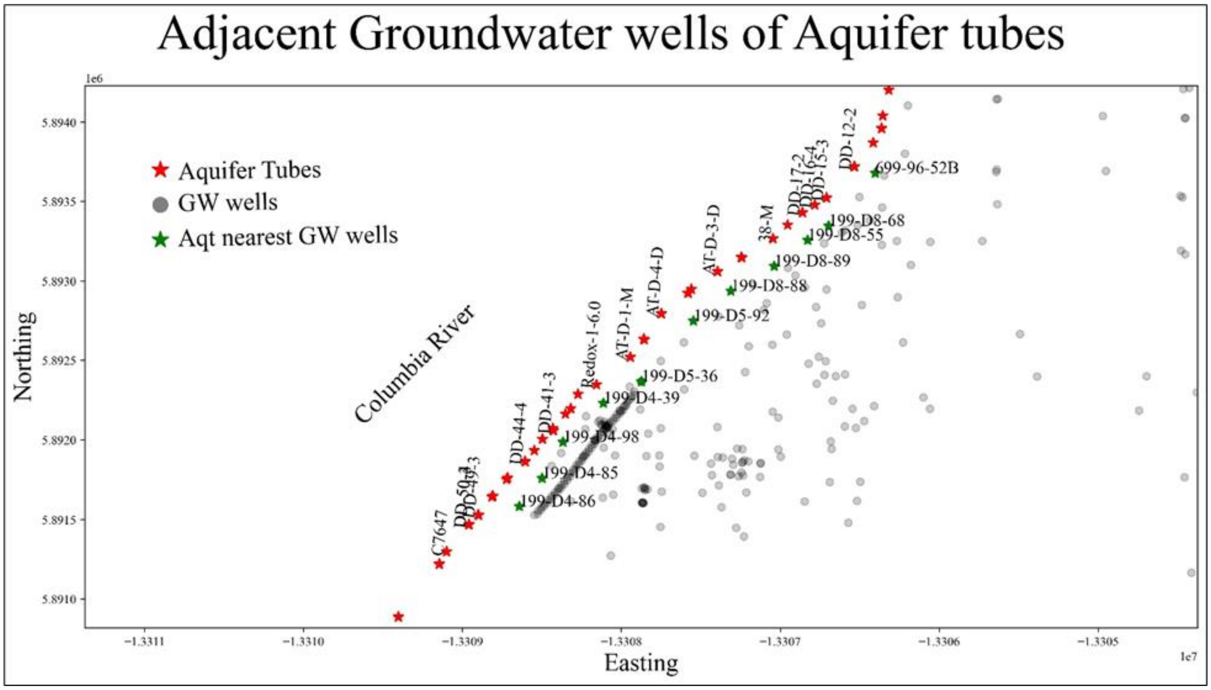

Figure 100. The identified nearest groundwater wells corresponding to the shoreline aquifer tubes.

The identified adjacency relation between the aquifer tubes and the groundwater wells for the OU 100-HRD is presented in Table 15.

Table 15. Shoreline Aquifer Tubes and Identified Nearest Groundwater Wells

Shoreline Aquifer tubes	Nearest groundwater wells
'38-M',	199-D8-89
'AT-D-1-M'	199-D5-36
, 'AT-D-3-D',	199-D8-88
'AT-D-4-D',	199-D5-92
'C7647',	199-D4-86
'DD-12-2',	699-96-52B
'DD-15-3',	199-D8-68
'DD-16-4',	199-D8-68
'DD-17-2',	199-D8-55
'DD-41-3',	199-D4-98
'DD-44-4',	199-D4-85
'DD-49-3',	199-D4-86
'DD-50-3',	199-D4-86
'DD-50-4',	199-D4-86
'Redox-1-6.0	199-D4-39

The directional and distance-wise spatial segmentation for AI/ML modeling predictor-target selection was followed as the current approach depicted in Figure 101. Currently, 500 m to 1500 m for distance and 210° to 390° for directional segmentation were considered.

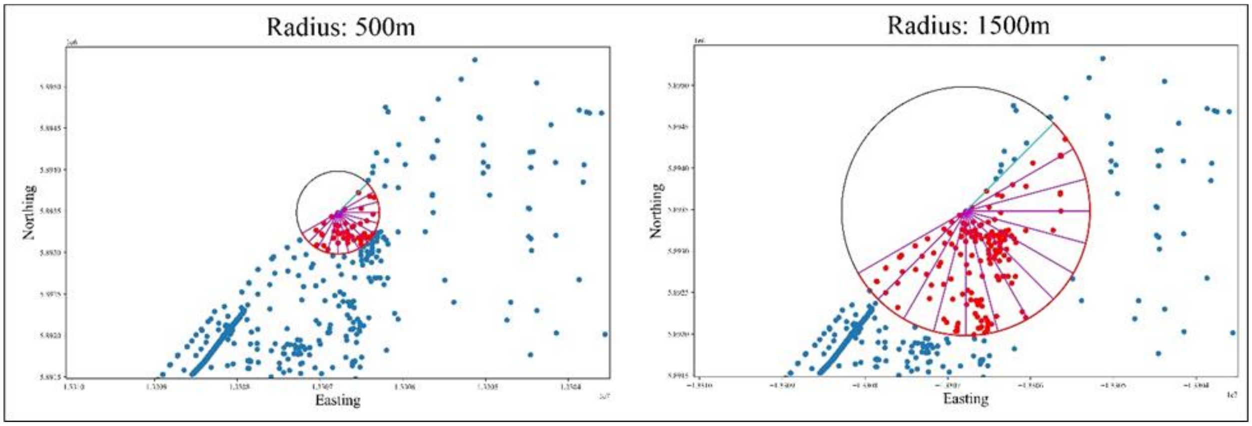

Figure 101. The directional and distance-wise spatial segmentation for AI/ML modeling predictor-target selection.

A demonstration of the capability of the pre-processing algorithm researched and developed is depicted in Figure 102 to identify input and output timeseries using spatial information given the radius and the direction of any specified area. As an instance, the input timeseries identification taking the groundwater well 199-D4-85 as a target timeseries in the AI/ML modeling is depicted in Figure 102.

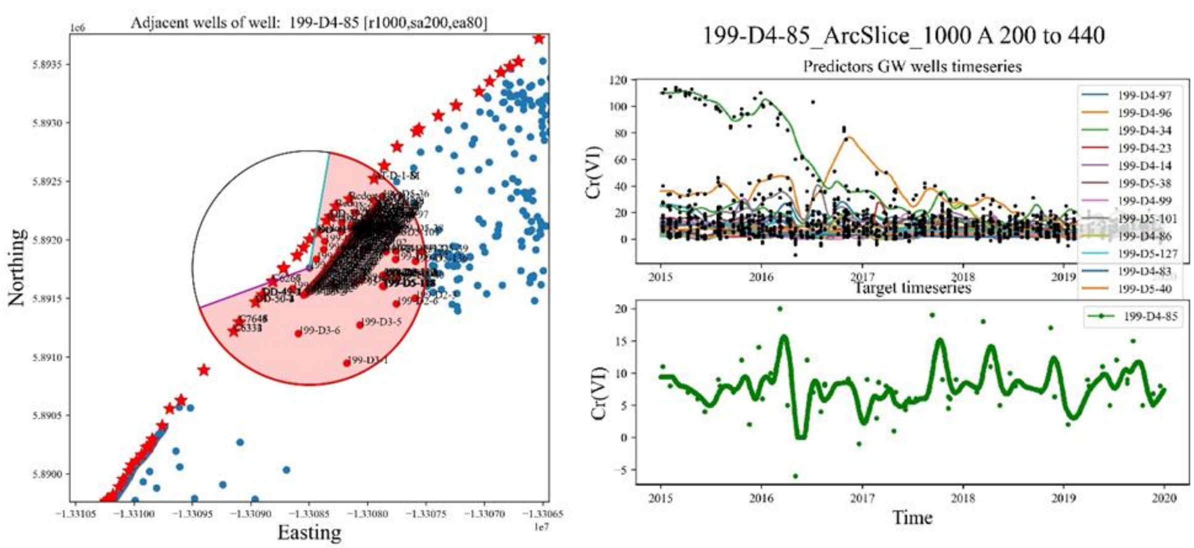

Figure 102. Data preprocessing algorithm result for near shoreline groundwater well 199-D4-85.

Subtask 7.2: Conclusions

Successful implementation of AI/ML algorithms to solve any problem entails a quality dataset with a balanced data density in the input and output variables. The data pre-processing and data exploration algorithms researched and developed under this subtask fulfill this requirement for the AI/ML application toward spatiotemporal relationship identification in the subsequent subtask

Subtask 7.2: References

[1] Peterson, Reid A., Edgar C. Buck, Jaehun Chun, Richard C. Daniel, Daniel L. Herting, Eugene S. Ilton, Gregg J. Lumetta, and Sue B. Clark. "Review of the scientific understanding of radioactive waste at the US DOE Hanford Site." *Environmental science & technology* 52, no. 2 (2018): 381-396.

[2] Kaur, Harsurinder, Husanbir Singh Pannu, and Avleen Kaur Malhi. "A systematic review on imbalanced data challenges in machine learning: Applications and solutions." *ACM Computing Surveys (CSUR)* 52, no. 4 (2019): 1-36.

Subtask 7.3: Research and Analysis of Groundwater and Surface Water Spatiotemporal Relationship with AI models (NEW)

Subtask 7.3: Introduction

To keep the Cr(VI) level within the acceptable limit, continuous monitoring and cleanup efforts are ongoing at the Hanford Site since the late 1990s. Pump-and-treat, in situ redox manipulation, soil flushing, and closely monitored natural attenuation are some of the cleanup techniques used to rehabilitate this contaminated site [1,2]. Six operable units (OU) are designated for these cleanup activities at this location: 100-BC, 100-KR, 100-NR, 100-HRD, 100-HRH, and 100-FR. Recent reports showed that significant progress has been made in cleaning up Cr(VI) at most of these operable units' groundwater cleanup targets. However, the cleanup target for surface water Cr(VI) has not been achieved for most of these operable units. Thus, there is ongoing research to explore the transport dynamics of the Cr(VI) in the groundwater and surface water for any probable relationship. The very dynamic character of the Columbia River and the confusing influence it has on the measured variables at the 100-Areas make it exceedingly difficult to explore any patterns in the spatiotemporal dataset through data analysis. Artificial intelligence (AI) and deep learning are two examples of data-driven technologies that can be very helpful in discovering patterns in this case where the pattern-revealing properties in the dataset may not be obvious.

Subtask 7.3: Objectives

The overall goal of this research is to couple long-term monitoring data of hexavalent chromium [Cr(VI)] with AI/ML models to identify temporal and spatial relationships of subsurface chromium transport.

Subtask 7.3: Methodology

In this research, using the historical dataset of groundwater monitoring data and leveraging artificial intelligence/machine learning (AI/ML), a method for spatiotemporal relationship exploration was developed. In this method, AI/ML modeling was applied to the time series data to extract relational information, such as the feature importance of the time series as a predictor. In machine learning, feature importance refers to a score assigned to an input feature based on how useful that feature was in predicting the target variable. From the various sources of the feature importance, decision tree-based importance calculation was chosen for the current AI/ML modeling approach. Specifically, a Random Forest ensemble algorithm was used which constructs many individual decision trees at the training phase. Each of those decision trees is a set of internal nodes and leaves where the features are selected based on some criteria, such as Gini impurity or information gain in the classification task and mean squared error (MSE) reduction in the regression task. For each feature, the average of the metric of selection criterion can be collected from the decision trees. Then the average over all the trees in the RF model would be the measure of the feature importance score for the features or predictor time series. In the spatial part of the method, distances between the predictors and target variable in the AI/ML were used as a metric. For the information fusion of this spatial metric to the temporal features from the AI/ML model, regression analysis was used.

Subtask 7.3: Results and Discussion

In the AI/ML approach for spatiotemporal relationship exploration between inland monitoring wells and shoreline hexavalent chromium [Cr(VI)] concentrations, the Columbia River shoreline adjacent groundwater wells' timeseries were chosen to be used as the proxy in the machine learning (ML) models for aquifer tubes' Cr(VI) concentration as mentioned earlier due to the sparsity of the aquifer tubes' timeseries data. The predictor groundwater wells around target groundwater wells are segregated with respect to various distances and directions from the target groundwater wells for ML modeling in the current approach. Some of the notable target groundwater wells explored are '199-D8-55', '199-D5-92', '199-D8-68', '199-D5-36', and '199-D4-39'. The testing performance of the ML models at various directions and radii for these target groundwater wells is presented in Table 16.

Table 16. ML Models MAE Errors for Various Starting Arc Angles

GW wells		Arc starting angle (deg)												
	Radius(m)	210	225	240	255	270	285	300	315	330	345	360	15	30
199-D8-55-36	500		1.9181									1.5426	2.0302	1.903
	750	1.9059	1.8936	1.7808	1.9129							1.5426	1.7876	1.4733
	1000	1.6838	1.8936	1.4493	1.9129	1.5967	1.8509	1.9212			1.7572	1.5426	1.7876	1.3479
	1250	1.6838	1.8936	1.4493	1.9129	1.4097	1.7447	1.9212			1.7572	1.5435	1.7876	1.3479
	1500	1.3096	1.7092	1.475	1.6799	1.4048	1.7447	1.9483			1.7572	1.5435	1.7876	1.3479
199-D5-92	500													
	750		4.7968							5.9021	6.2488		6.4375	6.6572
	1000	5.0644	4.4491	6.6706		6.5898				5.1078	6.084	6.7108	6.4375	6.1868
	1250	4.6205	4.3465	6.6706	7.1734	6.5904			5.9922	4.927	6.084	6.3752	6.4375	3.638
	1500	4.6205	3.4256	6.6706	6.9527	6.5984		6.124	5.6752	4.8968	6.0196	6.2633	6.4787	3.258
199-D8-68	500	2.7842	2.8952							2.4969		3.1997		3.1845
	750	2.4859	2.9192	2.9115	3.1011					2.4619		3.1997		3.0021
	1000	2.4859	2.4699	2.8605	2.8477			2.8492		2.4619		3.1997		3.0021
	1250	2.3635	2.4699	2.8927	2.8477	2.6481		2.8492		2.4619		2.9848		3.0021
	1500	2.3635	2.4699	2.5826	2.8284	2.6098	3.0597	2.8492		2.4619		2.9848		3.0021
199-D5-36	500	1.58	1.2778			0.4374								
	750	1.4477	1.2778			0.3158		0.2882	0.4011				0.846	
	1000	1.2833	1.1592			0.1816	0.8816	0.2737	0.4011				0.1906	
	1250	1.2833	0.9895		1.5789	0.1816	0.8816	0.2763	0.4011			0.444	0.1844	0.4382
	1500	1.2833	0.9895		1.5789	0.1816	0.8816	0.2763	0.4011	1.5574	0.2147	0.3095	0.1773	0.4355

	500	3.276	2.1382					3.4354	3.9667		3.9125			
	750	3.276	1.883					3.2324	3.684		3.8695			
199-D4-39	1000	3.276	1.4794			3.9736		3.2324	3.5418	3.8311	3.8695		3.3382	2.9569
	1250	3.276	1.4794			3.9736		3.2324	3.5662	3.8311	3.1199		3.1519	3.6161
	1500	3.276	1.4794			3.9736		3.2324	3.5662	3.8311	3.1383	3.757	3.4801	2.6091

For each of the above-mentioned proxy groundwater wells, ML models' performance at various arc angles within the radius of 1,500 m are presented in Figure 103 ***(a)*** to ***(e)*** with the MAE error color-coded for subjective assessment.

(a)199-D8-55

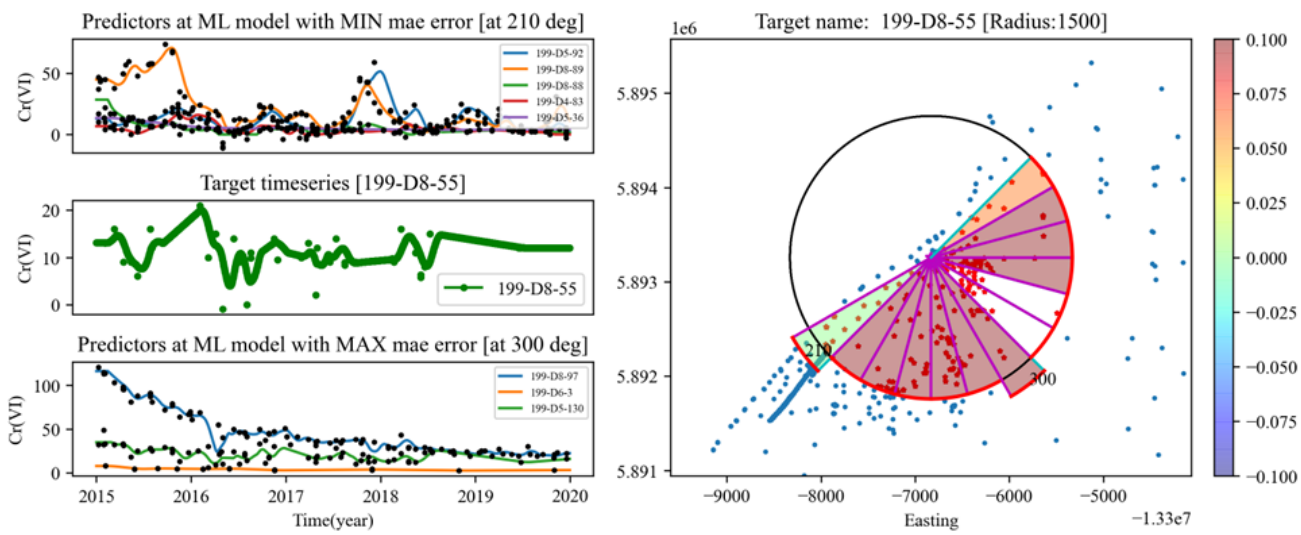

(b) 199-D5-92

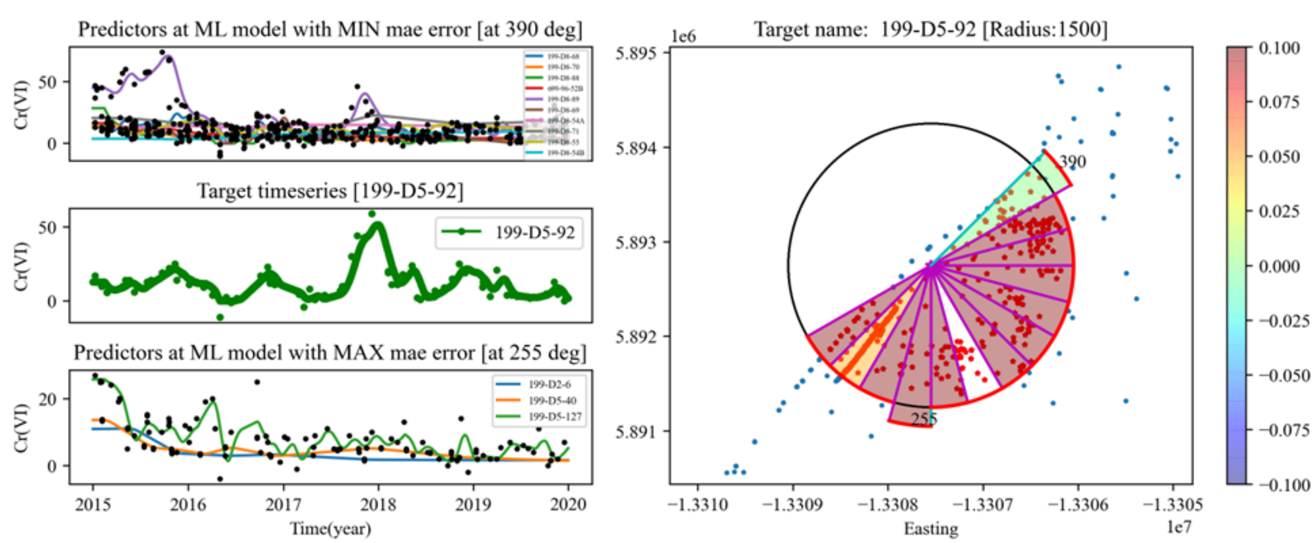

(c) 199-D8-68

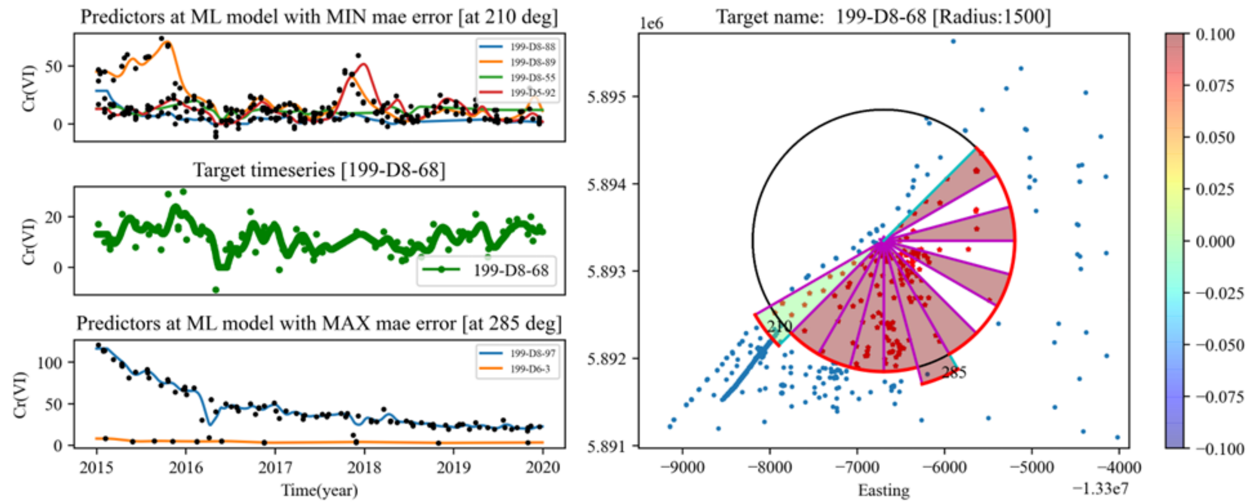

(d) 199-D5-36

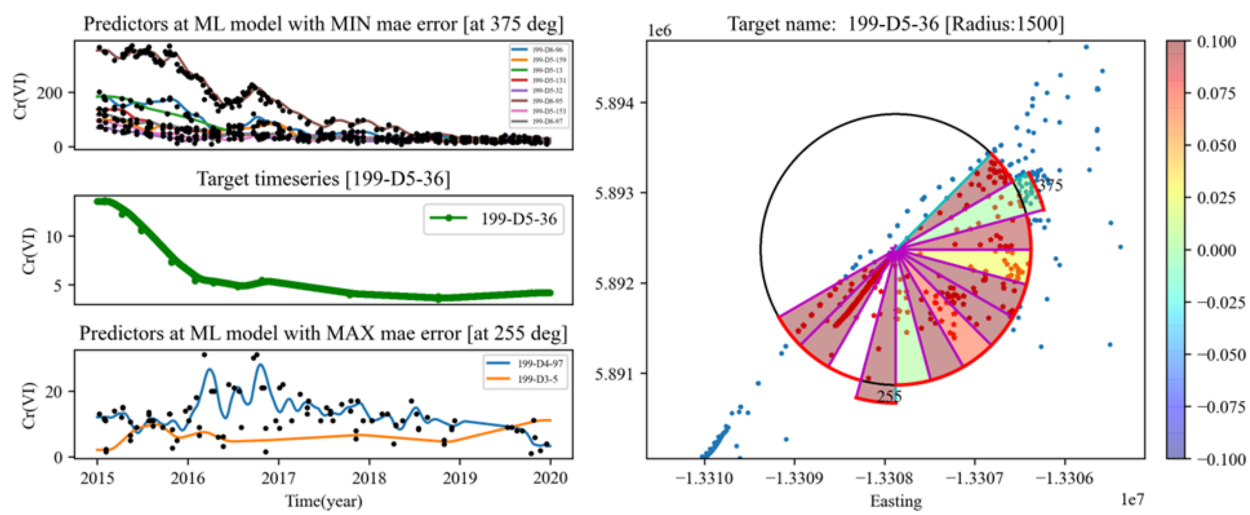

(e) 199-D4-39

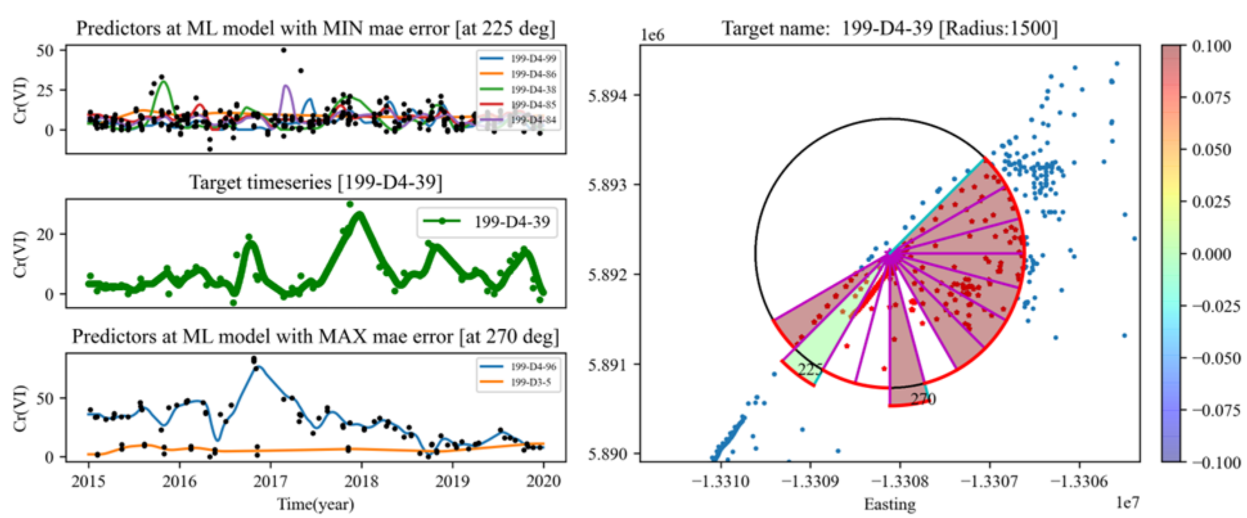

Figure 103. ML models' performance similarity for the radius of 1,500 m for proxy groundwater well '199-D8-55', '199-D5-92', '199-D8-68', '199-D5-36', and '199-D4-39'.

For each plot in Figure 103, the color-coded ML performance plot emphasizes the associated directions that resulted in the minimum and maximum MAE error in prediction by extending the associated arc triangles. Here the color bar indicates that the ML model with minimum MAE error should be shaded in towards most blue and the ML model with maximum MAE error should be shaded in towards most red. The predictors' timeseries in the best and worst-performing ML models are also presented in the corresponding plot for each of the groundwater wells. The results show that the minimum MAE error models associated with arc triangles are located approximately parallel and close to the shoreline, whereas the maximum MAE error models associated with arc triangles are located approximately perpendicular to the shoreline.

Some of the additional target groundwater wells explored are '199-D8-89', '199-D4-86', '199-D4-85', '199-D8-88', '699-96-52B', and '199-D4-98'. The testing performance of the ML models at various directions and radii for these target groundwater wells is presented in Table 17.

Table 17. ML models MAE errors for various starting arc angles

GW wells		Arc starting angle (deg)												
	Radius(m)	210	225	240	255	270	285	300	315	330	345	360	15	30
199-D8-89	500				8.444					3.9481			8.1001	11.1547
	750			11.6881	8.444					3.541			6.5361	7.9049
	1000			11.6881	8.444		6.5704	9.3413	5.8734	3.541	8.7163	5.4997	5.7852	4.0149
	1250	5.327	5.9606	6.4997	8.444	9.2442	6.2018	6.5671	5.8734	3.541	8.7163	5.4997	5.7852	3.4385
	1500	4.307	5.3485	5.9469	6.8606	9.4296	6.2661	6.5671	5.805	3.541	8.7163	5.4997	5.4688	3.4385
699-96-52B	500		1.9078	0.5872										
	750		1.9078	0.5872										
	1000	1.3462	0.7316	0.5896	0.9958	0.9083								
	1250	0.9553	0.6317	0.352	0.9958	0.7885								
	1500	0.6474	0.3244	0.2867	0.4898	0.7885						2.0026		
199-D4-86	500													
	750													
	1000											0.7338	0.5088	0.7584
	1250											0.4563	0.4191	0.7584
	1500										0.9678	0.473	0.5717	0.7584
199-D4-85	500													
	750													1.697
	1000											1.7877	1.7284	1.6389
	1250										1.6987	1.6701	1.7364	1.6389
	1500										1.636	1.7072	1.7372	1.6389
199-D4-98	500			1.9357									2.2271	2.1553
	750			1.9357							2.7025	2.5133	1.9592	1.7709
	1000			1.9357						2.5884	2.4694	2.6933	1.9592	1.7709
	1250			1.9357						2.3382	2.5498	2.6933	1.9275	1.8202
	1500			1.9357						2.3382	2.4237	2.6933	1.8835	1.8394

	500											1.3106	2.1877	
	750					1.3107			1.7622	1.3817		1.2544	2.1877	2.7739
199-D8-88	1000	2.7259	1.4637			1.3107		1.8874	1.3102	1.3817		1.2544	1.5503	2.7739
	1250	2.5554	0.9868	1.2769	1.2429	1.3107	2.7934	1.7787	1.1918	1.3156	1.521	1.2087	1.2606	1.0989
	1500	2.0534	0.9868	1.0752	1.2481	1.3132	2.7882	1.7407	1.205	1.3156	1.521	1.1015	1.2606	0.9511

For each of the above-mentioned proxy groundwater wells in Table 17, the ML models' performance at various arc angles within the radius of 1,500 m are presented in Figure 104 ***(a)*** to ***(e)*** with the MAE error color-coded for subjective assessment.

(a) 199-D8-89

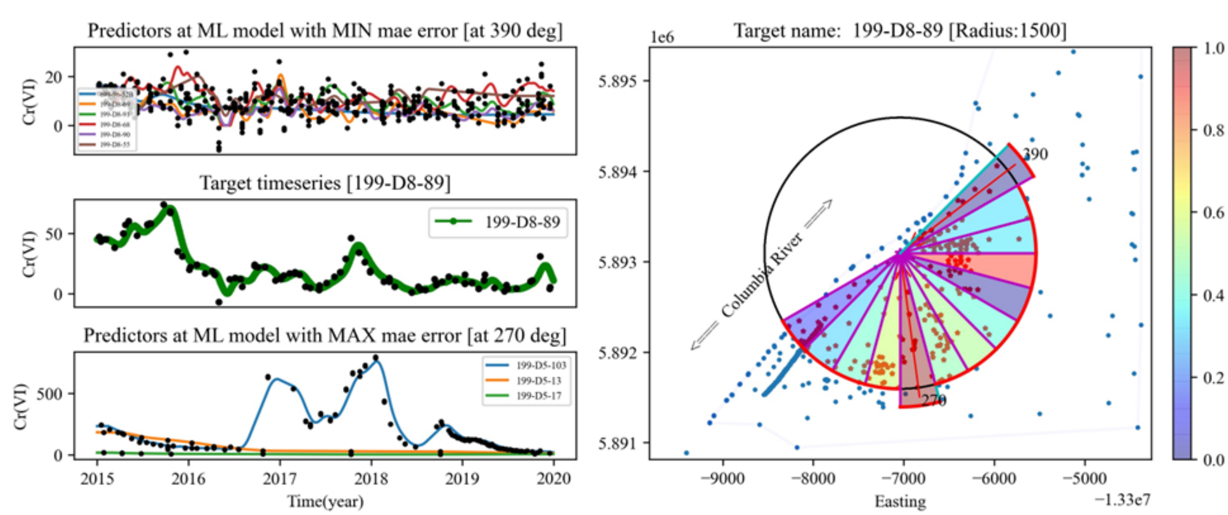

(b) 699-96-52B

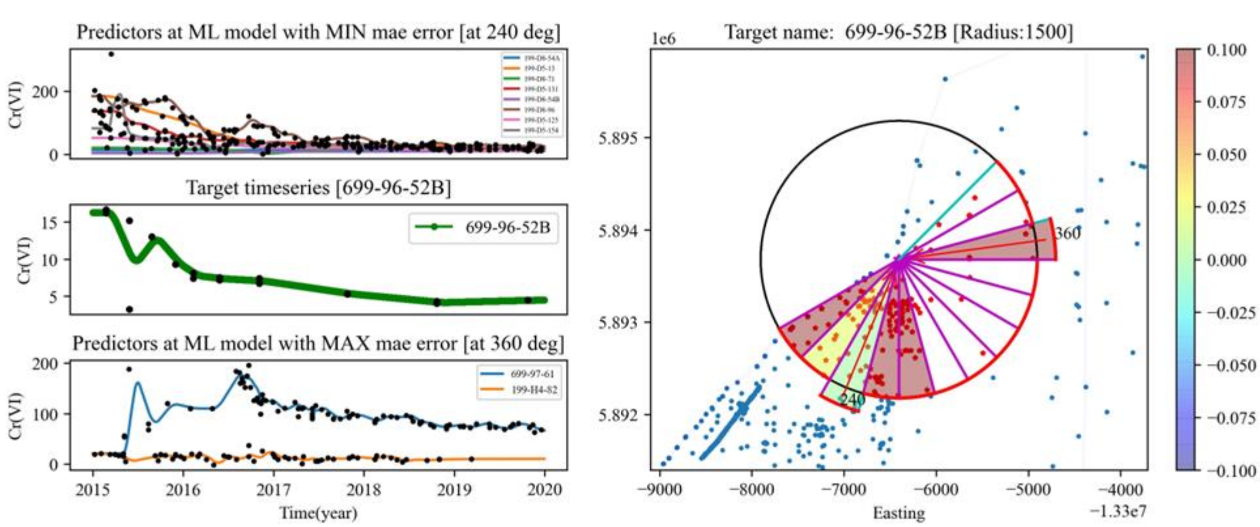

(c) 199-D4-86

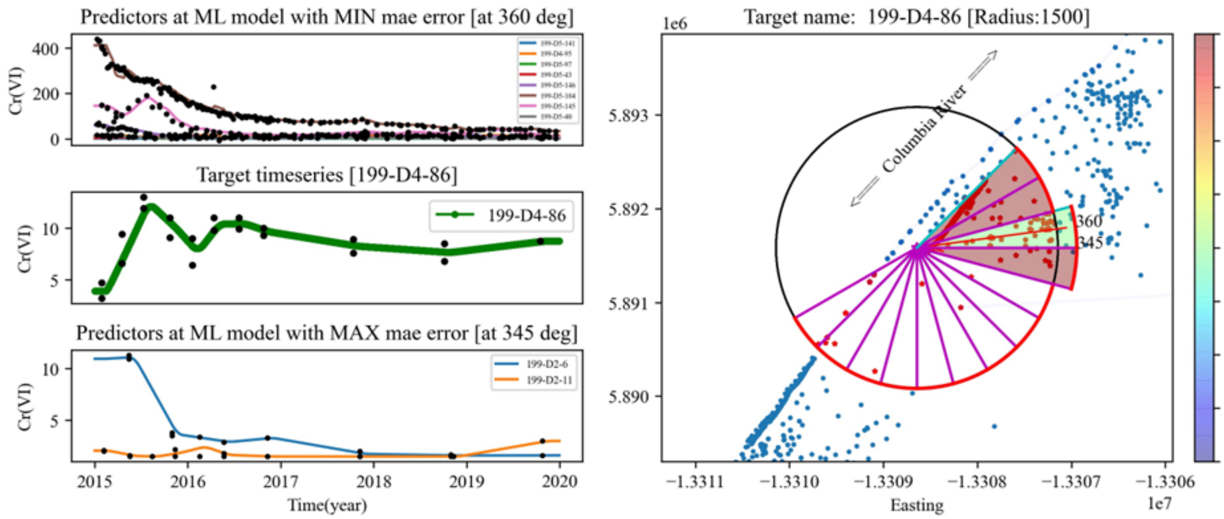

(d) 199-D4-85

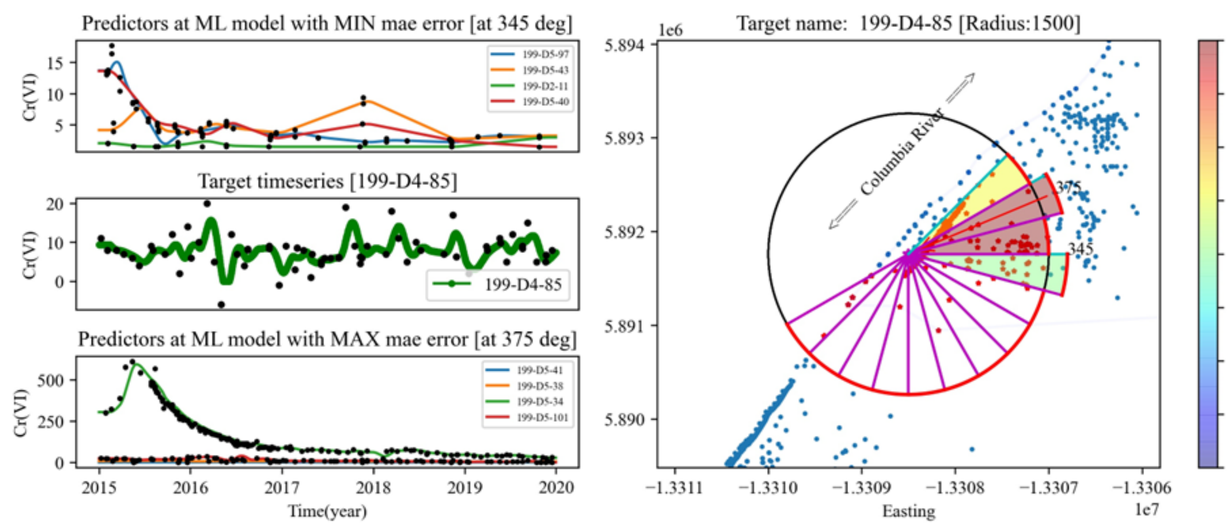

(e) 199-D4-98

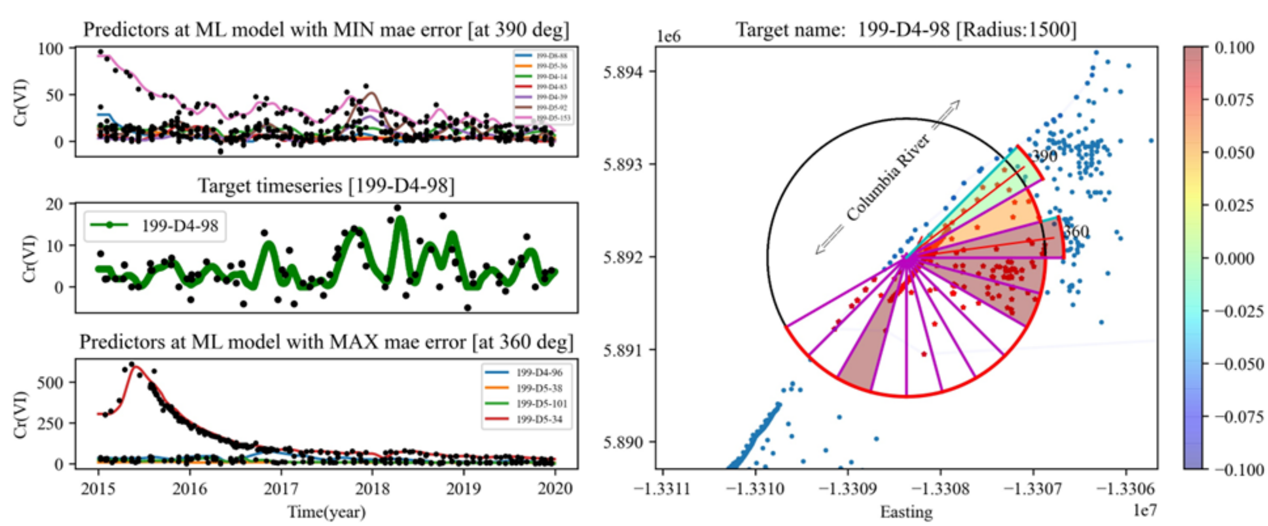

(f) 199-D8-88

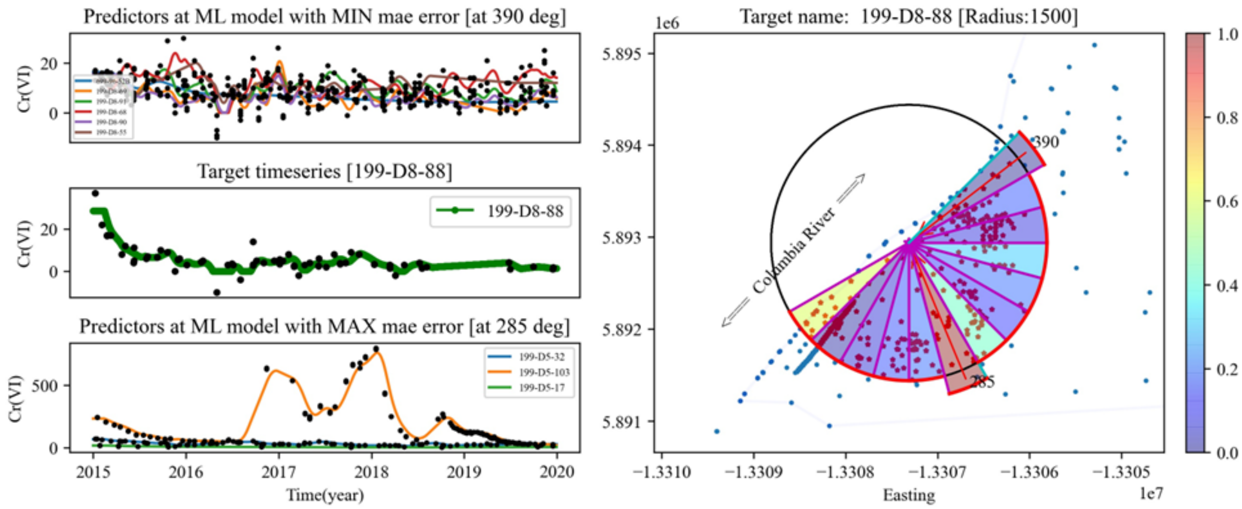

Figure 104. ML models' performance similarity for the radius of 1500 m for proxy groundwater well '199-D8-89','699-96-52B', '199-D4-86', '199-D4-85', '199-D4-98', and '199-D8-88'.

Afterward, the trend of similarity between the best and worst ML models' performing directions between aquifer tubes and groundwater was subjectively compared. Moreover, the best and worst ML models' performing directions among aquifer tubes, and groundwater wells were assessed individually.

(a) Directions associated with the ***minimum*** *MAE error ML model for various* ***aquifer tubes*** *as target*

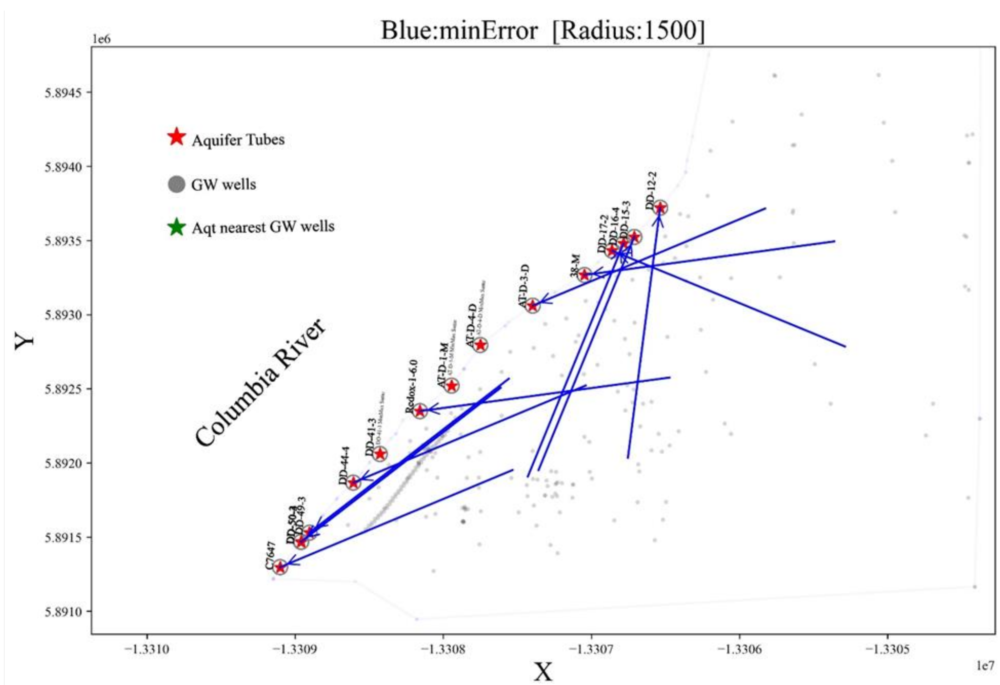

*(b) Directions associated with the **minimum** MAE error ML model for various **Groundwater wells** tubes as target*

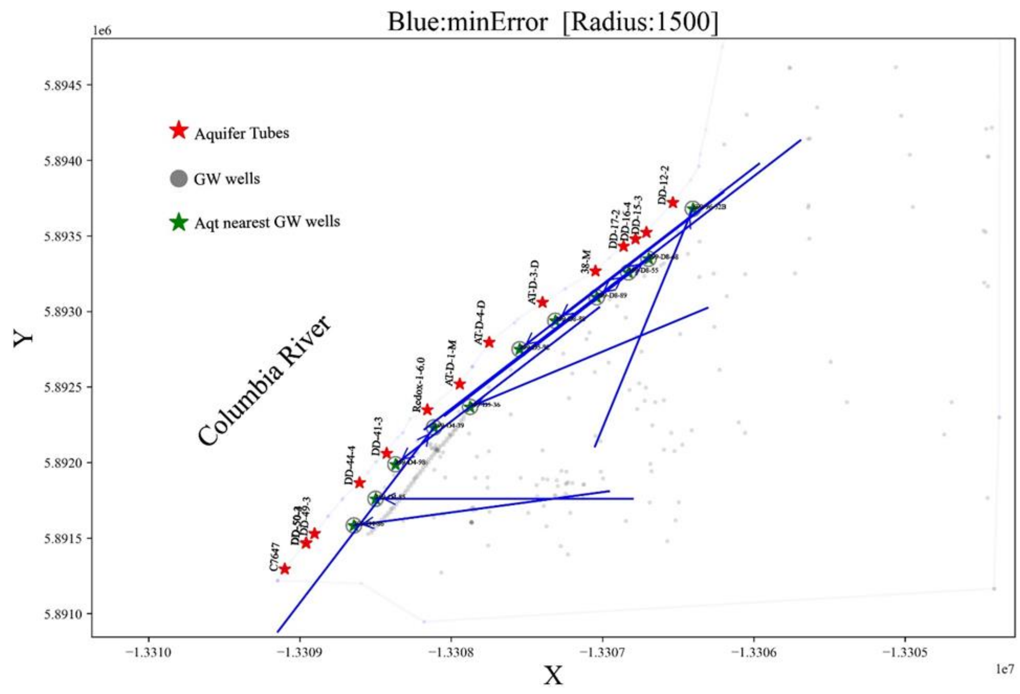

Figure 105. Comparison of (a) Directions associated with the minimum MAE error ML model for various aquifer tubes as the target, vs (b) Directions associated with the minimum MAE error ML model for various groundwater wells' tubes as the target.

*(a) Directions associated with the **maximum** MAE error ML model for various **aquifer tubes** as target*

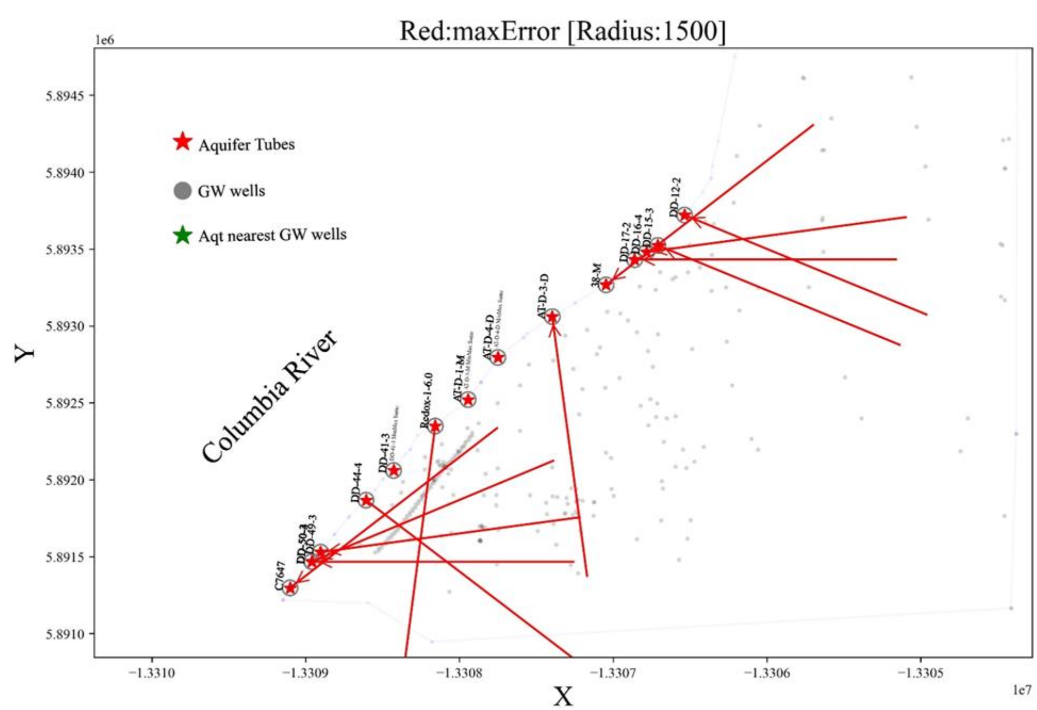

(b) Directions associated with the ***maximum*** *MAE error ML model for various* ***Groundwater wells*** *tubes as target*

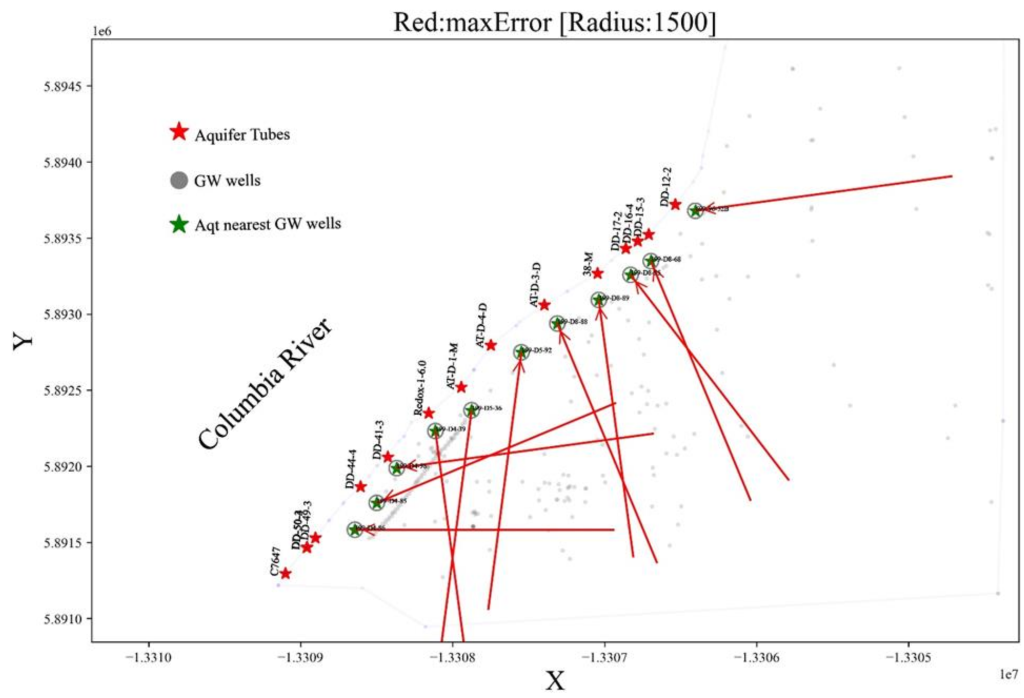

Figure 106. Comparison of (a) Directions associated with the maximum MAE error ML model for various aquifer tubes as the target, vs (b) Directions associated with the maximum MAE error ML model for various groundwater wells' tubes as the target.

In the assessment of the directions associated with ML model performance, the results show that the minimum MAE error models associated with arc triangles are located approximately parallel and close to the shoreline for proxy groundwaters wells, and an approximately opposite trend was observed for aquifer tubes where the directions are closely perpendicular to the shoreline which is depicted by Figure 105. However, for this set of comparisons between aquifer tubes and groundwater wells, a similar trend in the directional performance was observed when the maximum error directions were considered, which is approximately perpendicular to the river shoreline as presented by Figure 106. The combined result of the individual comparisons is presented in Figure 107 for directions associated with minimum and maximum prediction error ML models together for aquifer tubes and proxy groundwater wells.

*(a) Directions associated with the **minimum and maximum** MAE error ML model for various **aquifer tubes** as target*

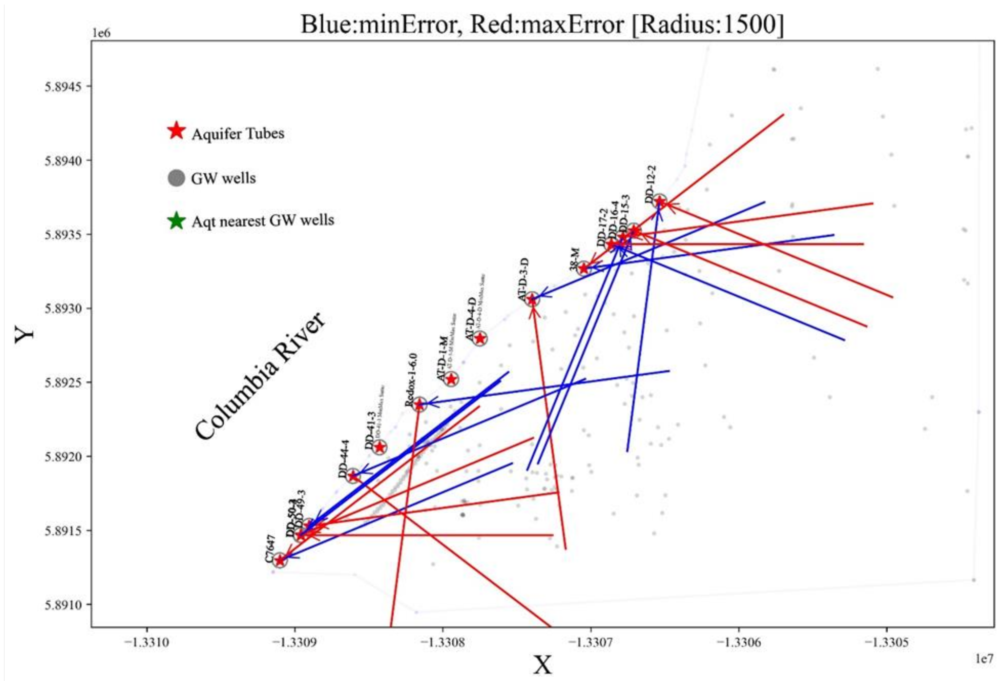

*(b) Directions associated with the **minimum and maximum** MAE error ML model for various **Groundwater wells** tubes as target*

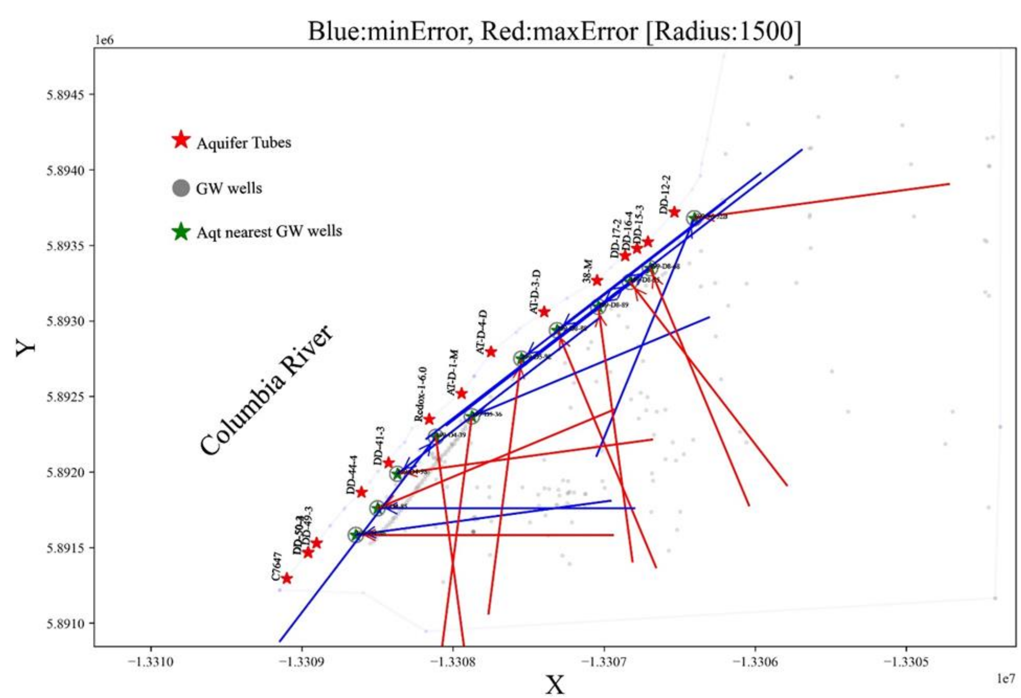

Figure 107. Comparison of (a) Directions associated with minimum and maximum MAE error ML model for various aquifer tubes as the target, vs (b) Directions associated with the minimum and maximum MAE error ML model for various groundwater wells' tubes as the target.

Subtask 7.3: Conclusions

The developed method can be used for spatiotemporal relationship exploration for individual target sensor locations as well as for the exploration of collective trends in a vast region. The application of the developed method on the demonstration dataset reveals direction preference in the spatiotemporal relation for individual surface water monitoring locations as well as the overall trend of the Cr(VI) concentration trend in the region of interest.

Subtask 7.3: References

[1] Abbott, John C. "Remediation efforts at DOE's Hanford site." *Federal Facilities Environmental Journal* 7, no. 1 (1996): 27-36.

[2] Gray, Robert H., and C. Dale Becker. "Environmental cleanup: the challenge at the Hanford Site, Washington, USA." *Environmental Management* 17, no. 4 (1993): 461-475.

TASK 8 AI FOR EM PROBLEM SET (SOIL AND GROUNDWATER) - DATA ANALYSIS AND VISUALIZATION OF SENSOR DATA FROM THE WELLS AT THE SRS F-AREA USING MACHINE LEARNING (LBNL, SRNL)

Subtask 8.4: Prototype Data interface development for the AI/ML System to support data ingestion and processing (NEW)

Subtask 8.4: Introduction

The mission of the Advanced Long-Term Environmental Monitoring Systems (ALTEMIS) project is to establish the overarching framework for the Department of Energy's (DOE) legacy site monitoring to ensure long-term environmental protection. The current monitoring program is based on the collection and analysis of samples of water from more than 100 stations that include groundwater-monitoring wells, surface water stations in the wetlands, and surface water stations in the local stream. In addition to this conventional groundwater sampling and laboratory analysis, in situ sensor deployment was proposed under the ALTEMIS project to advance this monitoring program. A data ingestion module will be critical for data storage and processing.

Subtask 8.4: Objectives

The objective of this subtask is to develop a prototype data interfacing module for the AI system. This type of module will help to ingest the time series and imagery data coming from the deployed sensors by the ALTEMIS project. This module will specifically contain submodules like data exploration, visualization, and preprocessing before the raw data from the sensors is to be used by the AI system.

Subtask 8.4: Methodology

I. API Exploration

The future sensor data that will be provided from the ALTEMIS project will be available through an application programming interface (API) called HydroVu API. The FIU Team spent some time going over the API documentation provided using the following link, ***https://www.hydrovu.com/public-api/docs/index.html***, which can be seen in Figure 108.

Figure 108. HydroVu API documentation.

The API provides access to a magnitude of information regarding the sensors. It provides longitude and latitude coordinates for each well as well as the sensor parameters, the readings, and much more. Getting a deep understanding of how to pull all this information into a consolidated place was crucial to perform preprocessing steps in subsequent stages.

Once the FIU team gained access to the HydroVu API the team explored the features available in the Graphic User Interface (GUI) of the HydroVu system. The GUI can be seen in Figure 109. Graphs of the sensor collected variables can be visualized such as pressure, temperature, depth, specific conductivity, and more. A map view of the sensors is also displayed in the top right corner of the GUI.

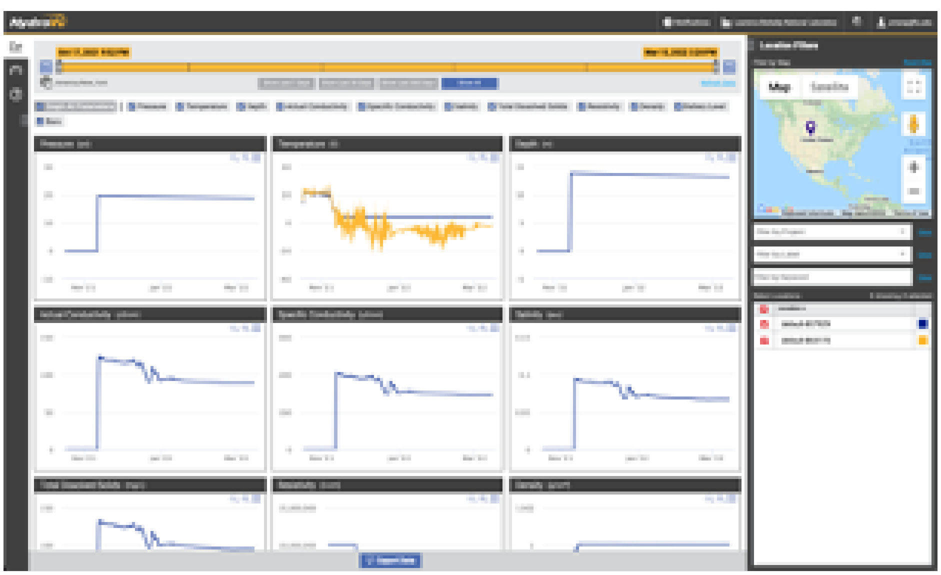

Figure 109. HydroVu graphical user interface.

Subtask 8.4: Results and Discussion

I. Retrieving sample API data using Python scripts

With proper access to the HydroVu API the FIU team was able to retrieve data using python code. The API has a few endpoints, the top two being the endpoint that provides well information such as the name and its spatial coordinates as well as an endpoint that provides data for each well and analyte. The raw requests are provided in JSON format, so transformations were necessary to make use of the data. The data was transformed into a format similar to the historical SRS F-Area dataset where the important columns are the "COLLECTION_DATE, STATION_ID, ANALYTE_NAME, RESULT, RESULT_UNITS". A sample of the transformed table is shown in Figure 110 below.

COLLECTION_DATE	STATION_ID	ANALYTE_NAME	RESULT	RESULT_UNITS
2021-10-18 17:00:00	default-857929	Pressure	-0.017385	psi
2021-10-18 18:00:00	default-857929	Pressure	-0.018447	psi
2021-10-18 19:00:00	default-857929	Pressure	-0.014484	psi
2021-10-18 21:00:00	default-857929	Pressure	-0.024750	psi
2021-10-18 22:00:00	default-857929	Pressure	-0.023332	psi
...	...	...	...	...
2021-10-18 22:00:00	default-863175	Baro	14.296474	psi
2021-10-18 23:00:00	default-863175	Baro	14.297346	psi
2021-10-19 00:00:00	default-863175	Baro	14.298885	psi
2021-10-19 01:00:00	default-863175	Baro	14.295509	psi
2021-10-19 02:00:00	default-863175	Baro	14.297779	psi

Figure 110. DataFrame transformed from raw HydroVu API data.

Although we can pull in data from the API, the endpoint for providing sensor readings returns data with only 10 records at a time. For this reason, we are required to make a request many times to acquire all the information. Unfortunately, after making over 250 API requests we received a "timeout error". With this problem, the FIU team still needs to figure out a workaround to properly acquire all the data.

One issue that was noticed was that the API only returned 10 records per call to the server and after executing about 250 calls, a timeout error would occur. To combat this issue, we ran a loop to keep calling the API to retrieve data so long as the last timestamp of the currently collected data is smaller than yesterday's timestamp. In other words, the script will continuously execute to retrieves data from the first timestamp in the dataset till yesterday's timestamp. This solves the issue where we only get 10 records per API call and now, we can retrieve all the available data. However, this did not solve the timeout issue. This obstacle was fixed using python's try and except method. This method allows the script to run a piece of code and "catch" an error if it occurs. In this case, every 250 API calls when the error occurs, the try and except method will ignore the error and resume downloading the data where it left off. The python code responsible for downloading all the data in the API is shown in Figure 111 below.

```python
for id, station_id in zip(locations.id, locations.name):
    last_tm = 0
    while(last_tm < yesterday):
        if(data.shape[0] == 0 and last_tm==0):
            last_tm = 0
        elif(data.shape[0] != 0 and last_tm==0):
            last_tm = 0
        else:
            last_tm = int(data['timestamp'].iloc[-1])
        try:
            print(last_tm)
            r = requests.get(url=f"https://www.hydrovu.com/public-api/v1/locations/{}/data?startTime={}".format(id, last_tm), headers=headers)
            parameters = pd.DataFrame(json.loads(r.text))
            params = pd.json_normalize(parameters['parameters'])[['parameterId', 'unitId', 'readings']]
            params = params.replace({"parameterId": param_unit_dict.parameters}).replace({"unitId": param_unit_dict.units})
            params = params.rename({"parameterId":"ANALYTE_NAME", "unitId":"RESULT_UNITS"}, axis=1)
            for i in range(params.shape[0]):
                curr = pd.DataFrame(params.readings[i])
                curr = curr.rename({"value":"RESULT"}, axis=1)
                curr['STATION_ID'] = station_id
                curr['ANALYTE_NAME'] = params.iloc[i]['ANALYTE_NAME']
                curr['RESULT_UNITS'] = params.iloc[i]['RESULT_UNITS']
                data = pd.concat([data, curr])
            last_tm = int(data['timestamp'].iloc[-1])
        except:
            print(count, "Resuming...")
            pass
```

Figure 111. Python code to download all the HydroVu API

Sometimes, when the error occurs and the code resumes where it left off, duplicate records are stored in the data frame, which is undesirable. Due to this, we remove all duplicate records once all of the data is retrieved.

II. API Data Preprocessing

One of the major components of this subtask is to preprocess the raw sensor data. With the module being able to retrieve raw data, preprocessing steps could be taken. Upon inspection, not all the sensors collect data at the same frequency; Some variables are collected every hour while others are collected every 30 minutes. To process the data in a uniform fashion, a resampling module will be created to have all the data at the same interval. To demonstrate the effects of using different resampling frequencies, we have plotted the transformation on the test sensor's temperature reading. This can be seen in Figure 112. The blue line represents the original/raw time series. Clearly there is quite a bit of variation daily, so taking the daily average may be more appropriate for future analysis shown in orange. Depending on the level of detail required for analysis, different frequencies may be selected. This module, however, only provided the tool to resample.

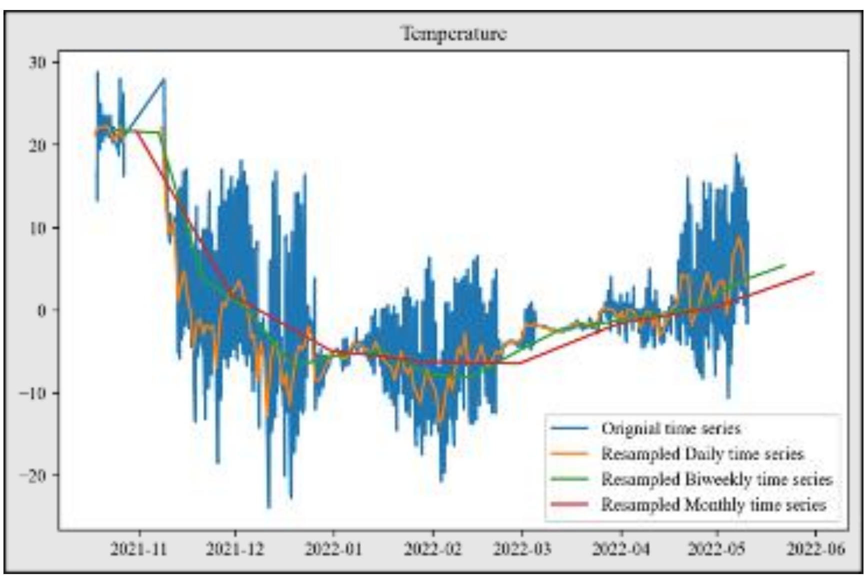

Figure 112. Test sensor temperature data resampled at different frequencies.

III. Storing sample data in SQL Server Database

To ensure that a reliable system is established for holding the latest InSitu sensor data, a SQL Server Database was created. To preserve a copy of the latest data a python script was devised to pull the API data and then push it to the SQL Server database. Once this data is secured on the database, it can be accessed from other systems and machine learning algorithms. A screenshot of SQL Server management studio with some of the data records stored on the database is shown below in Figure 113.

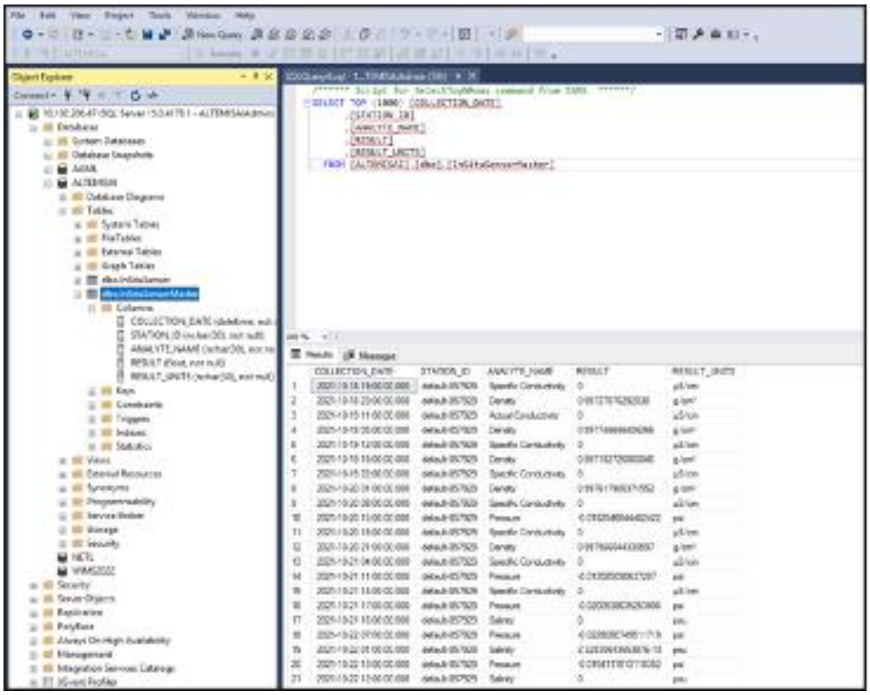

Figure 113. SQL Server Management Studio showing the InSitu Sensor Database.

Subtask 8.4: Conclusions

The FIU team has effectively established the framework for the upcoming creation of an AI interface. The team was able to obtain data from the HydroVu API, which houses the sensor information, store it in a SQL database, and preprocess it by resampling, for example.

Subtask 8.4: References

NA

Subtask 8.5: Development of the AI/ML-Based System to Perform Predictive Analytics using Datasets containing Time Series and Imagery Data from Sensors (NEW)

Subtask 8.5: Introduction

Florida International University (FIU), Savannah River National Lab (SRNL), and Lawrence Berkeley National Lab (LBNL) collaboratively worked with other ALTEMIS partners for the sensor location selection optimization at the Savannah River Site (SRS) F-Area using artificial intelligence and machine learning (AI/ML). The ALTEMIS team is scheduled to complete the installation of in-situ sensors (Aqua TROLL 200 and 500) in the latter half of 2022. With the installation of sensors, having models that can predict future analyte values given the live data is central for decision making.

Subtask 8.5: Objectives

The objective of this subtask is to build the foundation for the AI system in performing pattern identification, prediction, and anomaly detection, initially developed using the legacy dataset available for the SRS area which is the target site for sensor deployment under ALTEMIS project. With the time series from the newly deployed sensors (Aqua TROLL 200 and 500 sensors), the AI system will be tuned and tested. In this regard, FIU explored Recurrent Neural Network – Long Short-Term Memory (RNN-LSTM). The developed AI system will be generalizable to other DOE sites with similar sensor and AI system implementation.

Subtask 8.5: Methodology

I. Exploring Master and Proxy variables using PCA

The focus of this section was to identity F-Area's master and proxy variables using the historical dataset. The idea is to find the variables or analytes that contribute the most variability captured by the wells at the F-Area to get an overall understating of the site behavior. Our current approach was to apply Principal Component Analysis (PCA) to each well and examine the contribution of each analyte. PCA is a common Machine Learning (ML) tool that works primarily as a means of reducing the dimensionality of the given data through a means of compression. This process works by projecting data points onto several Principal Components (PCs) while maximizing the variance of the data [1]. This concept of projecting the datapoints is shown in Figure 114 [2].

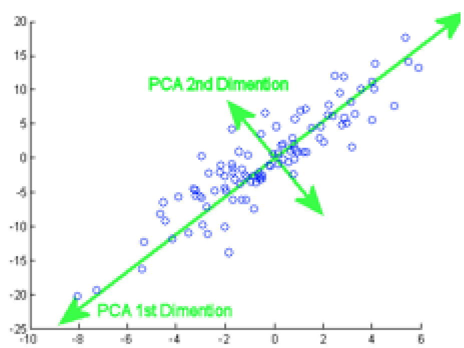

Figure 114. Visual explanation of PCA.

The main idea was to be able to rank the analytes by importance by using the following steps:

1. Preprocess the data to generate a table of analyte time series for each well. For example, one table would be created for well "FSB 95DR" where the rows represent the time index, and the columns represent each analyte recorded at that well.
2. PCA would then be applied to each table and all the PCs which explain up to 95% of the data's variability.
3. Lastly, the contributions of each analyte would be summed, and the list sorted by the highest sum of coefficients.

With this process, a ranking table would essentially be built for each well. The main idea is to count the occurrence of the top contributors of each well and determine which analytes appear most frequently across all of the wells, which represents the entire F-Area.

II. Contaminant Prediction using Machine Learning

One main curiosity was whether classical Machine Learning (ML) models could predict contaminant concentrations using a sensor collected variable. For this experiment, the time series of well FSB 95DR was examined due to its high availability of data and position near the F-Area plume. The analytes were also filtered by variables that will be sensed by the Aqua Troll 200 and 500 sensors. These variables include pH, reduction potential (RP), total dissolved solids (TDS), depth-to-water (DTW), specific conductance (SC), and water temperature (WT). In addition, the three main contaminants of concern, uranium-238, iodine-129 and tritium were kept in the data. When filtering with these conditions there was not enough data samples for RP and TDS, so they were omitted. With the remaining dataset the Pearson coefficient (PC) was calculated to reveal the variables with the highest correlation. The cells highlighted in green have the highest correlations (PC > 0.65). From these results specific conductance and uranium-238 were selected to perform predictions as it had the highest correlation of 0.873. With SC selected as the predictor and U-238 as the target variable, the next step was to apply various ML models on the data and evaluate their respective performance.

The data was split into a training and testing set where the first 70% of the data was reserved for training (roughly 1990 to 2009) and the remaining 30% reserved for the testing set (roughly 2010 to 2015). Six classical ML regression models were selected for evaluation: linear regression, stochastic gradient descent regression, kernel ridge regression, Bayesian ridge regression, gradient boosting regression and finally support vector machine.

III. Contaminant Prediction using Deep Learning

The same analysis was applied using Deep Learning (DL) models. Several varieties of long short-term memory (LSTM) models were employed for evaluating the performance of models being trained. Each DL model intakes 45 numbers, one per sample, and outputs the prediction for the next timestep. In other words, time steps are passed to the model and the model outputs the prediction. Using a timestep smaller than 45 resulted in weaker performance. First, a simple vanilla LSTM with 50 neurons followed by a dense layer was created. This resulted in a mean squared error (MSE) of 0.0032. A Bidirectional LSTM was also tested with 50 neurons but showed weaker performance compared to the vanilla model with a MSE of 0.0054. Lastly, a stacked LSTM model was trained where 2 LSTM layers were placed back-to-back followed by a dense layer.

Subtask 8.5: Results and Discussion

I. Exploring Master and Proxy variables using PCA

This approach was almost fully implemented, however, after discussing the method with the site mentor, an interesting point was brought up. The different PCs are usually orthogonal or perpendicular to each other. Summing up the PCs that reach the 95% explained variability that would not make any sense since each PC represents something different, pointing in opposing directions and would be “flattened”. This would likely result in skewed results where the rankings do not make sense. For this reason, this approach was deemed to be inconclusive.

II. Contaminant Prediction using Machine Learning

The MSE was used to assess the performance of each model. These results are shown in Table 18 below. The training and testing predictions of each model is also shown in Figure 115.

Table 18. Mean Square Errors of each ML Model

ML Model	MSE
LinearRegression	0.005255
SGDRegressor	0.037348
KernelRidge	0.001665
BayesianRidge	0.005260
GradientBoostingRegressor	0.017442
SVR	0.014346

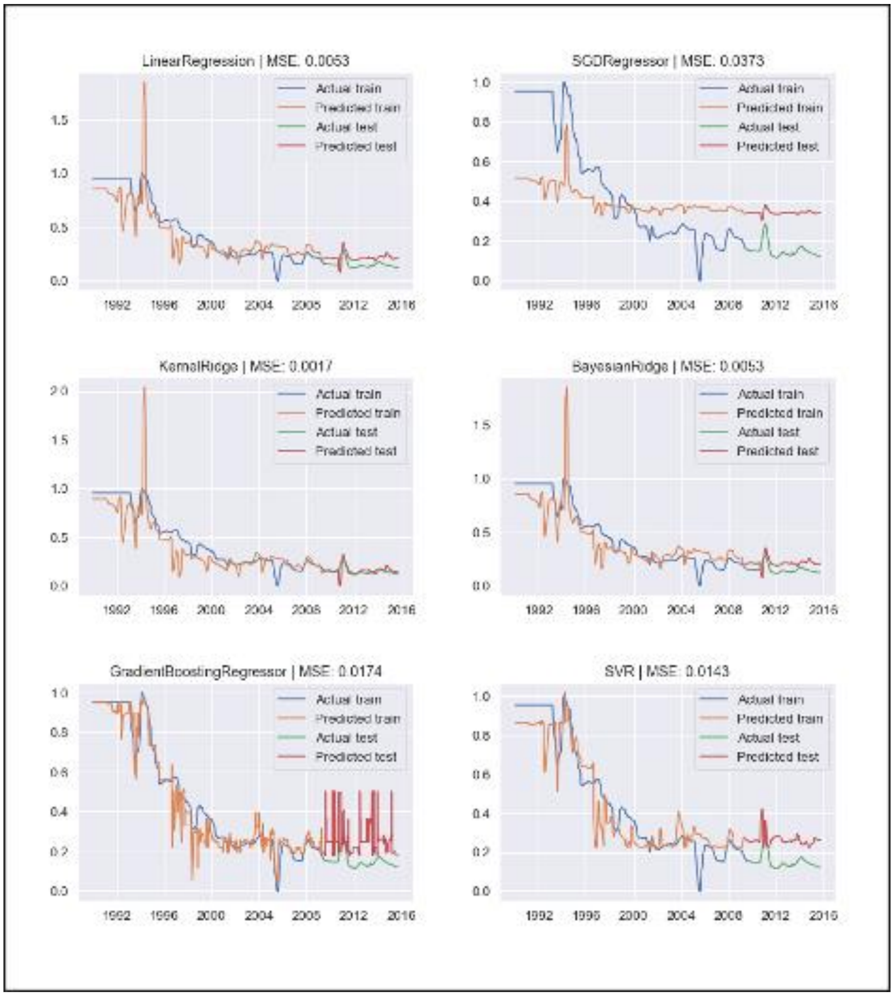

Figure 115. Training and testing predictions of each ML model.

As is evident in the MSE results, kernel ridge regression performed the best giving an error of 0.0016 on the testing set. It is also clear that the prediction best matches the actual concentration in the plot. Although the results are not bad by any means, most of the models did not generalize well on neither the training nor the testing set. This is probably since only one feature was used to make predictions. If the other variables, such as pH and depth-to-water for example are introduced, the results may be better.

III. Contaminant Prediction using Deep Learning

This model showed better results than the bidirectional LSTM model but not quite as good as the vanilla model. The performance of these three methods is shown in Figure 116.

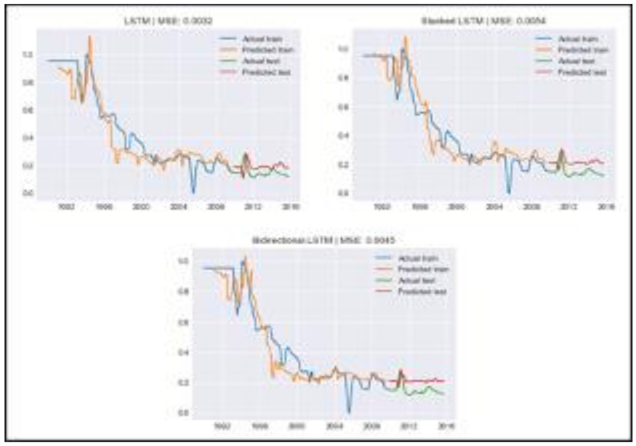

Figure 116. Training and testing predictions of each DL model.

The complexity of the prediction problem was also increased by incorporating multiple proxy variables as features to make predictions of uranium-238 using the same classical machine learning models that were previously used in December. The features that were added on top of specific conductance were water temperature, water depth, pH. With these four features, the same six ML models were trained and tested. These results are shown in Table 19 below. The training and testing predictions of each model is also shown in Figure 116. The best performing model was the support vector machine. Surprisingly however, the best performance for predicting U-238 remains the kernel ridge regression model that only had the one feature, specific conductance. It seems that for the ML modeling, the additional features did not contribute significant knowledge to predict uranium.

Table 19. Mean Square Errors of each ML Model (Multiple Features)

ML Model	MSE
LinearRegression	0.005182
SGDRegressor	0.024899
KernelRidge	0.006562
BayesianRidge	0.005197
GradientBoostingRegressor	0.011030
SVR	0.003002

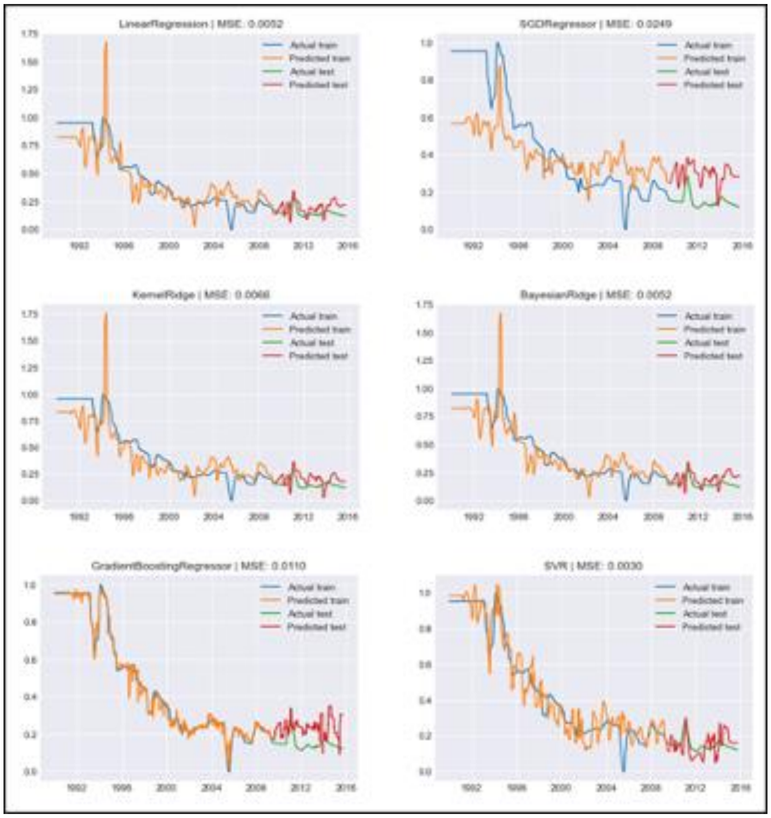

Figure 117. Training and testing predictions of each ML Model (multiple features)

As can be seen in Figure 117, the gradient booster regressor seems to perform the best during training but fails on the testing data.

The DL models were also tested to predict uranium-238 values using the four primary sensor collected variables: water temperature, pH, specific conductance, and the water table (depth or DEPTH_TO_WATER). To achieve this task, careful data manipulation was needed. First the data was filtered to only include the above listed analytes and filtered by the wells of interest for placing sensors (25 locations). In the dataset, each of the 25 columns for each analyte was sorted in lexicographical order to ensure that when the model is evaluated for performance, the proper well concentrations are compared to one another (e.g., True FSB 95DR values vs Predicted FSB 95DR values).

The Deep Learning model is composed of several LSTM layers consisting of 25, 50, 100, 100 neurons, respectively, followed by a dense layer of 25 neurons. The model needs to output 25 prediction values, one for each well, hence the reason for having 25 neurons in the last layer. The input for each well was arbitrarily selected as 60 values. In other words, the model takes in as input 60 previous values of each of the 4 input analytes for each well of the 25 wells and outputs a single value for the next time step for each of the 25 wells. This architecture is shown in Figure 118. This model still has plenty of room to be fine-tuned such as increasing the depth of the network (adding LSTM layers) and adjusting the number of values passed in as input instead of 60.

Layer (type)	Output Shape	Param #
lstm (LSTM)	(None, 60, 16)	10688
lstm_1 (LSTM)	(None, 60, 32)	6272
lstm_2 (LSTM)	(None, 60, 64)	24832
lstm_3 (LSTM)	(None, 64)	33024
dense (Dense)	(None, 25)	1625

Total params: 76,441
Trainable params: 76,441
Non-trainable params: 0

Figure 118. Deep Learning Model architecture.

The performance of the neural network was assessed by looking at the MSE on the testing set of each of the wells separately. The results are shown in Table 20. The results are sorted from the best performing predictions to the worst results. The time series plot of the train and test predictions are also shown in Figure 119. The visual predictions are consistent with the MSE metric. For example, the two best predicted wells, FSB120D and FSB 99D (0.003397, 0.004078 respectively) have test prediction and true values close to one another. The same is true for the lesser performing wells where the predicted time series deviates dramatically from the true values. Clearly, the network is learning on the input data since the training predictions follow the true values well, but overall performs poorly on the testing data. This indicates that the model needs to go deeper in order to generalize.

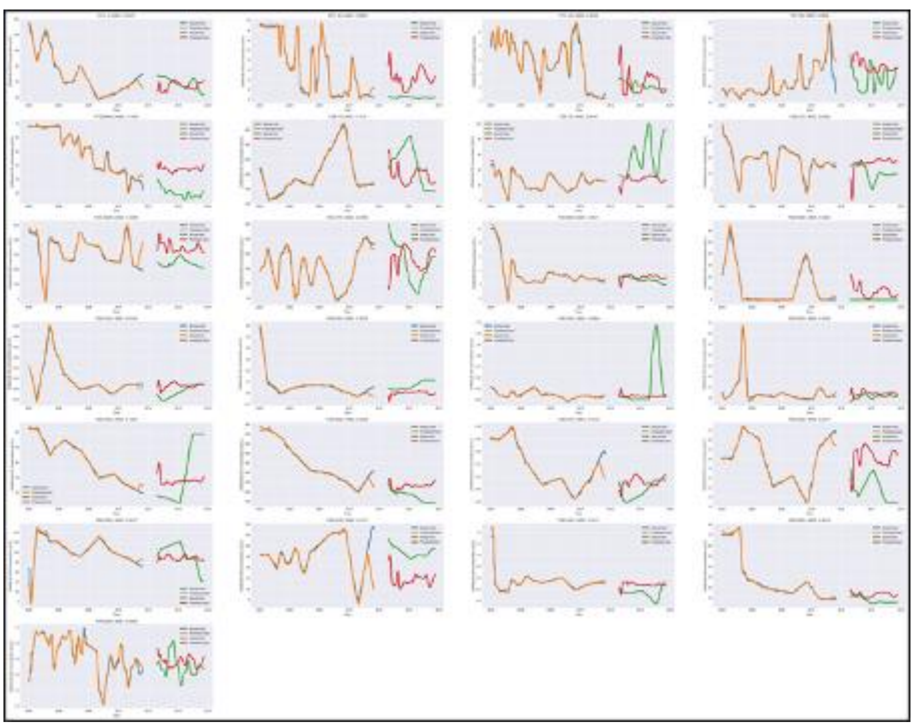

Figure 119. Deep learning model predictions for each well.

Table 20. Mean Square Errors of the testing set for each well using the same DL model sorted from best to worst.

Well name	MSE
FSB120D	0.003397
FSB 99D	0.004078
FEX 4	0.006953
FSB138D	0.007425
FSB116D	0.007883
FSB114D	0.014966
FSB135D	0.021066
FSB108D	0.022508
FPZ 6A	0.024303
FSB126D	0.025907
FSB 91D	0.028179
FSB130D	0.031664
FSB127D	0.031774
FSP204A	0.034619
FSB 95DR	0.055514
FPZ 6B	0.065643
FSB 79	0.081650
FPZ 4A	0.088865
FSB118D	0.096445
FSB 97D	0.099618
FPZ008AR	0.109162
FSB 78	0.111251
FSB132D	0.141650
FSB124D	0.150550
FSB128D	0.201747

Aside from the four variables that were being used to predict uranium concentrations, water depth, pH, specific conductance, and water temperature, in March the team added two additional features using an external dataset. The team found a python package called ***meteostat*** which allows us to get data on weather given GPS coordinates and elevation values. Since both the elevation and the latitudinal and longitudinal coordinates of each of the wells were available, it was possible to create a new feature for both precipitation and air temperature, which should have an influence on the water table dynamics.

After adding these two new features for each of the wells, the deep learning model used in March was retrained using this updated information. the model was trained on about 100 epochs and the results are tabulated and plotted in Table 21 and Figure 120 respectively. Compared to the results achieved in March, both the highest and lowest MSE values dropped slightly which indicates that the model is achieving slightly better performance. Overall, however, the model is currently not able to properly predict the uranium time series as can be seen visually in Figure 119. These results are indicating the need for a new strategy.

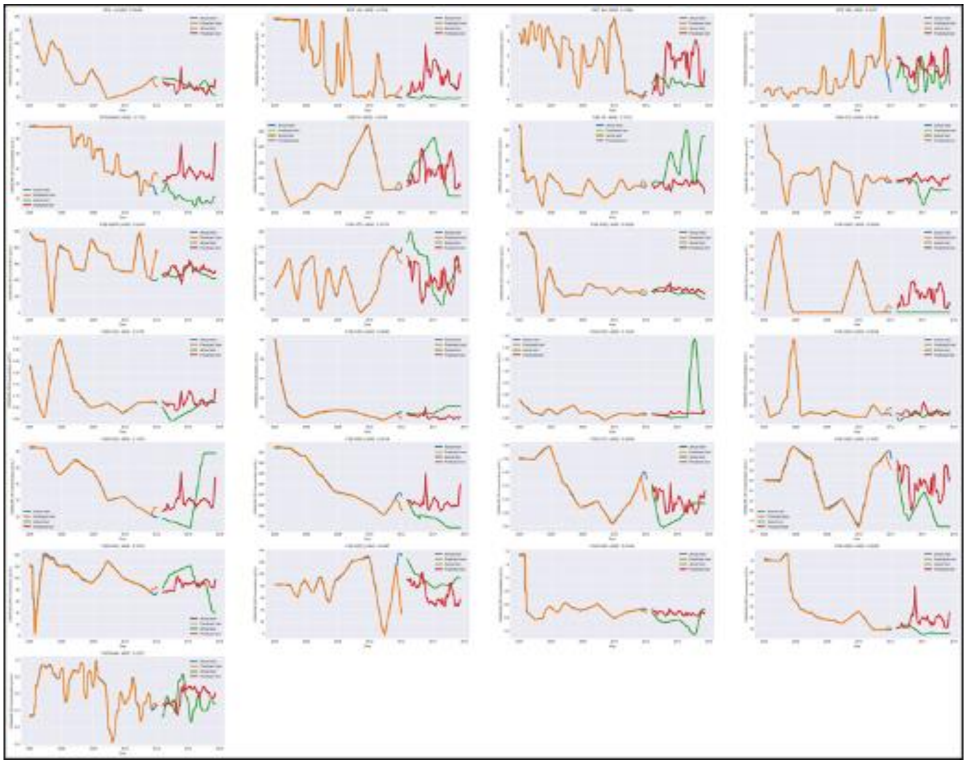

Figure 120. Deep learning model predictions for each well using the additional precipitation and temperature features.

Table 21. Mean Square Errors of the testing set for each well using the same DL model sorted from best to worst

Well name	MSE
FSB 99D	0.002592
FSB120D	0.003591
FSB 95DR	0.004716
FEX 4	0.005845
FSB116D	0.007970
FSB 91D	0.014560
FSB135D	0.016506
FSB114D	0.017638

FSB138D	0.025477
FSB130D	0.031183
FSP204A	0.037156
FPZ 6B	0.037240
FSB132D	0.038658
FSB127D	0.045526
FSB126D	0.051440
FSB108D	0.053606
FPZ 4A	0.070818
FSB 79	0.073227
FSB 78	0.076853
FSB 97D	0.077644
FSB118D	0.102503
FPZ 6A	0.108614
FPZ008AR	0.110113
FSB124D	0.147910
FSB128D	0.148713

Subtask 8.5: Conclusions

Deep learning methods seem to be the most appropriate approach to solving this problem. There are multiple possible directions for improving the current method for prediction. One suggestion would be to cluster the uranium time series so that wells that behave similarly are modeled together. Another method that could also help the prediction is developing deeper neural network models. This will come at a high cost in terms of time complexity to train the models, but if they can capture the complexities of the time series, then it will be worth exploring.

Subtask 8.5: References

[1] D. G. Chachlakis, A. Prater-Bennette, and P. P. Markopoulos, “L1-norm Tucker Tensor Decomposition,” IEEE Access, vol. 7, pp. 178454–178465, Nov. 2019, doi: 10.1109/ACCESS.2019.2955134.

[2] “pca_example.gif 499×375 pixels.” https://weigend.com/files/teaching/stanford/2008/stanford2008.wikispaces.com/file/view/pca_example.gif (accessed Dec. 08, 2021).

[3] M. Migliavacca et al., “The three major axes of terrestrial ecosystem function,” Nature, vol. 598, no. 7881, pp. 468–472, Oct. 2021, doi: 10.1038/s41586-021-03939-9.

CONFERENCE PARTICIPATION, PUBLICATIONS, AWARDS & ACADEMIC MILESTONES

Professional Conference Presentations and Proceedings

M. Komninakis, J. Sinicrope, K. Jiao, J. Nicholson, J. Wohlwend. Quantifying the Performance of Fixative Technologies under Impact Stress for D&D Activities, Waste Management 2022 Conference, Phoenix, AZ, March 2022.

**K. Jiao, J. Sinicrope, M. Komninakis, J. Perucina, P. Kohli, A. Vargas. Polymeric Micro-Ribbons Engineering for Wastes Oil and Mercury Removal from Water, Waste Management 2022 Conference, Phoenix, AZ, March 2022.

> **NOTE: Awarded “Best Poster Presentation” in Environmental Remediation Track 7.1 by WM Symposia.

H. Upadhyay, W. Quintero, L. Lagos. *Waste Information Management System with 2021-22 Waste Streams*. Waste Management 2022 Virtual Conference, Phoenix, AZ, March 2022.

A. Meray (DOE Fellow), H. Upadhyay, L. Lagos, M. Siddiquee, R. Serata, S. Sturla, S. Uhlemann, H. Wainwright, M. Denham, H. G. Raymat, C. Eddy-Dilek. *pyLEnM: An Open Source Machine Learning Framework for Long-term Water Quality Monitoring.* Waste Management 2022 Conference, Phoenix, AZ, March 2022.

A. Meray (DOE Fellow), S. Sturla, M. Siddiquee, R. Serata, S. Uhlemann, H. G. Raymat, M. Denham, H. Upadhyay, L. Lagos, S. Uhlemann, C. Eddy-Dilek, H. Wainwright. PyLEnM: A Machine Learning Framework for Long-Term Groundwater Contamination Monitoring Strategies (2022). Environmental Science & Technology 56 (9), 5973-5983. doi.org/10.1021/acs.est.1c07440

W. Quintero, H. Upadhyay, L. Lagos, S. Joshi. *D&D KM-IT 2022 Updates*. Waste Management 2022 Virtual Conference, Phoenix, AZ, March 2022.

R. Boza, S. Joshi, H. Upadhyay, L. Lagos. *Crack Detection Using Convolutional Neural Network Deployed on Mobile Platform.* 2021 ANS Winter Meeting and Technology Expo, November 30–December 3, 2021

S. Joshi, R. Boza, H. Upadhyay, W. Quintero, L. Lagos. *Mobile Platform for Structural Health Monitoring Using Convolutional Neural Network*. Waste Management 2022 Conference, Phoenix, AZ, March 2022

**H. Upadhyay, S. Joshi, W Quintero, L. Lagos. *Mobile Platform for Structural Health Monitoring Using Convolutional Neural Network*

> ** NOTE: Paper was awarded “ASME Best Oral Paper/Presentation Award” and “Superior Paper Award”, respectively, by WM Symposia 2022.

Student Conference Presentations and Awards

A. Meray (DOE Fellow), H. Upadhyay, L. Lagos, M. Siddiquee, H. Wainwright. *AI Approach to Predict Tritium Concentrations Using Specific Conductance as a Proxy Variable at the SRS F-Area*. Waste Management 2022 Conference, Phoenix, AZ, March 2022

Academic Milestones

DOE Fellow David Mareno (Class of 2018) graduated with a B.S. degree in computer engineering in Fall of 2021.

ACKNOWLEDGEMENTS

Funding for this research was provided by U.S. DOE Cooperative Agreement #DE-EM0005213. FIU's Applied Research Center would like to acknowledge the commitment of DOE-EM to this Waste and D&D Engineering and Technology Development project and to all the research being conducted as part of the Cooperative Agreement. The partnership between DOE EM and FIU has resulted in the development and training of outstanding minority STEM students that will benefit this country as a whole.

APPENDIX

The following documents are available at the DOE Research website for the Cooperative Agreement between the U.S. Department of Energy Office of Environmental Management and the Applied Research Center at Florida International University:
https://doeresearch.fiu.edu/SitePages/Welcome.aspx

FIU Year 2 Annual Research Review Presentations:

1. FIU Research Review - Project 1
2. FIU Research Review - Project 2
3. FIU Research Review - Project 3 – D&D
4. FIU Research Review - Project 3 – IT ML
5. FIU Research Review - Project 4 & 5
6. FIU Research Review - Project 4 - DOE Fellow Aubrey Litzinger
7. FIU Research Review - Project 4 - DOE Fellow Aurelien Meray
8. FIU Research Review - Project 4 - DOE Fellow Joel Adams
9. FIU Research Review - Project 4 - DOE Fellow Mariah Doughman
10. FIU Research Review - Project 4 - DOE Fellow Nicholas Espinal
11. FIU Research Review - Project 4 - DOE Fellow Philip Moore
12. FIU Research Review - Project 5 - DOE Fellow Olivia Bustillo
13. FIU Research Review - Project 5 - DOE Fellow Shawn Cameron
14. FIU Research Review - Wrap Up - Project 1
15. FIU Research Review - Wrap Up - Project 2
16. FIU Research Review - Wrap Up - Project 3 – D&D
17. FIU Research Review - Wrap Up - Project 3 – IT ML
18. FIU Research Review - Wrap Up - Project 4
19. FIU Research Review - Wrap Up - Project 5